University of Nottingham
UK | CHINA | MALAYSIA

Models and algorithms for the management of traffic flows with wireless charging lanes

Thesis submitted to the University of Nottingham for the degree of **Doctor of Philosophy, June 2024.**

FAN LIU

20319565

Supervised by

Zhen Tan
Hing Kai Chan
Liang Zheng

Signature _____

Date _____ / _____ / _____

Abstract

The rapid growth of Electric Vehicles (EVs) presents promising solutions to environmental and energy crises but introduces challenges in traffic management and charging infrastructure. This thesis explores advanced real-time traffic flow management models and algorithms specifically tailored for roads equipped with Wireless Charging Lanes (WCLs), a technology that allows EVs to charge while in motion. The primary objective is to optimize the overall operational efficiency (traffic and charging efficiencies) of the traffic systems with WCLs.

The research is structured around three key studies, each addressing different aspects of traffic management with WCLs. The first study explores a ramp metering control problem on WCLs, considering optimal traffic and charging efficiencies. First, we incorporate the state of charge (SOC) of electric vehicles (EVs) into the cell transmission model (CTM) in a mathematically convenient way, reformulating the model as a piecewise-affine (PWA) system. Using a hybrid model predictive control (MPC) approach, the control problem at each time stage is formulated as a mixed integer linear programming (MILP) problem, which is solved by well-established solvers. We conduct numerical experiments on an 8-km WCL for two sample scenarios and another with real traffic demand. We demonstrate both the efficacy and the limitation of ramp metering control in WCLs in terms of maximizing charging efficiency. We also reveal the inherent conflict be-

tween traffic efficiency and charging efficiency on a fully covered WCL. The proposed method and experiment results provide a novel tool and valuable insights for traffic authorities and policymakers regarding the management and operations of WCLs.

The second study addresses the variable speed limit (VSL) control problem in wireless charging lanes (WCLs), considering optimal traffic and charging efficiencies. Firstly, we introduce a system predictive model designed to anticipate the evolution of both traffic flow characteristics and the SOC of EVs with consideration of variable speed limits. The model is formulated as a PWA system through various linearization techniques. Subsequently, we propose a series of control models that account for the delicate balance between traffic and charging efficiencies, enabling the exploration of effective control strategies under varying priorities. The optimal control problem at each stage is cast as a MILP by a hybrid MPC approach. Our simulation results offer valuable insights for traffic operators engaged in the operation and management of WCLs.

The third study considers a dynamic pricing problem in a dual-lane system consisting of a general purpose lane (GPL) and a WCL. The electricity price is dynamically adjusted to affect the lane-choice behaviors of incoming EVs, thereby regulating the traffic assignment between the two lanes. The aim of dynamic pricing is to maximize operational efficiency (traffic efficiency and charging efficiency). First, we establish the dynamic traffic model tailored to the context of the dual-lane system by an Agent-Based Model (ABM) method, in which each EV acts as an independent agent with distinct characteristics. Next, we propose a model-free reinforcement learning (RL) algorithm, i.e., deep q-learning, to derive the optimal dynamic pricing strategy. A traditional machine learning (ML) method, that is, a classification and regression tree (CART) algorithm, and a static pric-

ing strategy are also proposed for comparison. The simulation results reveal that both the dynamic pricing strategies (CART and deep q-learning) outperform the static pricing strategy in maximizing operational efficiency. In particular, the deep q-learning algorithm demonstrates a superior capability in optimizing dynamic pricing strategies by leveraging system dynamics more effectively and future traffic demand information. These insights also contribute to the real-time management of WCLs. This study serves as pioneering work to explore dynamic pricing issues in a multi-lane system with WCLs. The methodology adopted in this paper serves as a template for other researchers interested in similar issues.

In summary, these studies contribute to the exploration of real-time traffic flow management problems in the context of WCLs, providing models and algorithms tailored to this traffic context. They also offer insights that aid traffic authorities and policymakers in managing systems equipped with WCLs. This thesis not only addresses significant gaps in real-time traffic management strategies for DWC scenarios but also lays a foundation for future research.

Acknowledgements

This thesis was completed at the University of Nottingham Ningbo China. As I submit this document, I extend my deepest appreciation to all individuals and organizations who have facilitated, supported, inspired, and traveled with me throughout my Ph.D.

Foremost, I owe a debt of gratitude to my supervisors—Prof. Zhen Tan and Prof. Hing Kai Chan from the University of Nottingham Ningbo China, and Prof. Liang Zheng from the School of Traffic and Transportation Engineering at Central South University. Their insightful guidance not only guided me toward the completion of this research, but also inspired and honed my academic abilities for future endeavors. Their unwavering support and constructive feedback were indispensable.

The authors also thank the internal assessor, Prof. Chandra Ade Irawan, and the external assessor, Prof. Nan Zheng from Monash University. Their commitment and valuable feedback significantly improved this thesis. My gratitude extends to the staff of the Graduate School at the University of Nottingham Ningbo China for their assistance with essential documentation throughout my Ph.D. program.

A special thanks goes to the many scholars who have been generous with their knowledge, advice, and time, especially those who engaged in enlightening discussions with me about philosophy, physics, and mathematics. I am equally grateful to my friends, whose companionship and unwavering support helped me navigate and overcome the challenges of the past four years.

Most importantly, I express my profound thanks to my family, especially my parents, whose unconditional love, support, and understanding have been my cornerstone. Despite the physical distances between us, their emotional support has been my constant.

My heartfelt thanks to everyone who has been a part of my journey.

Contents

List of Tables

List of Figures

Chapter 1

Introduction

1.1 Background of DWC technology for EVs

Electric vehicles (EVs) have become increasingly popular all over the world and they are expected to be the most promising transportation solution to the energy crisis and environmental pollution (Deflorio et al., 2015b; Jang, 2018; He et al., 2020). Recent increases in the adoption of electric cars have been driven mainly by government incentives and falling battery prices. According to data from the International Energy Agency, global EV sales increased by 41% in 2020 despite economic recessions caused by COVID-19, and the market is on track for a strong expansion expected in the next decade (IEA, 2021). However, the problem of charging is still a key barrier to the mass adoption of EVs, as most existing EVs are still charged by electric cables (Machura and Li, 2019). Long charging times and limited charging facilities greatly impede the convenience of charging, which further leads to 'range anxiety', where drivers worry about running out of energy before reaching their destination. Automotive research institutes have devoted considerable effort to reducing EV power consumption and

enhancing charging efficiency and battery capacity. At the same time, more flexible charging approaches have also been developed, such as battery swapping and static and dynamic wireless charging technology, as described below.

Battery swapping: In the context of battery swapping, a depleted EV battery is replaced with a fully charged one. Auto companies like Better Place and Tesla explored battery swapping technology but failed due to a lack of a unified standard or high costs compared to supercharging (Wu, 2021). Battery swapping still faces many challenges, the main one being that the electric parameters of EVs and batteries are difficult to standardize. In addition, few consumers will accept battery leasing solutions instead of owning the battery (Hans and Gupta, 2020). The only successful example of battery-swapping technology is the Chinese carmaker, NIO, which proposed a unique business model and launched its battery-swapping scheme in 2018. So far, NIO has built 175 battery-swap stations spread across China (an example is shown in Fig. 1.1a, although this number is still far from enough to support the large-scale application of battery-swapping.

Static wireless charging: In the context of static wireless charging, an EV is charged wirelessly at rest by electromagnetic induction between two coils. This charging technology allows EVs to get rid of charging cables and there is no physical contact during the charging process (see Fig. 1.1b). Static wireless charging enables a safer charging process without bulky cables, and it provides some unique advantages, such as 'park and charge'. However, static wireless charging is not significantly superior to traditional cable charging in terms of charging time and the charging facilities allocation. There has been considerable research into and testing of static wireless charging technology; however, since this charging mode is not the focus of this paper, interested readers can refer to Cirimele et al. (2018)

and Machura and Li (2019).

Dynamic wireless charging (DWC): In the context of DWC, EVs are charged wirelessly when in motion. Thus, DWC is also known as 'charging-while-driving' or 'in-motion charging'. The road equipped with the wireless chargers is called a wireless charging lane (WCL) (see Fig. 1.1c). Based on the power transfer principles, DWC technology for EVs can be categorized into two types: inductive Power Transfer and capacitive Power Transfer (Amjad et al., 2022). Inductive Power Transfer utilizes electromagnetic fields generated by coils embedded in the road. Energy is transferred through these coils to a receiver coil in the moving vehicle. The system typically involves a direct current power supply, which minimizes losses and can be integrated with renewable energy sources effectively. Unlike inductive systems, capacitive charging uses electric fields for power transfer. This method involves plates or capacitors that manage power transfer by the variation of electric fields across an air gap. While less common than inductive systems, capacitive methods are being explored for their potential in dynamic charging scenarios.

Since DWC technology was first proposed in the 1970s (Bolger et al., 1978), many carmakers and research institutions around the world have studied and developed it over the past few decades such as University of California, Berkeley (Chen et al., 2015a; Suh and Cho, 2017), Korea's Advanced Institute of Science and Technology (Kim et al., 2013a; Foote and Onar, 2017), and Bombardier Transportation (Cirimele et al., 2018). Numerous studies have been published based on DWC and many of them have indicated that it is likely the most promising charging mode. In addition, DWC can be implemented with other emerging techniques such as self-driving, in order to solve EV dispatching problems for system optimization. Although DWC is still in the experimental stage and has yet to be applied on a large scale,

there is little doubt that it has great practical value and market prospects. An empirical study has shown that it is expected that DWC technology will be first applied in commercial fleet vehicles such as buses, trucks, and port transport vehicles (Chen et al., 2017). From a transportation systems point of view, the great convenience and opportunities brought by DWC also come with notable challenges in traffic planning, management, and operations. For example, EV drivers' routing behaviors will be driven by state-of-charge (SOC) in addition to considering conventional factors such as travel time. EV drivers may also have to make new decisions, such as WCL speed choices according to their SOC profiles (Chen et al., 2016), while the complexities and uncertainties in the energy consumption of EVs and human factors are inherent (Jang, 2018). For another example, when WCLs are deployed on the highway, real-time traffic control measures (e.g. ramp metering and variable speed limit control) should consider not only traffic efficiency - enhancing traffic flow and reducing congestion - but also charging efficiency to ensure economic effectiveness (Panchal et al., 2018; Li et al., 2019). Here, charging efficiency is typically measured by the total energy transmitted to EVs, which also reflects the utilization rate of DWC facilities. Therefore, considering charging efficiency necessitates incorporating the EV's SOC into the dynamic traffic model. Moreover, since the energy obtained by an EV on the WCL is generally proportional to its travel time (given that the charging power is fixed), traffic efficiency and charging efficiency are inherently in conflict. Thus, problems such as traffic network design and traffic flow control are much more difficult to tackle when DWC EVs are introduced to the system.

(a) Battery Swapping

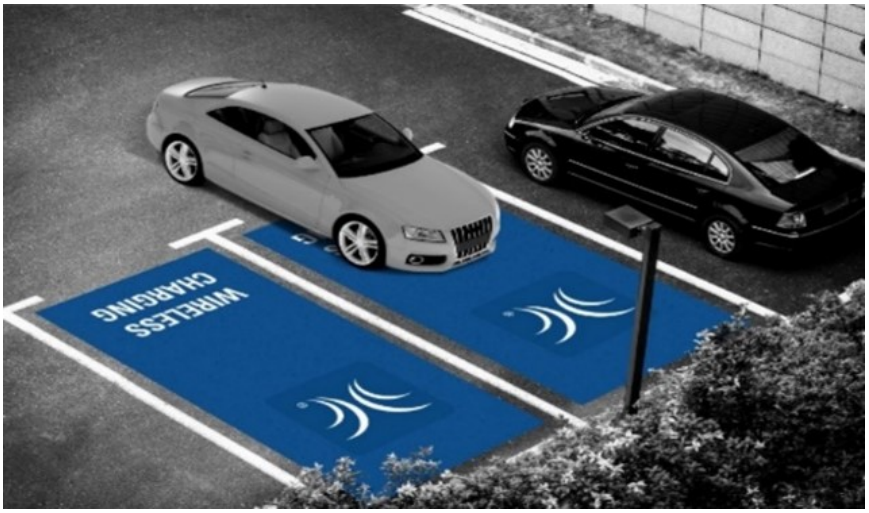

(b) Static Wireless Charging

(c) Dynamic Wireless Charging

Figure 1.1: Overview of Electric Vehicle Energy Solutions

1.2 Transportation systems management considering DWC EVs

The transportation systems management considering DWC EVs can be categorized into four aspects (Tan et al., 2022):

1. Development and features of DWC technology
2. Optimal allocation of WCLs
3. EV energy consumption analysis in WCL context
4. Billing and pricing for EVs on WCLs

The studies on the **Development and features of DWC technology** concentrate on its evolution, applications, and integration into EV systems. Originating in the 1970s, DWC has advanced significantly through contributions from global academic and corporate entities, like the University of California, Berkeley, and Korea's Advanced Institute of Science and Technology. DWC technology improves the utility of EVs by enabling in-motion charging, reducing vehicle weight and costs, and supporting autonomous driving technologies. However, its broader adoption faces challenges such as high costs and technical issues like maintaining efficient power transfer between moving coils. A detailed review is provided in Sec. 2.1.

Studies on **optimal allocation of WCLs** explore various research strategies to implement WCLs effectively across different traffic systems. These studies categorize allocation problems into micro- and macro-models, each addressing different scales of traffic systems. The micro-allocation models focus on optimizing WCL layouts along specific paths, minimizing installation costs, and adapting to precise vehicle requirements like SOC.

Macro-allocation models evaluate broader impacts on traffic systems, often employing network modeling to assess WCL effects on traffic flows and system-wide efficiencies. These studies utilize mathematical optimization techniques to balance costs, maximize energy delivery to EVs, and meet specific operational constraints like budget limits and SOC thresholds. Studies typically conclude with strategies that enhance charging efficiency and traffic management, recommending WCL configurations that align with varying urban and highway traffic conditions. A detailed review is provided in Sec. 2.2.

The studies on the **EV Energy Consumption Analysis in WCL Context** review the studies examining how WCLs affect EVs' energy consumption profile. These studies explore different scenarios including urban, highway, and motorway settings, and consider factors like vehicle speed, traffic density, and road type. Key findings suggest that energy consumption varies with traffic conditions, and urban environments present more challenges due to erratic driving patterns. Researchers utilize various models to simulate energy dynamics, incorporating factors like SOC, vehicle acceleration, and the specific configurations of WCL installations. This research is pivotal for optimizing the deployment of WCL to improve energy efficiency, manage traffic flows, and extend the range of EV driving. A detailed review is provided in Sec. 2.3.

The studies on the **Billing and Pricing for EVs on WCLs** explore diverse methodologies to economically integrate WCLs into the transport and power networks. They highlight the complexity of billing based on energy received and dynamic pricing strategies to influence EV routing to alleviate congestion. Research spans from micro-level tactics, such as individual vehicle charge management and pricing, to macro-scale analyses linking transportation behavior with power grid economics. These studies

often use game-theoretical models and user equilibrium principles to forecast the interactions between EV drivers and WCL providers, in order to efficiently balance system costs, road traffic, and power consumption. A detailed review is provided in Sec. 2.4.

1.3 Research motivation, questions, objectives, and contributions

Although various aspects of transportation management issues related to WCLs have been studied, real-time traffic management issues for WCLs have not been sufficiently explored. Traditional real-time traffic management focuses on improving traffic efficiency (TE) by improving traffic flow, reducing congestion, and minimizing travel time. However, integrating WCLs into traffic systems also introduces the need to optimize charging efficiency (CE) for economic effectiveness. This creates a dilemma for individual EVs: optimal traffic efficiency encourages faster travel, while optimal charging efficiency requires slower speeds to maximize energy replenishment, given the generally fixed charging power of WCLs. This conflict presents significant challenges for managing real-time traffic on WCLs, yet the current literature does not adequately emphasize the conflicting demands of optimizing both TE and CE. Addressing these challenges requires a comprehensive approach that considers both TE and CE from a modeling perspective, potentially by integrating the (SOC) of EVs into dynamic traffic models in a mathematically tractable way.

Thus, motivated by the need to bridge the gap between technological advancements in DWC and the practical challenges in real-time traffic management, we propose two research questions:

Research Question 1 How can traffic models and algorithms be developed to simultaneously optimize TE and CE in real-time traffic management for highway systems with WCLs?

Research Question 2 What managerial insights can be derived from the optimal traffic management strategies that balance TE and CE in highway systems with WCLs?

Our research objectives are twofold:

- Firstly, we aim to develop and propose models and algorithms specifically designed for real-time traffic management on WCLs. These tools are intended to be practical enough for implementation and adaptable for further enhancement by other practitioners.
- Secondly, we aim to provide valuable insights into real-time traffic management on WCLs that can assist policymakers and traffic departments. These insights are designed to bridge the gap between theoretical research and practical application.

Our contributions are outlined below:

- We explore three real-time traffic management challenges in traffic systems with WCLs: ramp metering control, variable speed limit control, and dynamic pricing. To our knowledge, this is pioneering work in the field.
- We introduce three novel dynamic traffic models tailored to each study's context, applicable at both macro and micro levels depending on specific requirements. Each model is complemented by a dedicated control

method, including both model-based methods like MPC and model-free approaches like deep Q-learning. Additionally, we develop a novel algorithm, *learning from K-nearest neighbors mode sequences (LKNMS)*, to accelerate the model-based control problems.

- Our simulation results reveal the inherent conflict between traffic and charging efficiency on WCLs, offering valuable insights into the operation and management of such traffic systems.

The thesis is organized as follows: Chapter 2 provides a comprehensive review of the existing literature related to transportation management on WCLs. Chapter 3 outlines the methodology employed in the three studies that form the core of this thesis. Chapter 4 presents the first study, which investigates Ramp Metering Control on WCLs. Chapter 5 details the second study, focusing on VSL control on WCLs. Chapter 6 covers the third study, which addresses the challenges of Dynamic Pricing on WCLs. Finally, Chapter 7 summarizes the key findings of the thesis, discusses the insights for transportation management, and suggests directions for future research.

Chapter 2

Literature Review[1]

This section gives a brief review of the studies related to WCLs in transportation systems. The databases we searched and the keywords we used are listed in Table. 2.1. We first searched all papers published from 2012 to 2024 that contained the search keywords. Then we retained those papers that are closely related to transportation systems management according to their abstracts. Finally, we also checked the references of these selected papers manually to identify additional relevant studies for the review. Our review is organized from four aspects: (1) Development and features of DWC technology; (2) Optimal allocation of WCLs; (3) EV energy consumption analysis in WCL context; (4) Billing and pricing for EVs on WCLs.

Table 2.1: Search keywords and database used.

Databases (2012 – 2024)	**Keywords searched**
ScienceDirect, Google Scholar, Web of Science, INFORMS Online Journals, IEEE Xplore, Wiley Online Library	wireless charging lane, dynamic wireless charging, in-motion charging, charging while driving, charging road, charging lane.

[1]This chapter has been published in the journal *Transportation systems management considering dynamic wireless charging electric vehicles: Review and prospects* (Tan et al., 2022).

2.1 Development and features of DWC technology

DWC technology was first proposed in the 1970s (Bolger et al., 1978) and has been studied and developed in the past few decades by many carmakers and research institutions around the world. Readers interested in the working principles of the DWC system can refer to Ahmad et al. (2017) and Panchal et al. (2018). Some of the pioneers in studying DWC are the University of California, Berkeley (Shladover, 2007; Chen et al., 2015a; Suh and Cho, 2017), Korea Advanced Institute of Science and Technology (Kim et al., 2013a; Foote and Onar, 2017; Suh and Cho, 2017) and Bombardier Transportation (Cirimele et al., 2018). A series of in-depth studies have demonstrated the feasibility of this technology. In addition, several real WCL projects have been tested and implemented in some other countries, such as the solar panel-equipped road in Jinan, China (Bloomberg, 2018), and many others have been planned. In the future, EVs and WCLs are likely to be more and more widely applied to traffic systems. Readers interested in more history of commercialization activities can refer to Jang (2018). At present, DWC is regarded as the most promising charging solution to EVs due to its various advantages, such as those listed below:

Extension of the driving range: EVs are allowed to charge while consuming energy, which can greatly extend the driving range, achieving an infinite range in the ideal case (Chopra and Bauer, 2011a). Thus, range anxiety can be effectively relieved or overcome (Jansuwan et al., 2021).

Reduction in battery size and vehicle weight: The technology can effectively reduce the number and capacity of the batteries, thereby reducing EV cost and weight (Duarte et al., 2021), which in turn helps save energy (Bi et al., 2019b). Bi et al. (2015) demonstrated that the battery

size of wireless charging buses can be reduced to one-fifth to one-third of the original size.

The economy of time and space: EV drivers do not need to spend extra charging time at a stationary point. Space occupied by charging facilities is negligible.

Facilitating EV sharing: Downtime due to static charging is a key barrier to the operation of EV car-sharing systems (Lin and Kuo, 2021). DWC provides a natural solution to this problem and thus helps to realize the environmental, mobility, and societal benefits of EV sharing.

Integration with other emerging technologies: DWC technology can be combined with other advanced technologies and control measures such as self-driving (Panchal et al., 2018) and platooning to improve EV charging efficiency (Jansuwan et al., 2021).

Potential for cost reduction in power networks: Bi-directional power transfer can be made more flexible and accessible by DWC, EV drivers can both charge and discharge their energy while driving, which can help shave peak load for power networks and thus reducing power generation cost (Nasr Esfahani et al., 2022).

Currently, the major challenges for the mass adoption of DWC are:

High cost: The construction of a DWC system requires a lot of powerful electronic devices and complex guide rails. Besides, regular maintenance is necessary. Its total cost is much higher than cable charging or static wireless charging.

Technical bottleneck: Trung and Diep (2021) demonstrated that the theoretical maximum efficiency of DWC can exceed 90%. However, the current efficiency of DWC is about 70–80% (Bi et al., 2016), that is, still

lower than the efficiency of plug-in charging and static wireless charging with a maximum efficiency of about 90%. The charging power is steady for static wireless charging, which is mainly controlled by two coils or pads. For DWC, however, the location of vehicles is constantly changing. Consequently, the receiver coils on the vehicles might be coupled with different transmitter coils on the road, which affects the charging efficiency. To reduce power loss, different power supply segments should be controlled differently (Tavakoli and Pantic, 2017). A perfect solution is to create the perfect alignment between the two coils by autonomous driving technology (Panchal et al., 2018).

The deployment and planning of WCLs in the traffic systems are also challenging considering various affecting factors and stakeholders, which have been discussed in many recent studies, as we will review in the following section.

2.2 Optimal allocation of WCLs

The optimal allocation problem is one of the most important problems in the system design of both WCLs and traditional charging facilities. So far, extensive research has been conducted to optimize the deployment of WCL in various scenarios. The optimal allocation of WCL is usually formulated into an optimization problem that achieves one or more of the following objectives: 1) Minimising social cost, including the construction cost of WCLs and the total travel time; 2) Maximising the total energy received by the EVs or the number of EVs that use WCLs; 3) Optimising battery size or charging power, and satisfy various constraints such the budget constraint and limits on EVs' SOCs.

In this subsection, we will first distinguish three different types of allocation problems and describe their general mathematical models. Then relevant studies for each type of model will be reviewed, hoping to give some concrete examples.

2.2.1 Problem classification

Jang (2018) classified the WCL allocation models into two categories according to the scope: the micro-allocation and the macro-allocation models. Microscopic allocation models optimize the WCL layout (e.g., segment length and location) on one or a few pre-defined path(s) on which the speed profile or required travel time of the EV is given. The objectives are typically minimizing the cost of the WCL facility. A basic micro-allocation model can be generally written as the following optimization problem:

$$\begin{aligned} \min_{x \in X} \quad & J(x) \\ \text{s.t.} \quad & r_p^{low}(d) \leq r_p(x,d) \leq r_p^{up}(d), \quad \forall d \in [0, l_p], \quad \forall p \in P \end{aligned} \tag{2.1}$$

where $\boldsymbol{x}$ is the decision vector encoding the WCL allocations (e.g., the starting and ending positions of each WCL segment on each path); J is the cost function to be minimized (e.g., the fixed and variable installation cost); r_p is a function describing the SOC level of the vehicle at any location d on path p, i.e., $r_p(\boldsymbol{x}, d)$ represents the SOC of the vehicle at location d on path p, and l_p is the length of path p; $r_p^{low}(d)$ and $r_p^{up}(d)$, respectively, are the given lower and upper limit of the SOC on path p, which can be location-dependent, e.g., initial SOC and target SOC when leaving the system (Schwerdfeger et al., 2022); P is the set of paths and X is the set of feasible allocations defined mainly by the geometric restrictions.

The continuous model formulation (2.1) is usually simplified by dividing the

paths into a set of equidistant small segments and restricting the allocation decisions to be segment-based, i.e., $\boldsymbol{x}$ to be a binary vector (e.g., (Ko et al., 2015; Liu and Song, 2017)). Also note that other decisions are often considered together in micro-allocation problems, such as buses' battery sizes and bus fleet sizes (e.g., Alwesabi et al. (2021)), in which case the decision vector $\boldsymbol{x}$ can be enlarged and other relevant elements can be added to the objective and constraints in model (2.1).

In contrast, macro-allocation models aim to evaluate the impact of the WCLs on the higher-level transportation systems perspective. They typically adopt a network-modeling approach and need to make high-level assumptions due to the models' greater scope, for example, the traffic demands for each origin-destination pair in the network are given. One key factor that distinguishes macro-allocation models is whether traffic flow distributions are allowed to be dependent on WCL allocation decisions. Studies that focused on cost-benefit analysis for a longer planning horizon or a broader scale typically assumed that traffic demand and flow distribution on the network are given. These models can be expressed generally as:

$$\begin{aligned} \min_{y \in Y} \quad & G(\boldsymbol{y}, \boldsymbol{f}) \\ \text{s.t.} \quad & s_{a,u}^{low} \leq s_{ua}(\boldsymbol{y}, \boldsymbol{f}) \leq s_{a,u}^{up}, \quad \forall u \in U, \forall a \in A \end{aligned} \tag{2.2}$$

where $\boldsymbol{y}$ is the decision vector encoding the WCL allocation plan, whose dimension is usually equal to the number of links in the network but can be larger in cases where, for example, the deployment decisions are sequential (e.g., Bi et al. (2019b)); $\boldsymbol{f}$ is the given link flow vector that may be defined for different types of users according to their features such as origin-destinations or vehicle classes; G is the cost function to be minimized, which usually involve both $\boldsymbol{y}$ and $\boldsymbol{f}$, e.g., the deployment cost and total travel time on the network; $s_{a,u}$ represents the SOC of the type-u user after passing link a, which generally depends on not only the allocation de-

cision $\boldsymbol{y}$ but also the flow distribution $\boldsymbol{f}$ (e.g., traffic flow affects the travel time thus the recharging time); $s_{a,u}^{low}$ and $s_{a,u}^{up}$, respectively, are the lower and upper limit of the type-u user's SOC after passing link a; U is the set of different user types; A is the set of links on the network and Y is the set of feasible allocations defined mainly by the budget constraints.

Other studies regarded flow distribution as endogenous by modeling the impact of WCL on EV drivers' route choices. So, instead of $\boldsymbol{f}$ being given, these models typically rely on some traffic assignment model for capturing how WCLs affect routing choices. Conceptually, such a model can be formed by including the flow conservation condition and one set of constraints that enforces the allocation-dependent flow distribution:

$$\begin{aligned} \min_{y\in Y, f\in F} \quad & G(\boldsymbol{y}, \boldsymbol{f}) \\ \text{s.t.} \quad & s_{a,u}^{low} \leq s_{ua}(\boldsymbol{y}, \boldsymbol{f}) \leq s_{a,u}^{up}, \quad \forall u \in U, \forall a \in A \qquad f = \Lambda(\boldsymbol{y}) \end{aligned} \tag{2.3}$$

where F is the set of feasible flow distributions that ensures flow conservation condition; Λ is the traffic assignment operator that maps the allocation decision y to a specific network flow $\boldsymbol{f}$, which is itself a nontrivial mathematical programming problem in general and also implicitly includes the interdependence between $\boldsymbol{f}$ and SOC variables. Thus, considering choice behavior under DWC obviously makes the allocation problem more challenging to solve. However, it is useful to generate more interesting insights for traffic planning and management. Similar to the micro-allocation problems, model (2.2) or (2.3) can be revised to incorporate other decisions into the macro allocation problems, such as the electricity prices (Liu et al., 2021).

2.2.2 Studies on micro-allocation models

One typical scenario for micro-allocation model analysis is On-Line Electric Vehicle (OLEV): a DWC bus-transit system first developed by the Korea Advanced Institute of Science and Technology (Miller et al., 2015). Numerous studies have proposed allocation models based on OLEV, either for a single bus route (Jang et al., 2015; Jeong et al., 2015; Ko et al., 2015; Jang et al., 2016a,b) or several bus routes (Mouhrim et al., 2016; Hwang et al., 2017; Liu and Song, 2017; Lee and Jang, 2017). The aim of these models is usually to find an optimal solution that minimizes the total cost, including battery cost and the cost of the DWC bus-transit system. Jeong et al. (2015) were the first to take the battery life into account when evaluating the total cost, and their result showed that battery life is an important factor in long-term economic analysis. Hwang et al. (2017) and Liu and Song (2017) considered the case of shared routes where a WCL could be shared by multiple electric bus lines. Doan et al. (2017) proposed an optimal control model to deal with the WCL allocation problem for autonomous EVs with a pre-determined speed profile on a single path. Lee and Jang (2017) proposed a model that jointly optimizes the allocation of WCLs and battery capacity in a multi-route public transit system. In addition, Liu and Song (2017) proposed a robust optimization model that selects the optimal location of charging lanes with the optimal battery size considering the uncertainty of travel time and energy consumption of electric buses.

Some studies also considered, in their micro-allocation problems, the scheduling decisions for electric buses, i.e., optimal assignment of electric buses to cover the whole timetable of the transit system. Alwesabi et al. (2020) developed an optimization model that first selects the DWC planning decisions including WCL location and battery sizes assuming fixed fleet size and then utilizes the results to optimize the required number of electric buses

in the system considering additional charging time and battery size constraints. The findings suggested that joint scheduling (where an electric bus can service several routes) with a single optimal battery size is more cost-efficient than disjoint scheduling (where an electric bus services only a specific route) with multiple optimal battery sizes. Alwesabi et al. (2021) further formulated a mixed integer linear programming (MILP) model which simultaneously optimizes the electric buses' schedule and WCL planning decisions considering the dependences among battery capacity, location of WCL, and fleet size. The model was applied to a real-world off-campus college transit system to minimize the total life cycle system cost.

A recent work by Schwerdfeger et al. (2022) discussed the WCL allocation problem for serving long-haul electric trucks on a highway road segment consisting of multiple original destination pairs. The study formulated a continuous optimization model that finds the cost-minimizing WCL deployment plan that respects the truck SOC requirements defined for each origin-destination pair. An exact solution approach was then proposed based on a MILP, which was applied to a 963-km-long Germany highway example. The results showed that only about 35% of the highway needs to be electrified, mainly the central segments to cover more traffic. The study also tested a faster solution approach which approximates the allocation plan by discrete variables, claiming it to be the first to quantify the loss in precision by using this less flexible discrete model compared to the continuous one.

Table 2.2 summarises the micro-allocation studies we reviewed by some key features including problem objectives, decision variables, model assumptions, etc.

Studies	Problem objective(s)	Decision variables	Key model assumptions	Other features
Jeong et al. (2015)	Minimising the battery and charging infrastructure costs	Battery size for each route and WCL locations	Linear energy charging and discharging functions are assumed.	Take battery life into account
Hwang et al. (2017)	Minimising the battery cost and power track cost	Battery size for each route and WCL locations	EVs operate on multiple routes. Homogeneous battery sizes are assumed.	The WCL is shared by multiple electric bus lines
Liu and Song (2017)	Minimising the total cost of batteries and DWPT facilities	Battery size for each route and WCL locations	Each bus line in the bus system operates on a fixed route	Using data obtained from the transportation center at Binghamton University
Alwesabi et al. (2020)	Minimising the total cost of batteries and the DWC facilities	WCL location and battery sizes	The fleet has a uniform model, type, and size.	Using data obtained from the transportation center at Binghamton University
Alwesabi et al. (2021)	Minimising total cost of battery size, the number of transmitters, and the fleet size	Battery size, WCL location, and bus fleet size	The fleet has a uniform model, type, and size.	Simultaneously optimize the integrated model of EB fleet size and DWC infrastructure planning

Table 2.2: Summary of representative studies on micro-allocation models.

2.2.3 Studies on macro-allocation models without considering route choices under WCL

Fuller (2016) evaluated the potential for WCL to extend the driving range and its economic benefits. A 200-mile range EV was assumed to travel on key California freeways in collaboration with both station-based static charging and DWC. The dynamic charging problem was formulated as a flow-based set covering problem which considers driving range and battery capacity constraints. An optimization model was constructed to find the optimal solution to the allocation of WCL with the aim of minimising the total investment cost. The model implicitly assumes that WCLs are deployed throughout the wireless charging links. Results indicated that a 200-mile range EV can complete most state-wide travel with the support of a 40 kW, 626-mile DWC system together with the existing static charging stations at some locations. The result also showed that DWC is a more cost-effective way of extending driving range than increasing battery capacity.

Bi et al. (2019b) considered the optimal deployment problem of WCLs in both spatial and temporal dimensions to minimize life cycle costs, greenhouse gas emissions, and energy burdens. The problem is for deploying WCLs on a network consisting of 154 links over a period of 20 years with decision variables defined for each year. A genetic algorithm was proposed to determine the optimal locations and the year of deployment. The results demonstrated that up to about 3% coverage of WCL can downsize EV battery capacity by up to 48%. It can also reduce life cycle greenhouse gas emissions and energy consumption by up to 9.0% and 6.8%, respectively.

Wang et al. (2019) pointed out that traffic lights have a significant impact on EV charging activity if WCL is deployed near signalized intersections. The study proposed an optimal deployment model that takes traffic lights

and regional energy supply-demand balance into account. Real traffic data sets were used to design the WCL deployment plan in urban areas. The results revealed that deploying all WCLs at intersections with heavy traffic flow may not be optimal when considering the balance between power supply and demand.

Mubarak et al. (2021) considered the deployment problem from the perspective of an urban planner. A mathematical model was suggested for determining the location and power capacities of WCLs (which were referred to as 'wireless charging stations') that minimizes investment cost while satisfying the recharging needs of all EVs in the network. The study can be extended to the deployment of the combination of static charging stations and WCLs. For simplification, the model treats user equilibrium-based traffic assignment as input which is unaffected by WCL allocations.

2.2.4 Studies on macro-allocation models considering route choices under WCL

Riemann et al. (2015) was among the first few studies that explored the WCL deployment problem. An extended flow-capturing location model was proposed to capture the interaction between the location of WCLs and the traffic flows on WCLs. The model considers drivers' routing behaviors based on the stochastic user equilibrium principle. Note that for model simplicity, the model adopts some unrealistic assumptions, for instance, an EV is fully charged once passing over a WCL, without considering its SOC.

Chen et al. (2016) modeled the trade-off between the amount of energy received and the extra travel time on WCLs. The basic assumption of the model is that the energy received on WCLs is proportional to the charging time while the energy consumption is proportional to the travel

distance. The drivers can decide the charging time on WCLs and may tend to move slowly to get more energy but incur longer travel time. Overtaking maneuvers are allowed in this study so that the speed choice on WCLs is not affected. Taking this point into consideration, they established a user equilibrium model to allocate the WCLs on the traffic network.

Chen et al. (2017) focused on the traffic scenario with both plug-in charging stations and WCLs along a long traffic corridor. The optimal deployment strategy was designed for two cases: 1) public provision, where the government was responsible for the construction and operation of charging facilities to minimize the total social cost; and 2) private provision, where two different charging facilities were built and operated by two different companies to maximize their own profits. The numerical results showed that, in the private provision scenario, WCLs were more competitive than charging stations in terms of profit; while in the public provision scenario, WCLs were more competitive for the drivers who valued time more than cost.

Liu and Song (2018) considered a WCL deployment problem assuming that DWC may only be used by plug-in hybrid electric trucks. A multi-class multi-criteria user equilibrium model was proposed for capturing different route choice behaviours of truck and passenger car drivers. In particular, while each passenger car only minimizes its travel time, the truck minimizes its generalized cost which consists of travel time, fuel, and electricity costs. The truck driver can decide its recharging time on a WCL. The study showed that the equilibrium flow distributions, in this case, may not be unique, so it further adopted a robust approach that optimizes the worst-case system cost under any equilibrium. A heuristic algorithm was developed for solving the robust optimization problem, which was shown to be effective based on three numerical examples.

Ngo et al. (2020) proposed a WCL deployment model based on a bi-level programming approach, where the upper-level problem considers the public infrastructure planner's minimization of total travel time or emissions, while the lower level is the user equilibrium problem. Note that in all the aforementioned macro-allocation studies, the deployment of WCLs was encoded by binary variables assuming either that DWC facilities were installed on the entire link or no DWC facilities were installed on the link. This implicitly limited the maximum efficiency of DWC resources and led to a sub-optimal deployment. Thus, Ngo et al. (2020) used a continuous variable to represent a fraction of the link equipped with DWC facilities.

He et al. (2020) suggested an optimal deployment model for WCLs considering their effects on drivers' route choices and road capacity. The paper indicated that overtaking maneuvers on the WCLs in heavy traffic would inevitably reduce the road capacity of a multi-lane system. The numerical results showed that the impacts of WCLs on road capacity drop and drivers' route choices are not negligible. It also pointed out that the deployment of WCLs required a relatively high charging power. This study was the first to incorporate the adverse effects of WCL on the traffic flow into the allocation model.

Liu et al. (2021) proposed a bi-level model for optimizing the deployment and electricity prices of WCL to minimize the total social cost. The logit-based stochastic user equilibrium model was used to consider EV drivers' routing and charging behaviors, and both WCL and static charging stations were considered. The numerical results showed that the optimal deployment and price strategy generated by the proposed model can reduce the total social cost by 14.25% compared to the case where no WCL is deployed. The results also showed that the social cost of WCL can be reduced by offering travelers more travel and charging information to support their path

choices. This was the first such study that explored the combined decision problem of deployment and pricing on WCLs while considering EV drivers' routing and recharging behaviors.

He et al. (2023) presents a detailed analysis of deploying and operating wireless charging lanes (WCLs) for electric freight vehicles (EFVs) using a data-driven, large-scale micro-simulation approach. The multi-objective mixed-integer programming model developed utilizes real-world trajectory data of EFVs to optimize WCL deployment. Objectives include maximizing saved charging time, minimizing charging costs, and minimizing negative traffic impacts. Initially tested on a small network, the model was then applied to a large-scale scenario in Beijing. Results indicate that DWC could significantly reduce charging time by approximately 0.08–0.11 hours per EFV per day, within a budget of $67 million, predicting a long-term net value of $140.83 million over 25 years. The model incorporates several simplifying assumptions for computational feasibility, such as constant vehicle speed on WCLs, which might not fully capture variable traffic conditions. Furthermore, it employs a genetic algorithm for solving the large-scale optimization, efficiently managing the multi-objective nature of the problem and allowing for robust testing of various deployment strategies across Beijing's complex urban landscape.

Wang et al. (2023) considers a comprehensive bi-level optimization study on the integrated deployment of charging infrastructures for Battery Electric Vehicles (BEVs) within a combined transportation and power grid network. The model aims to minimize total travel and power generation costs while adapting to dynamic user behaviors and grid demands. The decision variables includes the locations of charging lanes and stations, alongside the generation of electricity at each busbar. A significant strength of the model is its incorporation of realistic assumptions about BEV energy consump-

tion and recharging rates based on travel distances and charging times, which are influenced by user route choices. The assumption is grounded in practical traffic flow dynamics and power grid interactions. The simulation results highlight substantial improvements in network efficiency, with the optimized infrastructure setup potentially reducing travel and charging times by significant margins. Note that this paper builds upon and extends the work of previous studies like He et al. (2020) and Ngo et al. (2020), which have explored the impact of dynamic charging lanes on route choices and power grid stability but did not incorporate the integrated planning approach this paper achieves. By comparing these methodologies and results, this paper offers novel insights into the optimization of infrastructure investments while accounting for the intricate dependencies between traffic flows and power grid dynamics.

Table 2.3 summarises the macro-allocation studies we reviewed by some key features including problem objective, decision variables, model assumptions, model formulation, etc.

Table 2.3: Summary of representative studies on macro-allocation models.

Study (ordered by year)	**Problem objective(s)**	**Decision variable for WCL deployment**	**Key model assumptions**			**Model formulation and solution approach**	**Other features**
			EV energy consumption	**EV energy recharging**	**Traffic flow distribution**		
Riemann et al. (2015)	Maximising total EV flow captured by charging links	A link is either a regular or wireless charging link	Proportional to the travel distance	An EV becomes fully charged once passing over a WCL	Determined by stochastic user equilibrium principle	A mixed-integer nonlinear program approximated by MILP and solved in Cplex	
Fuller (2016)	Minimising the capital cost of WCLs	A link is either a regular or wireless charging link	Proportional to the travel distance	The range added by recharging on a charging link is a constant assuming vehicle speed of 65 miles per hour	Given trip information: origin-destination and passing nodes, one-day trip or two-day trip	A MILP solved by branch and bound algorithm in Cplex	Existing static charging stations in the network also considered
Chen et al. (2016)	Minimising total travel time	A link is either a regular or wireless charging link	Proportional to the travel distance	Proportional to the charging time	Determined by user equilibrium principle	A mathematical problem with complementarity constraints solved by an active-set based algorithm	The EV driver can decide its charging time on the WCL

Chen et al. (2017)	Minimising the social cost or maximizing the profit from pricing the charging facility	WCLs deployed along the traffic corridor are sufficiently long and can be intermittent	Proportional to the travel distance	Proportional to the travel time on the WCL with a constant vehicle speed	Fixed flow on a single link, DWC demand is determined by choice model	A nonlinear programming problem with some optimal solutions derived analytically	Charging stations are considered and assumed uniformly placed along the corridor, as in Nie and Ghamami (2013)
Liu and Song (2018)	Minimising the weighted sum of total travel time, fuel, and emission costs	A link is either a regular or a wireless charging link	The truck consumes fixed total energy on each link (weighted sum of fuel and electricity)	Proportional to the charging time	Determined by multiclass and multicriteria user equilibrium model	A semi-infinite min-max program solved by a penalty function and cutting plane-based heuristic	The truck driver can decide its charging time on the WCL
Bi et al. (2019b)	Minimising life cycle costs, or GHG emissions, or energy burdens	WCLs can be deployed on each link in any year over a 20-year period	Proportional to the travel distance	Recharging model was not considered due to the problem scale	Given by historical traffic data	An integer programming problem solved by genetic algorithm	

Wang et al. (2019)	Minimising the weighted sum of WCL deployment cost and the gap between power supply and demand	WCLs can be deployed on each approach near an intersection with varied lengths	Proportional to the travel distance	Proportional to the travel time on the WCL	Given by historical traffic data	A MILP solved by generalized benders decomposition algorithm	Focused on comparing the results for downtown, industrial, and residential regions
Ngo et al. (2020)	Minimising total travel time or total net energy consumption	WCL can be deployed partly on each link encoded by a fraction of the link length	Proportional to the travel distance	The additional range obtained by recharging is proportional to the travel distance on the WCL	Determined by the user equilibrium principle	A bi-level programming problem solved by a surrogate model-based algorithm	

He et al. (2023)	Maximizing saved charging time, minimizing charging cost, minimizing negative traffic impact	WCL deployment can be adjusted across a large-scale network	Proportional to travel distance	Proportional to charging time, assuming constant vehicle speed	Determined by a simulation of traffic flows	A multi-objective mixed-integer programming model solved by a genetic algorithm	Employed real-world EFV trajectory data for model validation and testing in Beijing
Wang et al. (2023)	Minimizing total travel and power generation costs	Locations of charging lanes and stations, electricity generation at each node	Proportional to travel distance	Proportional to charging time, influenced by route choices	Influenced by user equilibrium reflecting realistic traffic flows	A bi-level optimization problem solved using a mixed-integer linear programming approach after various reformulations	Incorporates realistic traffic and power grid interactions, enhancing the practical relevance of the model

2.3 EV energy consumption analysis in WCL context

Understanding EV energy consumption is essential to SOC prediction and traffic system management. Numerous studies have looked at EV energy consumption in general, and the main conclusion is that EV energy consumption depends on traffic parameters, such as speed, acceleration, vehicle features, and road/environmental conditions. EV energy consumption is particularly complex to estimate in the erratic driving conditions of urban traffic (Galvin, 2017). In this section, we will review a few recent studies that explicitly considered the WCL context.

Deflorio et al. (2015b) proposed a method for measuring the performance of wireless charging EVs in the freight distribution service scenario from both traffic and energy standpoints. In this work, the WCLs were assumed to be installed only on the rightmost lane of a three-lane road in the form of discrete charging zones. The energy consumption was assumed to be linearly dependent on the average speed while the energy supplement on WCLs was proportional to the occupancy time. Different charging needs were defined for EVs with low-level SOC and EVs with normal-level SOC. Different charging modes require different speeds. The simulation result showed that the maximum power required by EVs on WCLs is about 50% higher for heavy traffic than for light traffic.

Deflorio et al. (2016a) proposed an application of DWC in motorway scenarios and suggested a method to estimate the daily energy provided to EVs by the DWC. The assumptions of road structure, energy consumption, and management strategy were similar to those in Deflorio et al. (2015b). The result indicated that WCL is suitable for motorways between two nearby cities where a number of EVs travel between the two city centers.

García-Vázquez et al. (2017) compared the performance of WCLs in three different road stretches (urban, highway, motorway) in terms of power and energy requirements, and EV's SOC. The numerical results indicated that the energy transferred to the EVs was higher for urban stretches than highways, but the fluctuation of power required by the WCL system on highways was much lower than that required on urban stretches. The increase of the battery SOC was low (<2%). Thus, an additional lane at a slow speed might be necessary for EVs to replenish more energy on the highway. This result is consistent with the assumption in some other studies that EVs should drive more slowly on WCLs than on general-purpose lanes (GPLs). Besides, the power requirement in an urban stretch is strongly dependent on the type/hour of the day and seasonality, whereas this dependence is low on highways. The work also concluded that another factor affecting the energy consumption of EVs was acceleration.

He et al. (2018) explored the impact of WCL on travel time and energy consumption in a two-lane road system consisting of one WCL and one GPL. They pointed out that WCLs should be placed on the multi-lane system. EVs driving on WCLs should travel more slowly than on GPLs. In this case, the effect of charging behavior on traffic flow is inevitable. Hence, they incorporated EV charging behavior into the driving behavior model and modified the existing energy consumption model. The simulation results indicated that the implementation of WCL can reduce the road capacity by 8%–17% and increase EV energy consumption by 3%–14% due to the frequent lane-changing behaviors of EVs. This result is consistent with the findings of He et al. (2020) regarding the adverse effect of overtaking maneuvers on road capacity. Both He et al. (2018) and He et al. (2020) revealed that the deployment of WCL in a multi-road system is worth considering, which may further influence the macro design.

Jansuwan et al. (2021) proposed an evaluation framework for an automated electric transportation system where cooperative EVs are charged by WCLs equipped on the road and can form platoons automatically. Road capacity, EV energy consumption, and 'well-to-wheel' emissions are measured for a simple ramp–mainline road system based on microscopic traffic simulation. The simulation concluded that the maximum range of an EV can be extended remarkably, for example, the range can be doubled even for the relatively low charging efficiency of 55% at a speed of 65 miles per hour. In particular, it was found that besides the enhancement of mainline capacity, platooning has significant power-saving benefits due to the aerodynamic advantage it creates by reducing the resistance force of the vehicles. Compared to the manual control mode, cooperative platooning resulted in much smoother speed and power profiles, which contributed to further energy savings. However, supporting WCLs with conventional (renewable) energy resulted in CO2 emissions 2–5 times higher than super ultra-low emission/partial zero emission vehicles.

2.4 Billing and pricing for EVs on WCLs

Billing and pricing the electricity for EVs driving on the WCL are the core problems in the commercialisation of the DWC technology and play an important role in the operations and management of WCLs. Given that the charging behavior occurs while the vehicles are in motion, the design of both billing and pricing strategies is challenging. For instance, billing should depend on the amount of energy received by each EV, rather than how long an EV drives on the WCL (Hussain et al., 2017). Electricity prices can also differ on different WCLs to affect the route choice of EV drivers and thus the traffic flow pattern in the transportation network for

mitigating congestion (He et al., 2013).

So far, relatively few studies have explored the billing and pricing problem for DWC. Ou et al. (2015) took into account the mobile characteristics of EV charging loads and investigated how the locational marginal pricing (LMP) of the power network is affected by DWC. Hussain et al. (2017) pointed out that the entry detection-based strategy, though works well for road toll systems, is not fair for EV billing on WCLs, as it ignores the fact that EVs with higher SOC may not opt to get recharged when traveling on the WCL. The study then presented a safe and privacy-aware framework for billing and authentication of OLEV driving on the WCL, which assumes that the WCL is composed of multiple charging zones, each can deliver a constant amount of energy and the billing was zone-based.

Several studies discussed the DWC pricing strategy considering its impact on EV drivers' choice behavior on transportation networks. For example, as we reviewed in Sec. 2.2.4, the study by Liu et al. (2021) considered a problem of optimizing the link-specific electricity prices together with the WCL deployment decisions on traffic networks. This study assumed that EV drivers can decide their routes and the amount of electricity recharged at WCLs so as to minimize their generalized travel cost consisting of travel time and recharging cost.

Wang et al. (2020) proposed an interesting charging pricing and vehicle scheduling algorithm based on a double-layer game model. The lower layer is the game between EVs, in which each EV is considered selfish, aiming to avoid detours and pay less for the electricity while gaining sufficient power to travel. A potential game theoretical model was used and the existence of Nash equilibrium was proved. The upper layer is the game between WCLs and EVs. EVs hope to reduce the charging cost while WCLs hope to raise the profit of electricity sales. The reverse Stackelberg game was used to

model the price function between WCLs and EVs. The simulation results demonstrated that the proposed double-layer game model can achieve a fair balance effect on both EV and WCL benefits.

At a larger system level, the WCL pricing problem can also be formulated by modeling the interaction between the transportation and power networks are considered. An early study by He et al. (2013) proposed both the first-best and second-best integrated pricing of roads and electricity pricing of DWC from the government agency's perspective. The first-best pricing model assumes that the transportation and power networks are both managed by a government agency whose goal is to minimize the total cost of power generation and travel time by charging locational marginal price at each bus of the power network and external travel time and energy cost on each link of the transportation network. The second-best pricing model assumes that the government agency only manages the transportation network to minimize the total travel time and energy consumption by designing the toll of each charging link, it has to ensure a positive revenue and follow the location marginal prices set by the power network. Numerical examples were used to offer insights into the proposed pricing method and demonstrate its effectiveness in improving social welfare.

Manshadi et al. (2018) proposed an interesting decentralized optimization framework considering interdependence among the electricity network and the transportation network: changes in the price of electricity affect EV drivers' routing choice and the associated distribution of traffic flow volume in the transportation network. The changes of charging demand caused by drivers' decisions affect the price of electricity in turn. EVs' routing behaviors in the transportation network were assumed to be captured by the user equilibrium principle. Note that the study considered the impact of traffic congestion on the economics of the electricity network, although the

additional charging time caused by traffic congestion was not considered.

Nasr Esfahani et al. (2022) designed an optimal pricing approach for bidirectional WCLs in coupled transportation and power networks. The proposed electricity pricing scheme can buy energy from and sell energy to EVs, with the objective of minimizing the total system cost of power generation, travel time, as well as the cost of purchasing electricity from EVs. In addition to EV's cost of travel time and energy recharging (i.e., grid-to-vehicle, G2V), the benefits of discharging energy to the power grid (i.e., vehicle-to-grid, V2G) were also included in the user equilibrium model. A bi-level optimization problem was then formulated to solve for the optimal buying price for electricity on each charging link, assuming that the selling price for electricity on each link is determined by LMP. The effectiveness of the proposed bidirectional charging model in reducing peak load and EVs' charging cost was validated by three numerical examples.

2.5 Research gaps

Previous sections have discussed various aspects of transportation management, particularly the optimal allocation of WCLs. However, real-time traffic management issues for WCLs remain underdeveloped. As mentioned in Sec. 1.3, addressing the real-time traffic management issues requires a comprehensive approach that considers both TE and CE from the modeling perspective, potentially by integrating the SOC of EVs into dynamic traffic models in a mathematically tractable way.

However, integrating EVs' SOC into the dynamic traffic model is challenging. The main difficulty is the complexity of the EV energy profiles. With WCLs, energy replenishment of an EV can also occur en-route alongside energy consumption. This obviously makes EV routing decisions more com-

plicated than that for a traditional setting with no DWC facilities (Chen et al., 2016). EV's energy replenishment on WCLs is commonly assumed proportional to the recharging time (Deflorio et al., 2015a), though a recent study assumed that the charging power can be SOC-dependent in DWC (Fernández et al., 2022). In fact, energy recharging typically becomes slower during the constant voltage phase in traditional cabled charging (Pelletier et al., 2016). However, the existence and the level of such nonlinearity in recharging seems under-investigated in the DWC setting, which is worth further research and may lead to new implications for traffic systems management. Meanwhile, the energy consumption of an EV is complicated to model, since it depends on various factors such as speed, acceleration, driving environment (e.g., road gradient), and type of vehicle Fontana (2013); Zhang et al. (2020); Fernández et al. (2022). Moreover, extensive research has demonstrated that EVs show different energy consumption characteristics in urban areas and on freeways (Wu et al., 2015; García-Vázquez et al., 2017) due to differences in the range of speed and acceleration profile. According to the context, different modeling choices and parameter settings should be used to derive meaningful results. Among these factors, speed and acceleration are the dominant factors for EV energy consumption and are highly dependent on the traffic states on the roads, yet most of the aforementioned macro-allocation models have simply assumed for model tractability that the energy consumption of an EV is proportional to the travel distance (see Table 2.3). This simplification significantly compromises accuracy, as it only approximates the dependence of energy consumption on vehicle speed but ignores vehicle acceleration. In the real-time management context, the complexity of EV energy profiles should be well captured.

Besides, since the key in SOC prediction is modeling the dependence of EVs' energy consumption on the dynamic traffic state (Tan et al., 2022),

scrutinizing the interplay between SOC, traffic state, and driving behaviors is necessary for real-time traffic modeling and control. In particular, the dynamic modeling of SOC must account for the spatial variation of traffic states, as an EV's real-time SOC depends on its initial SOC and the energy replenished and consumed along its trajectory. This calls for tracking of the vehicle's location, which is something traditional macroscopic traffic flow models (e.g., the CTM) are incapable of as they are routinely designed to predict only the evolution of traffic flow parameters. To this end, there is a notable need to study how to integrate EVs' location dynamics and their SOC into the traffic flow model.

In summary, real-time traffic management issues of WCLs are still in the nascent stages. The dynamic traffic models for DWC scenarios need to be established, the main difficulty of which is the integration of SOC of EVs. In addition, algorithms specifically designed for these real-time management challenges have not been explored sufficiently. Consequently, there remains a significant gap in deriving actionable insights for effective traffic management on WCLs.

Therefore, in the three studies presented in this thesis, we address these gaps by incorporating EVs' SOC into the traffic models in a contextually appropriate manner and by selecting suitable control methods. In Studies 1 and 2, we explore a ramp metering control and a variable speed limit control, respectively, on highways fully covered by WCLs. We model the traffic flow dynamics using the CTM and integrate EVs' SOC into the model through a mesoscopic approach. A model-based control method, MPC, is employed in both studies, thus contributing to the research gap in real-time traffic management on WCLs. Realizing the limitations of a fully covered WCL design in simultaneously optimizing TE and CE, in study 3, we focus on a multi-lane traffic system with WCLs, where the WCL is

deployed on a single lane. Here, we investigate a dynamic pricing problem within this system. Given EV and lane heterogeneity, we adopt an ABM to simulate the traffic flow dynamics. Consequently, a model-free method, DRL, is utilized to derive the optimal pricing strategy. This study addresses the gap in real-time traffic management within multi-lane systems.

Chapter 3

Research Methodology

This section outlines the research methodologies utilized in this thesis, focusing on the chosen models and algorithms and their justification. Table 3.1 provides a summary of the fundamental methods employed across three distinct studies, detailing aspects such as real-time traffic management strategy, WCL context, the scale of traffic models, control methods, and programming languages. The methodologies selected are tailored to best address specific problems, reflecting a problem-driven approach in our research.

Table 3.1: Comparison between the methodologies used in the three studies

Studies	1	2	3
Real-time traffic management strategy	Ramp metering control	Variable speed limit control	Dynamic pricing
Context of WCLs	The WCL is fully covered on the road	The WCL is fully covered on the road	The WCL is deployed on one lane of a multi-lane system
Scale of the traffic model	Macroscopic traffic flow model (CTM)	Macroscopic traffic flow model (CTM)	Microscopic (simplified car-following model)
Control method	Model-based method (Hybrid MPC)	Model-based method (Hybrid MPC), together with the LKNMS algorithm proposed for reducing the scale of the MILP	Model-free method (deep q-learning). Traditional machine learning techniques such as decision tree algorithms are also used for comparison
Control objectives	TE & CE	TE & CE	TE & CE
Decision variables	Metering rates of the on-ramps	Speed limits of each road segment	Charging price
Main constraints	Maximum metering rates, Maximum rate of change of metering rates, Maximum traffic density	Maximum speed limits, Maximum rate of change of speed limits, Maximum speed limit difference between adjacent segments, Maximum traffic density	Pre-defined discrete charging price
Programming language	Matlab	Matlab	Python/NetLogo

3.1 Models and Algorithms for Studies 1 and 2

In studies 1 and 2, we consider a ramp metering control and a variable speed limit control problem, respectively. These two control problems are among the most common real-time traffic control strategies on highways. We utilize a macroscopic traffic flow model, specifically the CTM, to establish the traffic dynamics. This model has been typically used in these control problems in the literature for several reasons:

1. **Scope of Analysis**: Macroscopic traffic flow models such as the CTM describe the aggregate behavior of traffic by simplifying the complex interactions of numerous vehicles into manageable flow dynamics. They have been used extensively in highway traffic management (Daganzo, 1995). The characteristic of these models makes them particularly advantageous for strategies like ramp metering and variable speed limit control, which aim to regulate overall traffic flow rather than focusing on individual vehicles. This broader perspective is essential for an effective implementation of these control measures, enhancing their impact on traffic congestion and safety.

2. **Efficiency and Simplicity**: The CTM, known for its computational efficiency and simplicity, offers a practical approach to simulating traffic flows across large networks. This model translates the complex behaviors of individual vehicles into cumulative flow and density, greatly simplifying the analysis and implementation of traffic management strategies. The widespread use of CTM in traffic management underscores its reliability and effectiveness in various traffic scenarios (Lighthill and Whitham, 1955).

3. **Integration with Control Systems**: The integration of macroscopic models like the CTM with control systems allows for effective real-time management of traffic conditions. These models provide a robust framework for implementing dynamic strategies such as ramp metering and variable speed limits, crucial for responding to real-time traffic demands and conditions.

Based on the adoption of CTM, we have implemented a model-based control strategy, namely MPC. MPC has been widely used in traffic control tasks due to its ability to handle multiple inputs and outputs simultaneously and to explicitly manage system constraints (Bellemans et al., 2006; Maggi et al., 2015; Koehler et al., 2016; Schmitt et al., 2017; Qiu and Du, 2023). It has been shown to perform better than some traditional traffic control methods such as proportional integral derivative (PID) controllers (Rawlings et al., 2017). In studies 1 and 2, we adopt a hybrid MPC approach. Hybrid MPC is tailored to the hybrid systems characterized by both continuous dynamics and discrete events. The CTM, due to the PWA relationship between the flow and density, can be reformulated into a PWA system. Using a hybrid MPC approach, the control problem at each time stage can be cast as a MILP problem, which can be solved by well-established solvers. The overall modelling framework of studies 1 and 2 are shown in Fig. 3.1. The framework integrates exogenous inputs and real-time system states into a hybrid MPC controller, which uses a predictive model to optimize control sequences. These sequences are determined by solving an MILP problem, taking into account control objectives and constraints. The optimized control inputs are then applied to the highway system, ensuring efficient traffic management.

However, as the scale of MILP grows, it might become mathematically intractable. Hence, in study 2, we propose an algorithm, *learning from*

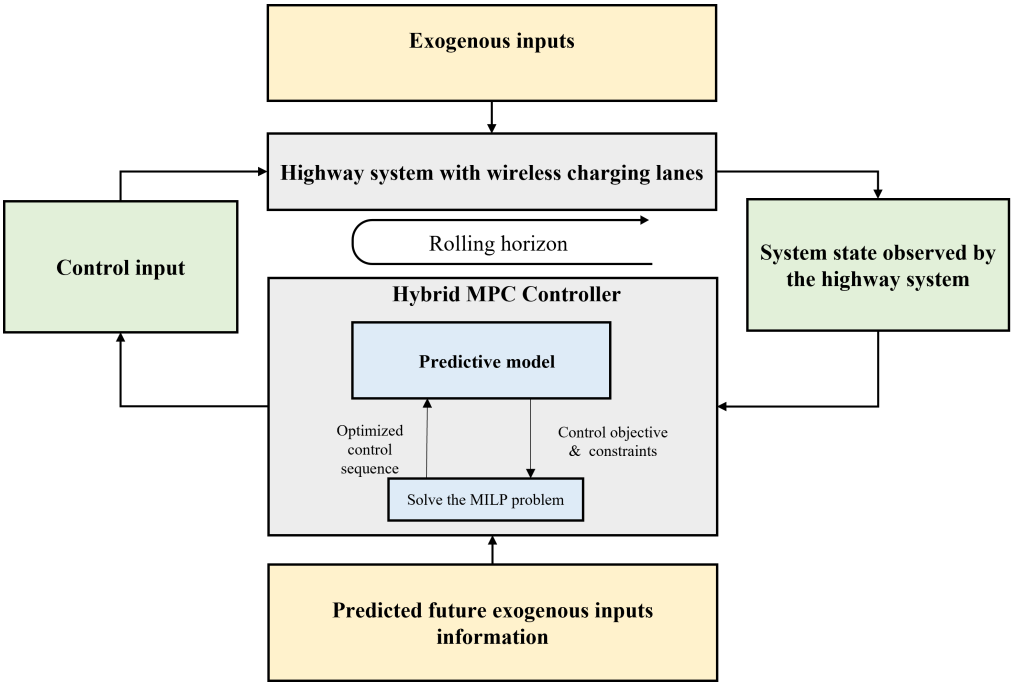

Figure 3.1: Modelling framework for studies 1 and 2

K-nearest neighbors mode sequences (LKNMS), to scale down the MILP generated by hybrid MPC. The algorithm is motivated by the observation that the set of states in a high-dimensional PWA system (each state corresponding to an integer variable if the PWA system is well-posed) that can be reached from a given initial state is constrained. This observation implies that, by predicting the reachable states before solving a given MILP problem, it is feasible to eliminate the inactive integer variables and their associated logical constraints. The prediction of the reachable states of a given initial state can be driven by the historical solution data or the generated data (data sampled in a high-dimensional PWA system). In the *LKNMS* algorithm, the reachable states of a given initial state $\boldsymbol{x}_0$ are predicted using the solution information (configuration of binary variables) its K-nearest neighbors. Details are elaborated in Sec. 5.4.3. Then by eliminating the inactive integer variables (corresponding to the unreachable states), the scale of the MILP can be greatly reduced. The reduced MILP will generate an optimal or a sub-optimal solution of the original MILP. This algorithm leverages the historical solution information and the

structure of the MILP and is designed to be simple-yet-effective and easy to implement.

3.2 Models and Algorithms for Study 3

Different from the WCL context assumed in studies 1 and 2, where the WCL is fully covered on the road, in study 3 we consider a dual-lane system comprising one GPL and one WCL. Each EV behaves as an autonomous agent with distinct attributes. Due to the heterogeneity of the road system and EVs, adopting a macroscopic traffic flow model (which assumes homogenization of traffic flow) is not suitable; instead, a microscopic model is necessary.

Given the model assumptions for the considered traffic context, we adopt an ABM to simulate the traffic dynamics. ABM provides a flexible platform for modeling the diverse behaviors of individual drivers and their interactions, which significantly influence overall traffic flow and system performance. This microscopic approach is particularly effective in environments where individual vehicle behaviors and interactions directly impact the system's dynamics, such as in mixed traffic lanes where charging and non-charging vehicles coexist.

However, ABM does not fit the typical model-based method used in traffic management for several reasons:

- ABMs focus on individual behaviors and detailed interactions, which do not readily aggregate into the simplified, higher-level variables required for model-based control strategies such as MPC, which often rely on aggregate measures of flow and density rather than detailed agent states.
- The computational complexity of ABMs, which increases significantly

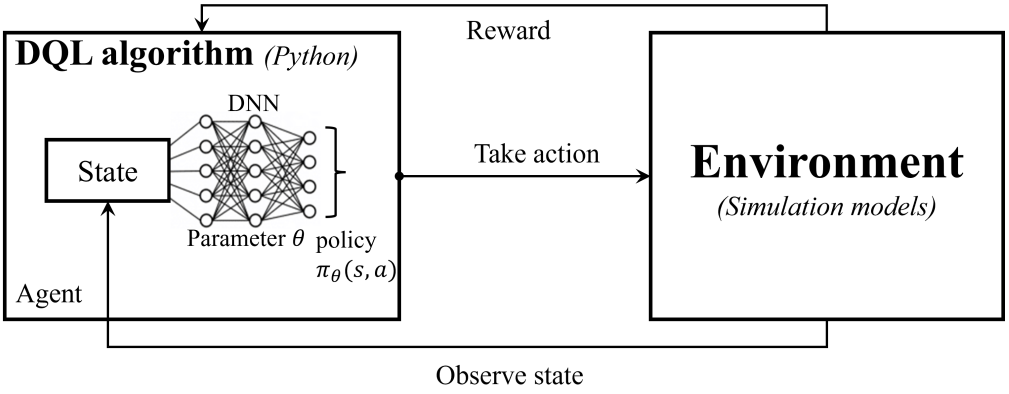

Figure 3.2: Modelling framework for study 3

with the number of agents and the complexity of their interactions, along with the extended run times and data requirements, makes real-time optimization and control particularly challenging. Integrating ABM with control systems that require quick, repeated computations for real-time decision-making is problematic, as it hinders the ability to make swift, effective decisions.

In this study, we adopt a model-free method for the dynamic pricing problem. We utilize a typical Deep Reinforcement Learning (DRL) approach, deep q-learning, which is selected as the most suitable method for our ABM where the state space is continuous and the action space is discretized. Meanwhile, a traditional machine learning technique, the CART, is adopted for comparison with the deep q-learning method in the performance of dynamic pricing strategies. The use of DRL allows for the optimization of pricing strategies based on the complex, dynamic interactions captured by the ABM, providing a robust framework for adaptive, real-time traffic and charging management in a heterogeneous traffic environment. The overall modelling framework of study 3 and 2 are shown in Fig. 3.2. The detailed modelling framework is given in Sec. 6.5.

To sum up, the methodology adopted in this thesis is driven by the specifics of the problems. The models and algorithms employed across different

studies are chosen based on specific traffic problems and model assumptions to address distinct aspects of real-time traffic management in the DWC context. This principle ensures that our strategies are both effective and appropriately aligned with the underlying challenges of managing traffic flow.

Chapter 4

Ramp metering control on wireless charging lanes considering optimal traffic and charging efficiencies[1]

4.1 Introduction

In recent years, the popularity of electric vehicles (EVs) has grown exponentially worldwide due to their potential to conserve energy and reduce emissions (Jang, 2018; He et al., 2020). For instance, global sales of EVs have surged to over 10 million in 2022, which is three times the figure recorded in 2020 (McKerracher, 2023). However, to realize their full potential, EVs need to overcome some challenges, including limited driving range, long charging times, and inadequate charging infrastructure. To address these issues, in addition to ongoing advancements in battery tech-

[1]This chapter has been published in the journal *IEEE Transactions on Intelligent Transportation Systems* (Liu et al., 2024).

nology, more advanced charging methods have emerged, such as battery swapping and wireless charging. Of these alternatives, dynamic wireless charging (DWC), whose common enabling mechanism is inductive power transfer charging (Ahmad et al., 2017), shows particular promise because of its superior convenience. In the context of DWC, charging infrastructures are installed beneath the road surface to facilitate DWC, allowing EVs to receive energy while driving without requiring a physical connection. These specialized roads are referred to as WCLs. Such advanced technology liberates EVs from stationary charging stations, and can thereby greatly extend their driving range (Mohamed et al., 2019; Chopra and Bauer, 2011b). Thus, the EV market is expected to experience further expansion and advancement with the large-scale adoption of dynamic wireless charging technology.

Since the 1970s, DWC technology has undergone extensive development and testing by numerous research institutions and EV manufacturers worldwide. Some pioneers include the University of California, Berkeley (Chen et al., 2015b; Suh and Cho, 2017), the Korea Advanced Institute of Science and Technology (Kim et al., 2013b; Foote and Onar, 2017; Suh and Cho, 2017), and Bombardier Transportation (Cirimele et al., 2018). Recent pilot projects have been launched, such as a 1.65 km WCL system in Michigan, USA, built by the Israeli company ElectReon in 2022 Fletcher (2023), and a 21 km WCL system in southern Sweden, built by the Swedish Transport Administration Lewis (2023) in 2023. Moreover, DWC EVs have also attracted considerable attention from the research community. A comprehensive review of transportation management issues related to DWC EVs is presented in Chapter 2, where four research directions are summarized: 1) The development and features of DWC technology; 2) Optimal allocation of WCLs; 3) EV energy consumption analysis in a WCL context; 4) Billing and pricing for EVs on WCLs. The study also outlines impending

research needs and prospects. In particular, they highlight a significant research gap in real-time control considering DWC EVs. This unaddressed research gap motivated the present study. However, we have encountered two major challenges in addressing this gap.

The first challenge is the lack of a predictive model, specifically concerning the state-of-charge (SOC) of EVs. Real-time traffic control is typically based on macroscopic traffic flow models that describe the aggregate behavior of traffic such as density, speed, and flow. In traditional traffic scenarios, the primary goal is to improve traffic efficiency (TE) which can be expressed as a function of density and flow. In the DWC scenario, charging efficiency (CE) should also be considered for the sake of economic effectiveness (Li et al., 2019; Panchal et al., 2018). Hence, EVs' SOC should be incorporated into the predictive model. However, SOC generally refers to a property of a single EV, rather than an aggregate behavior of EVs. It thereby raises a question: "How can EVs' SOC be incorporated into the macroscopic traffic flow (e.g., the cell transmission model, which has been extended in many ways to meet the requirements of various scenarios)?". A feasible modelling method is given in (Tan et al., 2022). First, they pointed out that the key to modelling EVs' SOC is to formulate its dependence on dynamic traffic state (density and speed). Next, they proposed a high-level discrete-time dynamic system model, in which the EVs are grouped according to their entry time. In this way, EVs' SOC is incorporated into the model by a mesoscopic approach, which is described as a function of traffic flow parameters. However, specific model formulations have not been established for an application.

Another challenge is designing a flexible control model. The main difficulty lies in the inherent conflict between TE, i.e., the throughput of the road, and CE, i.e., the total net energy replenishment of EVs. Traditional traffic

control, for example, ramp metering control, aims at reducing overall traffic congestion by regulating the volume of on-ramp flows. However, in the DWC scenario, a lower traffic speed favored by traffic congestion results in a higher energy replenishment of EVs (per unit distance) but a lower energy consumption (per unit distance). In other words, tolerating a certain level of traffic congestion can increase EVs' SOC level, which contributes to CE. Therefore, when both TE and CE are considered (e.g., to charge EVs as much as possible within a specified traffic delay range), the control model requires a meticulous design. Given the inherent conflict between TE and CE, representing both in the objective function through linear weighting may not yield an optimal solution. A more effective approach is treating one as the primary control objective and the other as a constraint. In this regard, a model-based control approach is handy, as one can explicitly handle the constraints involved.

To address these challenges, we explore a ramp metering control problem in the DWC scenario, as a pioneer study in exploring real-time traffic control problems on WCLs. First, we describe the traffic flow dynamics using the cell transmission model (CTM) and incorporate the SOC dynamics into it in a mathematically tractable way. We then formulate the model as a Piecewise Affine (PWA) system, similar to the approach presented in (Thai and Bayen, 2014). By employing a hybrid model predictive control (MPC) approach, the control problem at each time stage is transformed into a Mixed-Integer Linear Programming (MILP) problem that can be conveniently solved using well-established solvers. The state-feedback control law can also be extracted offline using an explicit MPC approach, significantly reducing the online computational cost (Tan and Gao, 2018). This framework of combining hybrid MPC with CTM has been proven effective in traffic control tasks such as ramp metering (Koehler et al., 2016) and dynamic pricing for high-occupancy toll lanes (Tan and Gao, 2018). More-

over, we adopt a closed-loop MPC, which can dynamically adjust its control actions based on real-time feedback. This control strategy inherently accommodates modeling inaccuracies and external disturbances, effectively mitigating the impacts of such deviations from the anticipated model behaviors. The primary contributions of this study are outlined below:

- We address the real-time traffic control problem within the context of WCLs. To our knowledge, we are pioneers in exploring the real-time traffic control challenges posed by WCLs.
- We innovatively incorporate the SOC dynamics of EVs into the CTM in a mesoscopic method in which the functional relationship between macroscopic traffic flow parameters and EVs' SOC is established. Then we develop a ramp metering control model considering both TE and CE.
- Our theoretical analyses and simulation results reveal the inherent conflict between TE and CE, yielding insights for real-time traffic management and operations on WCLs.

The rest of the chapter is organized as follows: Section 4.4 states the problem considered in this study. Section 4.5 presents the formulations of the predictive model. Section 4.6 describes the formulations of the control model for the ramp metering control problem. Section 4.7 conducts the numerical experiments. Section 4.8 presents simulation results and discussions. Section 4.10 provides the conclusion of this chapter and points out its limitations and future research directions.

4.2 Related work

As outlined in Sec. 4.1, the dynamic traffic models specifically designed for DWC scenarios remain unexplored. Therefore, this section primarily

explores studies that implement MPC, particularly hybrid MPC, to address ramp metering problems.

Bellemans et al. (2006) evaluates the efficacy of MPC against ALINEA in the context of motorway ramp metering. They model the traffic dynamics by the fundamental diagram. Their MPC framework seeks to minimize the total time spent, incorporating a penalty term for fluctuations in control inputs. Through simulations of a typical morning rush hour, the study demonstrates that the MPC controllers not only surpass the performance of ALINEA-based controllers but also offer enhanced stability.

Maggi et al. (2015) aims to reduce congestion in freeway systems via ramp metering, comparing different MPC-based traffic controllers. The study utilizes both a standard CTM and a modified version that incorporates the capacity drop phenomenon. These models help simulate the dynamic behaviors of freeway systems. The optimization challenges are addressed through different Finite Horizon Optimal Control Problems, focusing on minimizing congested states. The problems are formulated as a MILP to ensure efficient computational performance. Results demonstrate that while the modified CTM used in some MPC schemes did increase computational times, it did not always translate into clear advantages in controlling congestion, which suggests further research using microsimulators might be needed to evaluate these models effectively.

Koehler et al. (2016) presents a robust Hybrid MPC approach for ramp metering, where the authors formulate the CTM into a PWA system, subsequently managed via hybrid MPC. Their optimal control problem aims to minimize deviations from equilibrium states within the system, structuring the optimization problem as a Mixed Integer Quadratic Problem (MIQP). The efficacy of their controllers is assessed using two key metrics: total travel time and total travel distance, both derived from macroscopic traffic

flow parameters.

Schmitt et al. (2017) delves into the ramp metering problem on a freeway stretch modeled by the CTM, proposing MPC for optimal control over a finite horizon with the goal of minimizing the Total Time Spent. While MPC is theoretically apt, empirical evidence from practical freeway applications suggests that it may not consistently outperform simpler, distributed feedback policies. They address the absence of theoretical backing for these empirical observations by comparing distributed, non-predictive policies against the theoretically optimal solution under ideal conditions of perfect model knowledge and monotonic traffic dynamics. It introduces a novel, distributed, non-predictive policy, establishing sufficient optimality conditions for minimizing the Total Time Spent and confirming through a case study with real-world traffic data that these conditions are seldom breached. Furthermore, simulations under non-ideal conditions—highlighting model mismatches—suggest that the widely used ALINEA policy closely approximates the ideal control in both control behavior and performance.

Similar to Bellemans et al. (2006) and Koehler et al. (2016), Tan and Gao (2018) also employs the CTM together with hybrid MPC. The authors introduce a hybrid MPC-based dynamic tolling strategy for managing high-occupancy toll (HOT) lanes with multiple access points. This model proactively plans and coordinates toll rates for different origin-destination (OD) pairs, ensuring adaptive lane utilization based on real-time demand and boundary conditions. The optimal tolling rates are determined via a one-to-one mapping from optimal toll entry flows, with the overall hybrid MPC problem being formulated as a MILP problem, which is solved in an online fashion. It can be also solved in an offline fashion by explicit MPC by which an explicit control law is extracted by multi-parametric program-

ming techniques. Their optimal control problem aims to minimize the total person travel time and the effort involved. Validation through a numerical experiment on a representative freeway segment demonstrates the model's capability to dynamically adjust tolls in response to changing demands and boundary conditions, driving the system towards a new equilibrium that minimizes total person delay.

Qiu and Du (2023) develops a synchronization control strategy for two Connected and Autonomous Vehicles (CAVs) initially separated by other vehicles, aiming for them to smoothly approach each other and maintain a stable car-following mode without compromising traffic safety and efficiency. The study introduces a hybrid model combining micro- and macro-traffic flow dynamics, employing MPC embedded with a mixed-integer nonlinear programming (MINLP) problem. This model integrates established car-following models for microscopic vehicle movements and the CTM for macroscopic traffic dynamics. The MINLP targets multi-objective optimization, balancing synchronization and traffic efficiencies. The complex problem structure necessitates an adaptive control strategy, accounting for different traffic scenarios and CAV penetrations. Their numerical experiments indicated that the synchronization control performance improved significantly with higher CAV penetration, with the time required for synchronization decreasing as CAV penetration increased. For example, synchronization time was reduced by 27% when CAV penetration increased from 20% to 40%, with further reductions as penetration increased to 60%. However, the effect was diminishing beyond certain levels.

In summary, these papers underscore the increasingly prevalent application of the CTM in conjunction with hybrid MPC real-time traffic management. The integration of CTM with Hybrid MPC has demonstrated significant efficacy, showcasing its ability to enhance the precision and efficiency of

traffic control strategies. These methodologies not only cater to complex traffic dynamics by accurately modeling and predicting traffic flows but also facilitate the efficient implementation of control actions in various real-time traffic scenarios. This mainstream approach has proven to be effective in optimizing traffic flow, reducing congestion, and improving overall traffic system performance. In this study, we adopt this CTM and hybrid MPC framework. We innovate by incorporating EVs' SOC (a microscopic property) into the CTM (a macroscopic traffic flow model) through a mesoscopic approach. We then formulate the model into a well-posed PWA system, preparing it for integration with hybrid MPC.

4.3 Methodology

4.3.1 MPC

This section offers a comprehensive introduction to MPC. Initially developed in the late 1970s, MPC has evolved from simple applications to a robust, advanced model-based control strategy that leverages explicit dynamic models of the process to forecast future states and make optimal control decisions (Qin and Badgwell, 2003). Unlike traditional control strategies such as Proportional-Integral-Derivative (PID) and Linear Quadratic Regulator (LQR), MPC is distinguished by its ability to handle multiple inputs and outputs simultaneously and to manage system constraints explicitly. This capability makes MPC particularly suitable for complex industrial scenarios where the demand for precision and optimality is high (Camacho and Bordons, 2004).

MPC's adoption has been driven by its superiority in dealing with constraints and multi-variable control problems, which are common in indus-

tries like chemicals, petrochemicals, and refining (Qin and Badgwell, 2003). Furthermore, its foundation on the receding horizon principle — which involves constantly updating predictions and optimizations as new data becomes available — provides a dynamic framework that significantly enhances the adaptability and performance of control systems in comparison to static frameworks used by PID and LQR (Rawlings et al., 2017). These unique features have propelled MPC to the forefront of control technology, offering substantial improvements in efficiency and safety over conventional control techniques. The next sections delve into the critical components of MPC, namely the predictive and control models, illustrating their roles and interrelations within the broader framework of MPC.

The predictive model is an essential ingredient in MPC, which forecasts the system's future outputs based on current and past inputs and states. These models can be linear or nonlinear and are crucial for the accuracy and effectiveness of the MPC. Its mathematical formulation can be expressed as:

$$\boldsymbol{x}(t+1) = \boldsymbol{A}\boldsymbol{x}(t) + \boldsymbol{B}\boldsymbol{u}(t) + \boldsymbol{w}(t) \tag{4.1}$$

Here, $\boldsymbol{x}(t)$ and $\boldsymbol{u}(t)$ are the state vector and control input at time t, respectively. $\boldsymbol{A}$ and $\boldsymbol{B}$ are coefficient matrices, and $\boldsymbol{w}(t)$ represents noise.

The control model in MPC, which determines the control actions, may differ from the prediction model. While the prediction model forecasts future states, the control model is used to calculate the control inputs that will guide the system toward its target states. These models can be identical but are often tailored separately to optimize performance and computational efficiency. The control horizon in MPC, denoted as N, determines the number of future steps over which predictions are made and optimizations are performed. The choice of N affects both the performance and computational load of the control system. The length of the control hori-

zon influences the foresight of the control actions. A longer horizon can anticipate future events better but requires more computational resources (Lee and Cooley, 1997). At each time step, MPC solves an optimization problem to determine the optimal control actions that minimize a cost function based on predicted future states and inputs. The optimization problem can be expressed generally as:

$$\min_{\{\boldsymbol{u}(t|t)\}_t^{t+N-1}} \quad J = \sum_{t}^{t+N-1} G(\boldsymbol{x}(t|t), \boldsymbol{u}(t|t)) \tag{4.2}$$

$$\text{s.t.} \quad \boldsymbol{x}(t+1|t) = f(\boldsymbol{x}(t|t), \boldsymbol{u}(t|t)), \quad \text{for } t \text{ to } t+N-1, \tag{4.3}$$

$$\boldsymbol{x}(t|t) \text{ is given}, \tag{4.4}$$

$$\boldsymbol{u}_{\min} \leq \boldsymbol{u}(t|t) \leq \boldsymbol{u}_{\max}, \quad \text{for } t \text{ to } t+N-1, \tag{4.5}$$

$$\text{additional state and input constraints.} \tag{4.6}$$

Here, J represents the cumulative cost over the control horizon N, which evaluates the control objectives, such as minimizing the energy use or deviation from a set point. The function $G(\boldsymbol{x}, \boldsymbol{u})$ is the stage cost at each timestep, indicating the immediate cost associated with the state $\boldsymbol{x}$ and control input $\boldsymbol{u}$.

The notation $\boldsymbol{x}(t+1|t)$ represents the predicted state at time $t+1$, given the system state and control input up to time t (Mayne et al., 2000). The variable $\{\boldsymbol{u}(t|t)\}_t^{t+N-1}$ represents the sequence of future control inputs from time t to $t+N-1$, which are the decision variables in the optimization problem.

MPC uses the receding horizon principle, where the optimization is performed over a moving time window, and only the first control input $\boldsymbol{u}(t|t)$ is implemented. This process is repeated at each sampling instant, with the horizon shifting forward, ensuring that control actions are continually updated based on the latest available measurements. While MPC funda-

mentally computes the control actions in an open-loop setting, namely, by predicting future states and planning a control sequence over the prediction horizon, it operates in practice with a closed-loop mechanism due to its execution strategy. Each control action, although computed based on predictions and without intervening feedback, is only temporarily valid. The 'open-loop' nature is confined to the computation of the control sequence, not its execution. Once the first control input $\boldsymbol{u}(t|t)$ is applied, MPC obtains the new system state from the latest measurements. This feedback turns the strategy into a closed-loop control, where the controller's decisions are continually adjusted based on actual system responses rather than solely on predicted behavior. In essence, the process iteratively refines the control inputs, adapting to any disturbances, model inaccuracies, or unexpected system changes. This dynamic adjustment is crucial for dealing with real-world complexities and uncertainties, providing a robust control mechanism that can effectively respond to a changing environment.

4.3.2 Hybrid MPC

This section gives a comprehensive introduction to hybrid MPC. Hybrid MPC extends the principles of standard MPC to hybrid systems. A hybrid system is a type of system that includes both continuous variables and discrete events. Hybrid MPC has been effectively applied in automotive control systems (Falcone et al., 2007; Di Cairano et al., 2012), robotic systems (Wei et al., 2013; Kong et al., 2023), and traffic management (Frejo et al., 2014; Tan and Gao, 2018; Zhang et al., 2022). Common hybrid systems are the Mixed Logical Dynamical (MLD) systems and PWA systems (Bemporad and Morari, 1999; Borrelli et al., 2017):

- **Mixed Logical Dynamical (MLD) Systems:** MLD systems are de-

scribed by a combination of linear dynamic equations, logical conditions, and inequalities that represent both the system's dynamics and the control logic. MLD systems allow for the modeling of interactions between continuous variables and binary decisions, which is essential for applications involving complex switching processes and mode-dependent behaviors. MLD systems are commonly employed in the areas such as power systems, robotics, etc.

- **Piecewise Affine (PWA) Systems:** PWA systems are characterized by partitioning the state space into regions within which the system dynamics are described by different affine functions. This model is particularly useful for systems where the behavior changes distinctly across different operating regimes or conditions. Besides, a PWA system has significant flexibility in approximating nonlinear dynamics. A PWA system can approximate any nonlinear system to any desired degree of accuracy, provided a sufficient number of partitions in the state space are allowed. However, the challenge with PWA systems lies in the complexity that increases with the number of partitions: more partitions require more complex control logic and computational resources, potentially making the real-time implementation more demanding. Therefore, while PWA systems offer a powerful tool for approximating nonlinear systems, their practical application must balance approximation accuracy with computational feasibility.

The fundamental connection between MLD and PWA systems lies in their ability to model hybrid dynamics, although they do so in structurally different ways. MLD systems provide a comprehensive framework that directly integrates logical rules into dynamic models, making them ideal for control applications that involve explicit mode switching and decision-making. In contrast, PWA systems focus more on the piecewise linear representation

of the dynamics, suitable for scenarios where the system's behavior can be distinctly segmented into linear regimes. In this chapter, we formulate the predictive model of hybrid MPC into a PWA system in a mathematically convenient way (see Sec. 4.5.4). The modeling framework is depicted in Fig. 4.1 in which the highway system with WCLs refers to the real-world traffic system.

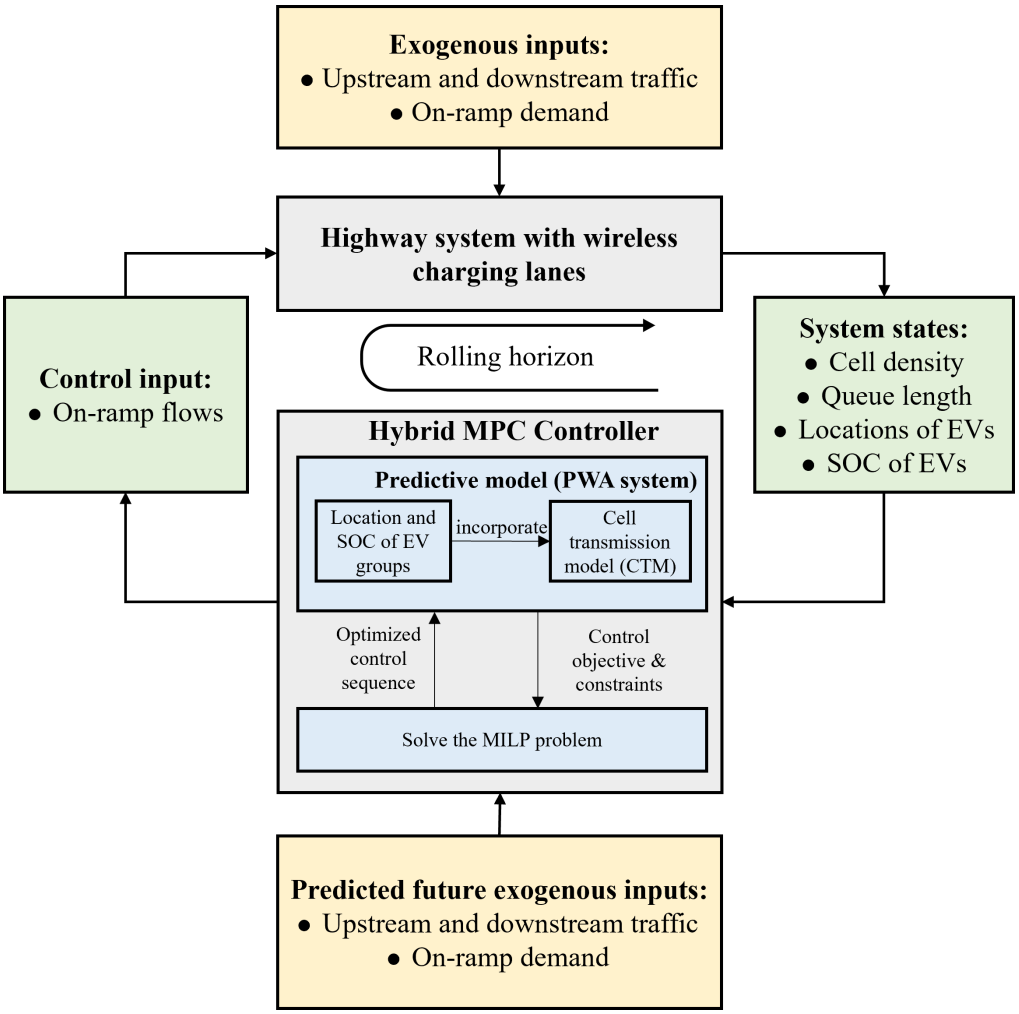

Figure 4.1: Modelling framework

The Hybrid MPC problem can be expressed as:

$$\min_{\{\boldsymbol{u}(t|t),\boldsymbol{d}(t|t)\}_t^{t+N-1}} \quad J = \sum_{t}^{t+N-1} G(\boldsymbol{x}(t|t), \boldsymbol{u}(t|t), \boldsymbol{d}(t|t)) \tag{4.7}$$

$$\text{s.t.} \quad \boldsymbol{x}(t+1|t) = f(\boldsymbol{x}(t|t), \boldsymbol{u}(t|t), \boldsymbol{d}(t|t)), \tag{4.8}$$

$$\boldsymbol{u}(t|t) \in U, \quad \boldsymbol{d}(t|t) \in \{0,1\}^m, \tag{4.9}$$

$$\text{additional constraints on } \boldsymbol{x}(t|t), \boldsymbol{u}(t|t), \text{ and } \boldsymbol{d}(t|t). \tag{4.10}$$

where $\boldsymbol{x}(t|t)$ represents the state vector of the system at time t, conditioned on all available information up to time t. The vector $\boldsymbol{u}(t|t)$ denotes the continuous control inputs applied at time t, and $\boldsymbol{d}(t|t)$ represents the discrete control decisions, typically binary or integer values reflecting operational modes or on/off control actions. J is the objective function representing the cumulative cost over the control horizon N, which evaluates control objectives such as minimizing total travel time or maximizing the total energy. The stage cost function G quantifies the immediate cost associated with the state and control inputs at each time step, while f describes the system dynamics, mapping the current state and inputs to the next state.

Hybrid MPC integrates the flexibility of handling both discrete and continuous dynamics, optimizing complex decision-making processes involving continuous control and discrete mode selections. However, the computational complexity and the need for detailed, accurate modeling of interactions between different system components remain significant challenges. Following the intricate demands of Hybrid MPC, Explicit MPC offers a promising alternative by pre-calculating and simplifying the control actions needed for different scenarios. Explicit MPC is based on the principle of solving the MPC problem offline to generate explicit solutions, usually in the form of PWA functions that map the current state directly to the control inputs.

Explicit MPC works by computing the optimal control laws offline using parametric optimization. This approach partitions the state space into regions, within each of which the control law can be expressed as a simple affine function of the state. During real-time operation, the system identifies which region the current state belongs to and applies the corresponding pre-computed control law, significantly reducing the computational load during execution (Alessio and Bemporad, 2009). This method transforms the typically computationally intensive online optimization process of MPC into a simple lookup and evaluation procedure, offering considerable computational savings, especially for systems with limited processing capabilities or those requiring very fast response times.

Despite its advantages in reducing computational demands, explicit MPC has limitations. The first is its scalability. As the number of states or the complexity of the system increases, the number of regions in the state space can grow exponentially, making the offline computation and storage of the control laws infeasible. The second is its ability to resist external interference. Explicit MPC may struggle to effectively respond to unforeseen external disturbances. Since the control actions are derived from predetermined mappings without real-time optimization, the system's ability to react dynamically to unexpected changes or disturbances is limited. In scenarios where external disturbances are significant and frequent, this can lead to sub-optimal performance or the need for frequent recalculations of the control laws. Therefore, explicit MPC is generally best suited for simpler scenarios where system conditions and external disturbances are predictable and well-defined (Bemporad et al., 2002).

4.3.3 Solution method

We employ the Gurobi Optimizer, a state-of-the-art solver for MILP problems, to solve the optimization problem formulated in the hybrid MPC framework. Gurobi is renowned for its efficiency and robustness in handling large-scale MILP problems, which is crucial given the complexity of hybrid systems where both continuous and discrete decision variables are present (Gurobi Optimization, LLC, 2024).

The hybrid MPC problem is formulated into a series of MILP problems. These problems typically involve minimizing a linear or PWA objective function subject to linear constraints, where some of the decision variables are binary or integer-valued, reflecting the hybrid nature of the system (Bemporad and Morari, 1999).

Gurobi approaches the solution of MILP problems using a combination of advanced algorithms. It employs branch-and-bound techniques to explore the feasible region, efficiently navigating through potential solutions by systematically partitioning the problem space into smaller sub-problems (Land and Doig, 2010). At each node of the branch-and-bound tree, Gurobi solves a linear relaxation of the MILP, where integer constraints are temporarily relaxed, allowing the solver to handle continuous variables more easily. This relaxation provides a lower bound on the objective function value. If the solution of the relaxed problem yields integer values for the discrete variables, it represents a feasible solution for the original MILP. Otherwise, Gurobi uses cutting planes (Gomory, 1960) and heuristics (Lenstra and Rinnooy Kan, 1978) to refine the search, improving the bounds and guiding the branch-and-bound process toward an optimal solution.

The solver also incorporates pre-solve techniques to reduce problem size and complexity before the main branch-and-bound process begins. These

techniques involve simplifying constraints, removing redundant variables, and detecting infeasibilities early in the process, which can significantly accelerate the overall computation (Bixby, 2002).

Given the computational intensity of solving MILP problems, Gurobi's parallel processing capabilities are leveraged to enhance performance. By distributing the computational workload across multiple processors, Gurobi can explore different branches of the search tree simultaneously, thus reducing the overall solution time.

In summary, Gurobi employs a series of advanced algorithms to solve the MILP problems generated by the hybrid MPC framework. Its ability to efficiently handle the combination of continuous and discrete variables ensures that optimal control strategies can be efficiently calculated, even for complex real-time traffic management scenarios. Both the performance of the solution algorithms is given and discussed in Sec. 4.8.2.

4.4 Problem statement

This study addresses a ramp metering control problem in a DWC scenario, in which the WCLs are fully deployed on a highway system with on- and off-ramps and dedicated to servicing DWC EVs. All EVs are assumed to have similar specifications (type, battery, etc.) and aim to charge on the WCL and maintain maximum speed whenever possible. Facilitated by an advanced Intelligent Transportation System (ITS), we assume that real-time traffic information including mainstream and on-ramp traffic demands, downstream traffic conditions, and EV-related demand (e.g., initial SOC, minimum permissible SOC, target SOC, and target travel time) can be collected. Traffic operators decide whether to prioritize TE or CE based on the specific scenario requirements. The on-ramp flows are controlled

accordingly.

In the following, we discuss two key considerations of the real-time control on the WCL: 1) Energy consumption characteristic of EVs, and 2) Inherent conflict between TE and CE.

4.4.1 Energy consumption characteristic of EVs

The energy consumption of EVs depends on various factors including speed, acceleration profiles, the use of auxiliary systems that are affected by traffic conditions, driving behaviors, and weather conditions (De Cauwer et al., 2017; Zhang et al., 2020). Among these factors, speed profile stands as the predominant determinant. As a result, a speed-dependent energy consumption rate (defined as the energy consumption per unit time in this study) is commonly adopted in traffic problems related to DWC (Deflorio et al., 2015a; García-Vázquez et al., 2017; Fernández et al., 2022), which is more practical than the studies Chen et al. (2016); Fuller (2016); He et al. (2020) where the energy consumption rate is assumed simply to be proportional to the travel distance. However, the speed-dependent energy consumption rate does not explicitly account for the longitudinal dynamics of vehicles including traction, resistances, and braking (Hulagu and Celikoglu, 2021), expressed as acceleration and deceleration. To capture more accurate SOC dynamics, in this study, we incorporate the acceleration into the SOC dynamics, which is approximated by the average speed difference between adjacent time steps.

The consumption-to-speed curve for EVs is significantly different from that for fuel vehicles because of the fundamental difference in their propulsion systems (electric motors and internal combustion engines). The major difference lies in their optimal operating speeds for maximum energy effi-

ciency. In this chapter, we introduce the term "energy-efficient speed" to specifically refer to the optimal operating speeds that correspond to the lowest energy consumption per unit distance. The energy-efficient speed of a fuel vehicle is commonly above 80 km/h (U.S. Department of Energy, 2024), higher than that of an EV, which is commonly below 60 km/h. The study Galvin (2017) investigated the effects of speed on energy consumption in the laboratory. Eight commonly sold EVs, including the Nissan SV, Mitsubishi, and Chevrolet, were used as test subjects. The results indicated that energy-efficient speeds ranged from 50 to 60 km/h. When speeds exceeded this range, there was a significant increase in their energy consumption per kilometer.

4.4.2 Inherent conflict between TE and CE

As mentioned, the range of energy-efficient speeds of EVs (50 to 60 km/h) is notably lower than the free-flow speed on common highways. More importantly, a lower driving speed contributes to more charging time for EVs. However, a higher TE calls for fast movement of vehicles. Hence, an inherent conflict arises between TE and CE.

To intuitively illustrate the influence of speed on the EVs' SOC, a numerical example is provided. Suppose an EV moves on a 15-kW WCL at a steady speed and with a fixed charging power. The impacts of its speed on its energy consumption (per km) and energy replenishment (per km) are depicted in Fig. 4.2a where the speed ranges from 30 to 140 km/h. It can be seen that the energy consumption of EVs shows a significant increase when the speed exceeds 50 km/h while its energy replenishment continuously decreases. As a result, the net energy replenishment EVs decreases steadily as speed increases. When the speed exceeds approximately 90 km/h or so, the energy replenishment is insufficient to compensate for

the energy consumption, as shown in Fig. 4.2b. Hence, due to the specific physical properties of electric motors and the unique nature of DWC, an inherent conflict arises between TE and CE. To what extent do these two factors conflict? Is there a trade-off between them? We believe that these questions are worth exploring through simulations before the widespread application of DWC technology.

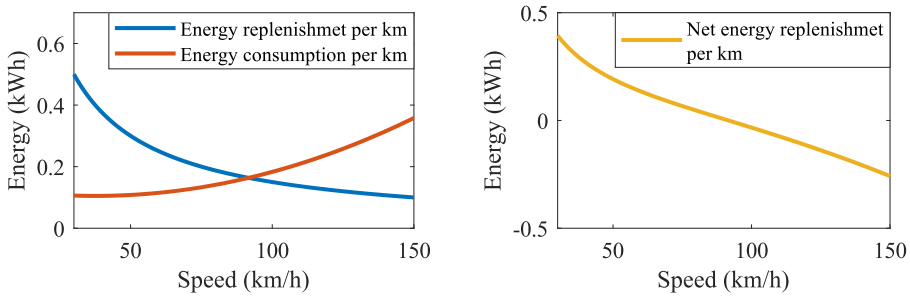

(a) (b)

Figure 4.2: The impact of speed on EVs' CE on WCLs.
Fig. 4.2a depicts the energy consumption rate against speed according to laboratory data used in Galvin (2017), and the energy replenishment rate against speed (inversely proportional to speed due to the constant charging power). Fig. 4.2b depicts the net energy replenishment rate against speed.

4.5 Predictive model

This section outlines the model formulations of the proposed predictive model. The model is formulated as a PWA system. Sec. 4.5.1 describes the dynamics of traffic flow including cell density, $\boldsymbol{n}$ and queue length, $\boldsymbol{e}$; Sec. 4.5.2 describes the dynamics of EVs' speed, $\boldsymbol{v}$, and energy consumption rate, $\boldsymbol{p}$. Sec. 4.5.3 describes the dynamics of EVs' location, $\boldsymbol{l}$, and EVs' SOC, $\boldsymbol{s}$. Sec. 4.5.4 defines the dynamics of the overall system. In the numerical experiments, we use the predictive model to simulate the real highway system, where the upstream/downstream traffic and on-ramp demand are assumed predictable by the advanced ITS. The model parameters and variables are summarized in Table. 4.1. Note that the unit for

all parameters and variables associated with the SOC is expressed as a percentage, offering numerical convenience for calculations.

Table 4.1: Parameters

Symbols	Definitions	Units
Parameters		
Δt	Length of time step	sec
N	Number of cells	/
N_s	Number of SOC levels	/
β_i	Split ratio of cell i	/
$v_{f,i}$	Free flow speed within cell i	cell/period
v_e	Energy-efficient speed	cell/period
L	Length of the road i	cell
w_i	Congestion wave speed =of cell i	cell
E_r	Normalized charging power per unit time	percent
Q_{max}	Energy consumption rate for v_f	percent
Q_{ene}	Energy consumption rate for v_e	percent
P_{aux}	Power of auxiliary systems	percent
T_{tot}	Total simulation time	period
Variables		
$q_{m,i}$	Flow capacity of cell i	veh/period
n_i	Density of cell i	veh/cell
n_j	Jam density of cell i	veh/cell
n_c	Critical density	veh/cell
n_e	Energy-efficient density	veh/cell
e_i	On-ramp queue	veh/cell
r_i	On-ramp flows of cell i	veh/cell
d_i	On-ramp demand of cell i	veh/cell
v_i	Real-time speed of EVs within cell i	cell/period
p_i	Energy consumption rate of cell i	percent
a_i	Acceleration of the traffic within cell i	cell/period^2
τ	Time traveled of EVs	period
τ_o^m	Maximal travel time	period
l_o^τ	Location of an EV with origin o	/
$l_{e,i}$	Location of the end of cell i	/
$s_{o,\omega}^\tau$	SOC of EVs	percent
$s_{o,\omega}^{tar}$	Target SOC	percent
s^{min}	Minimum permissible SOC of EVs	percent

4.5.1 Dynamics of traffic flow

We consider a freeway segment that is divided into N cells, as shown in Fig. 4.3. Each cell has the same length of normalized 1 while other parameters are cell-specific. Each cell has at most one on- and off-ramp. The time step is indexed by t and has length Δt. Based on the CTM (Daganzo, 1995), the flow from cell i to cell $i+1$ at time t, denoted as $q_i(t)$, equals the minimum of the three quantities (Daganzo, 1995): the number of vehicles that can be sent by cell i to $i+1$, $v_{f,i}n_i(t)$; the number of vehicles that can be received by cell $i+1$ from i, $w_{i+1}(n_{j,i} - n_{i+1}(t))$; and the flow capacity, $q_{M,i}$, namely, the maximum number of vehicles that can travel from cell i to $i+1$ at each time step. Then $q_i(t)$, for $i = 1, ..., N$ is expressed as:

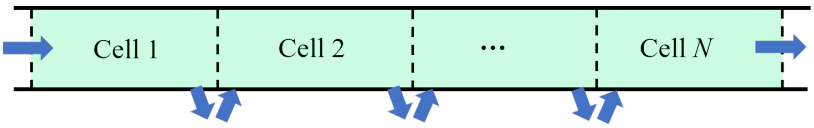

Figure 4.3: Freeway segment with ramps

$$q_i(t) = \min[v_{f,i}n_i(t), q_{M,i}, w_{i+1}(n_{j,i} - n_{i+1}(t))], \tag{4.11}$$

where n_i is the density cell i at time t; $n_{j,i}$ is the jam density of cell i; $v_{f,i}$,$w_i \in (0, 1]$ are the normalized free-flow speed and congestion wave speed of cell i, respectively. Considering the on-ramps, (4.11) is rewritten as Gomes and Horowitz (2006):

$$q_i(t) = \min[\beta_i v_{f,i}n_i(t), \beta_i q_{M,i}, w_{i+1}(n_{j,i} - n_{i+1}(t) - r_{i+1}(t))]. \tag{4.12}$$

where β_i is the split ratio of q_i that is defined as the ratio of the vehicles entering cell $i+1$ to the vehicles leaving cell i. r_i is the on-ramp flow of cell

i that can not exceed the following limits (Gomes and Horowitz, 2006):

$$r_i(t) \leq v_{f,i} n_i(t), \tag{4.13a}$$

$$r_i(t) \leq w_{i+1}(n_{j,i} - n_{i+1}(t) - r_{i+1}(t)), \tag{4.13b}$$

$$r_i(t) \leq r_i^{max}, \tag{4.13c}$$

$$r_i(t) \leq e_i(t) + d_i(t). \tag{4.13d}$$

(4.13a) and (4.13b) indicate that the on-ramp flows can not exceed the flows between cells for the sake of traffic stability needs; (4.13c) applies an on-ramp flow capacity; (4.13d) is the traffic demand limit. Based on conversation laws, the cell density n_i, and on-ramp queue e_i are updated as:

$$n_i(t+1) = n_i(t) + r_i(t) + q_{i-1}(t) - q_i(t)/\beta_i, \tag{4.14a}$$

$$e_i(t+1) = e_i(t) - r_i(t) + d_i(t). \tag{4.14b}$$

4.5.2 Dynamics of EVs' speed and energy consumption rate

First, the triangular fundamental diagram (FD) (Fig. 4.4) describes the relationship between the flow within cell i, denoted as $\overline{q}_i$, and its density, n_i:

$$\overline{q}_i(t) = \min[v_{f,i} n_i(t), w_{i+1}(n_{j,i} - n_i(t))],$$

Then the average traffic speed in cell i can be expressed as a function of density Hadiuzzaman and Qiu (2013); Mao et al. (2022), denoted as v_i:

$$v_i = \frac{\overline{q}_i}{n_i} = \min[v_{f,i}, w_{i+1}(\frac{n_{j,i}}{n_i} - 1)], \tag{4.15}$$

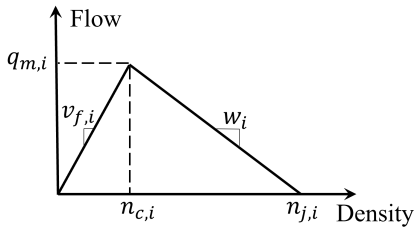

(a) Flow vs Density

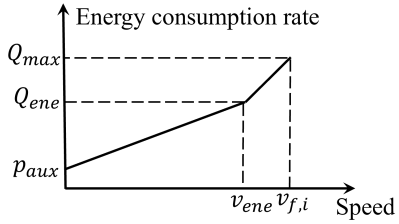

(b) Energy consumption vs Speed

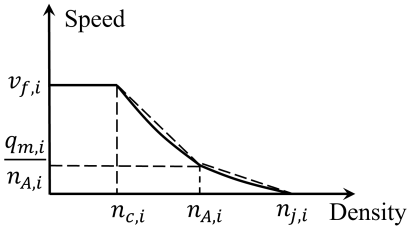

(c) Speed vs Density

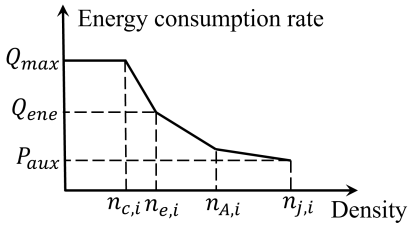

(d) Energy consumption vs Density

Figure 4.4: Relationships among flow, density, speed and consumption rate

Here v_i is a nonlinear function of n_i, which can be approximated by a PWA function (hereafter denoted as $\hat{v}_i$). Let $n_{z,i}^{pwa}$ be the zth nodes, $z = 1, ..., Z$, resulting in $Z-1$ partitions. Let $f_z^v(\cdot)$, $z = 1, ..., Z-1$ be the affine function on zth partition. Then $\hat{v}_i$ is defined as:

$$\hat{v}_i = \begin{cases} f_{1,i}^v(n_i), & \text{if } n_{1,i}^{pwa} \leq n_i < n_{2,i}^{pwa}, \\ \quad \vdots & \\ f_{Z-1,i}^v(n_i), & \text{if } n_{Z-1,i}^{pwa} \leq n_i \leq n_{Z,i}^{pwa}, \end{cases} \tag{4.16}$$

where $z_{1,i} = 0$, $z_{2,i} = n_{c,i}$, $z_{Z,i} = n_{j,i}$, $f_1^v(n_i) = v_{f,i}$ while other points are optional. Fig. 4.4 depicts an example of $\hat{v}_i$ with three nodes where $n_{A,i}$ is the midpoint between $n_{c,i}$ and $n_{j,i}$. The energy consumption rate p_i can be expressed as a nonlinear function of speed and acceleration according to the laboratory tests(Galvin, 2017):

$$p_i = k_1 v_i + k_2 v_i^2 + k_3 v_i^3 + k_4 v_i a_i + P_{aux}, \tag{4.17}$$

where k_1, k_2, k_3, k_4 are the coefficients to be derived empirically. We further incorporate the energy used by various auxiliary systems (e.g., air conditioner) into the function (Adriano et al., 2014), denoted as a constant, P_{aux}. Then we divide p_i into two parts. The first part is the speed-dependent energy consumption rate, $p_i^V = k_1 v_i + k_2 v_i^2 + k_3 v_i^3 + P_{aux}$, which can be approximated as a PWA function of speed delimited by a set of nodes, denoted as $\hat{p}_i^V$. Fig. 4.4b shows an example with two partitions delimited by the energy-efficient speed v_e, where Q_{max}, Q_{ene} denote the maximum consumption rate, energy-efficient consumption rate, respectively. Based on (4.16), the function can be further expressed as a PWA function of n_i, as shown in Fig. 4.4d.

The second part, $p_i^A = k_4 v_i a_i$, encodes the effect of acceleration on the energy consumption of EVs, which is a bilinear function of speed and acceleration. First, the acceleration is defined as the change in the average traffic speed within a specific cell over a time step: $a_i(t) = \hat{v}_i(t+1) - \hat{v}_i(t)$. Based on (4.14) and (4.15), both $\hat{v}_i(t+1)$ and $\hat{v}_i(t)$ can be expressed as PWA functions of $n_i(t)$ and $r_i(t)$. For simplicity, we assume that $n_i(t+1)$ shares the same partition as $n_i(t)$. Then a_i can be approximated in the same way as (4.16):

$$\hat{a}_i = \begin{cases} f_{1,i}^a(n_i, r_i), & if\ n_{1,i}^{pwa} \le n_i < n_{2,i}^{pwa}, \\ \quad \vdots & \\ f_{Z-1,i}^a(n_i, r_i), & if\ n_{Z-1,i}^{pwa} \le n_i \le n_{Z,i}^{pwa}. \end{cases} \tag{4.18}$$

Then we linearize the bilinear function using McCormick Envelopes Mc-

Cormick (1976):

$$\hat{p}_i^A \geq k_4(a^L v_i + a_i v_i^L - a^L v_i^L),$$
$$\hat{p}_i^A \geq k_4(a^U v_i + a_i v_i^U - a^U v_i^U),$$
$$\hat{p}_i^A \leq k_4(a^U v_i + a_i v_i^L - a^U v_i^L),$$
$$\hat{p}_i^A \leq k_4(a_i v_i^U + a^L v_i - a^L v_i^U),$$

where the superscripts L, U represent the lower and upper bounds of the corresponding variables. In this case, $v_i^U = v_{f,i}$ while a^L, a^U, v_i^L are user-defined based on the degree of traffic stability and traffic congestion under consideration. Then the energy consumption rate of EVs can be expressed as:

$$\hat{p}_i = \hat{p}_i^V + \hat{p}_i^A. \tag{4.19}$$

4.5.3 Dynamics of EVs' location and SOC

Expanding upon the high-level discrete-time dynamic system model proposed in (Tan et al., 2022), we group EVs based on their entry time $\tau \in \{0, ..., \bar{\tau}\}$ and origin $o \in \{1, ..., N\}$. Here $\bar{\tau}$ (subscript o omitted) is an integer representing the maximum number of time steps required to travel from the origin o to the end of the WCL. Its value is user-defined, depending on the worst possible congestion levels one would expect. Let l_o^τ denote the location of EVs that entered the road from the origin o and have traveled on the road for τ steps.

Considering that EVs with different SOC levels may have various charging requirements, we further group them based on their initial SOC levels. Let $s_{o,\omega}^\tau$ denote the SOC level of EVs that entered τ time steps ago from origin o, where $\omega \in \{1, 2, ..., N_s\}$ represents the discrete initial SOC level. The

number and range of SOC levels are user-defined. EVs with different SOC levels are assumed to exit the off-ramps proportionally. Then the EVs' location and SOC can be updated as follows in the predictive model:

$$l_o^{\tau+1}(t+1) = l_o^{\tau}(t) + \hat{v}_i(t), \tag{4.20}$$

$$s_{o,\omega}^{\tau+1}(t+1) = s_{o,\omega}^{\tau}(t) - \hat{p}_i(t) + E_r, \tag{4.21}$$

where $o \in \{1, ..., N\}$, $\omega = \{1, ..., N_s\}$, E_r is the energy replenishment rate which is normally a constant as assumed in Deflorio et al. (2015a,b, 2016b); Deflorio and Castello (2017); Li et al. (2019). Note that index i in (4.21) satisfies $l_{e,i-1} \leq l_o^{\tau}(t) < l_{e,i}$. Let $s_{o,w}^{tmn}(t)$ denote the terminal SOC (i.e., the SOC when reaching the end of the WCL) at time t, then we have:

$$s_{o,w}^{tmn}(t) = s_{o,w}^{\tau}(t), \tag{4.22}$$

where τ satisfies $l_o^{\tau} > l_{e,N}$ and $l_o^{\tau+1} \leq l_{e,N}$.

4.5.4 Dynamics of the overall PWA system

Let the state vector be $\boldsymbol{x} = [\boldsymbol{n}^{\mathrm{T}}, \boldsymbol{e}^{\mathrm{T}}, \boldsymbol{l}^{\mathrm{T}}, \boldsymbol{s}^{\mathrm{T}}]^{\mathrm{T}}$ and the input vector be $\boldsymbol{u} = [\boldsymbol{d}^{\mathrm{T}}, \boldsymbol{r}^{\mathrm{T}}, \boldsymbol{v}^{\mathrm{T}}, \boldsymbol{p}^{\mathrm{T}}, \boldsymbol{q}^{\mathrm{T}}]^{\mathrm{T}}$ where $\boldsymbol{n} = [n_1, ..., n_N]^{\mathrm{T}}$, $\boldsymbol{e}, \boldsymbol{d}, \boldsymbol{r}, \boldsymbol{v}, \boldsymbol{p}$ are defined in the same way as $\boldsymbol{n}$. $\boldsymbol{q} = [q_0, ..., q_{N+1}]^{\mathrm{T}}$. The location and SOC of EVs are defined as: $\boldsymbol{l} = [\boldsymbol{l}_1, ..., \boldsymbol{l}_N]^{\mathrm{T}}$, $\boldsymbol{s} = \{\boldsymbol{s}_{o,\omega}\}$ where $\boldsymbol{l}_o, o \in \{1, ..., N\}$ is a vector consisting of the location of EVs with the same origin but different entry times, defined as $\boldsymbol{l}_o = [l_o^{\bar{\tau}}, ..., l_o^0]$. $\boldsymbol{s}_{o,\omega}$ is defined in a similar way as $\boldsymbol{l}_o$. Note that only the on-ramp flows $\boldsymbol{r}$ are controlled inputs while other variables in the input vectors are auxiliary variables. Let the output vector be $\boldsymbol{y} = \{\boldsymbol{s}^{tmn}\}^{\mathrm{T}}$ where $\boldsymbol{s}^{tmn} = \{s_{o,\omega}^{tmn}\}$.

Based on (4.12), (4.14), (4.16), (4.18)-(4.21), the dynamics of the overall

PWA system can be compactly expressed as:

$$\boldsymbol{x}(t+1) = f^x(\boldsymbol{x}(t), \boldsymbol{u}(t)), \tag{4.23}$$

$$\boldsymbol{y}(t+1) = f^y(\boldsymbol{x}(t)), \tag{4.24}$$

where $f^x(\cdot,\cdot)$ and $f^y(\cdot)$ encode the mapping from $(\boldsymbol{x}(t), \boldsymbol{u}(t))$ to $\boldsymbol{x}(t+1)$ and from $\boldsymbol{x}(t)$ to $\boldsymbol{y}(t+1)$, respectively.

4.6 Control model

In this section, we propose a hybrid MPC ramp metering control model based on the PWA predictive model presented in the previous section. We designed three controllers with different objectives and constraints. Controller #1 is for mimicking the no-control case. Controller #2 and #3 are designed to maximize CE and TE, respectively.

Controller #3 is designed to maximize TE. The control problem is expressed as a tracking problem, wherein the reference density is set slightly below the critical density (here we adopt a coefficient ψ of 0.9) to ensure traffic stability. At each time step, the controller #3 generates control

inputs by solving a MILP problem:

$$\min_{\boldsymbol{u}_t,...,\boldsymbol{u}_{t+P-1}} J_1(t) = \sum_{p=1}^{P} \|\boldsymbol{K}_1(\boldsymbol{n}_{t+p} - \psi \boldsymbol{n}_c)\|_1 \tag{4.25a}$$

$$\text{s.t. } (4.23),\ (4.24) \tag{4.25b}$$

$$\boldsymbol{x}(t) = \boldsymbol{x}_t, \tag{4.25c}$$

$$\boldsymbol{x}_{t+p+1} = f^x(\boldsymbol{x}_{t+p}, \boldsymbol{u}_{t+p}),\ p = 1, ..., P, \tag{4.25d}$$

$$\boldsymbol{y}_{t+p+1} = f^y(\boldsymbol{x}_{t+p}),\ p = 1, ..., P-1, \tag{4.25e}$$

$$\boldsymbol{x}^{min} \leq \boldsymbol{x}_{t+p} \leq \boldsymbol{x}^{max},\ p = 1, ..., P-1, \tag{4.25f}$$

$$\boldsymbol{u}_{t+p}^{min} \leq \boldsymbol{u}_{t+p} \leq \boldsymbol{u}_{t+p}^{max},\ p = 1, ..., P-1, \tag{4.25g}$$

$$\boldsymbol{\eta}_1 \boldsymbol{x}_{t+p} + \boldsymbol{\eta}_2 \boldsymbol{u}_{t+p} \leq \boldsymbol{\eta}_3,\ p = 1, ..., P-1, \tag{4.25h}$$

$$\Delta \boldsymbol{u}^{min} \leq \boldsymbol{u}_{t+p} - \boldsymbol{u}_{t+p-1} \leq \Delta \boldsymbol{u}^{max},\ p = 1, ..., P-1, \tag{4.25i}$$

where $\boldsymbol{n}_c = [n_{c,1}, ..., n_{c,N}]^{\mathrm{T}}$, $\boldsymbol{K}_1 = [\kappa^0, ..., \kappa^N]$ is a N-dimensional vector characterized by an exponential decay ($\gamma < 1$). (4.25b)-(4.25e) are system dynamics constraints. In (4.25c), the initial state $\boldsymbol{x}(t)$ in the predictive model is equal to the observed system state $\boldsymbol{x}_t$. (4.25f) are the state constraints. The upper bound of n_i and e_i are $n_{j,i}$ and e_i^{max}, respectively, while their lower bounds are $\mathbf{0}$. The upper bound of $\boldsymbol{l}$ and $\boldsymbol{s}$ are assigned their maximum possible values. Their lower bounds depend on the target travel time, lowest permissible SOC, and target SOC. (4.25g) encodes the constraints (4.13c) and the equality constraints on the on-ramp demand $\boldsymbol{d}$. (4.25i) are the constraints on the delta changes of $\boldsymbol{u}$. The values depend on the need for safety and stability of traffic flow Tan and Gao (2018). (4.25h) encodes the joint state-input constraints (4.13a), (4.13b), and (4.13d).

Controller #2 is designed to maximize CE. The objective function is to maximize the terminal SOC of EVs $\boldsymbol{s}^{tmn}$. At each time step, a MILP

problem is solved:

$$\max_{\boldsymbol{u}_t \dots \boldsymbol{u}_{t+P-1}} J_2(t) = \|\boldsymbol{K}_2 \boldsymbol{s}_{t+P}^{tmn}\|_1$$
$$\text{s.t. } (4.25a)\text{-}(4.25h),$$

where $\boldsymbol{K}_2$ is a vector of ones.

Controller #1 is for mimicking the no-control case in which the vehicles in the queue tend to enter the road whenever possible. Hence, the control objective can be set to minimize the sum of the on-ramp queue length:

$$\min_{\boldsymbol{u}_t \dots \boldsymbol{u}_{t+P-1}} J_2(t) = \|\boldsymbol{K}_1 \boldsymbol{e}\|_1$$
$$\text{s.t. } (4.25b)\text{-}(4.25h).$$

4.7 Numerical experiments

We consider an 8-km WCL segmented into three cells ($N = 3$) with two on-ramps located at cells 2 and 3 and two off-ramps located at cells 1 and 2. We simulate three traffic scenarios. In Scenarios #1 and #2, we design two simple cases to mainly test the effectiveness of the controller in responding to typical changes in the highway system. In Scenario #3, we utilize real-world traffic data to verify the potential of the control model.

In Scenario #1, upstream and downstream densities remain at a medium level, $n_0 = n_4 = 60$. The road capacity, $q_{m,i}$, remains a constant value of 15. The on-ramp demands d_2 and d_3 initiate at a low level and subsequently experience a period of increase (see Fig. 4.5a). In Scenario #2, upstream and downstream densities remain at a medium level (60), while the road capacity experiences a temporary decrease for a defined period

(see Fig. 4.5b). The on-ramp demands d_2 and d_3 remain consistently low throughout. Other parameters are summarized in Table 4.2. To explore the possible trade-off between TE and CE, we further consider EV-related demand in the two scenarios. In Scenarios #1, we introduce constraints $l_1^{15} \geq 3$, $l_2^{11} \geq 3$ into Controller #2, indicating that EVs entering from on-ramps 1 and 2 aim to traverse the road within 7.5 minutes and 5.5 minutes, respectively. This modified controller is denoted as Controller #2*. In Scenarios #2, we introduce constraints $s_{1,1}^{tmn} \geq 40$, $s_{2,1}^{tmn} \geq 35$ into Controller #3, indicating that the EVs from on-ramps 1 and 2 with a low initial SOC level aim to gain at least 10% and 5% net energy replenishment, respectively. This modified controller is denoted as Controller #3*.

Table 4.2: Parameter used in numerical experiments

Δt	T_{tot}	n_c	β	v_f	N_s	k_4	γ
30	80	60	0.85	0.25	2	4	0.9
n_j	n_e	n_e	v_e	w	$s_{1,1}^0$	$s_{2,1}^0$	τ_1^m
160	72	110	0.2	0.15	30	30	20
Q_{max}	Q_{ene}	P_{aux}	E_r	e_i^{max}	$s_{1,2}^0$	$s_{2,2}^0$	τ_2^m
0.33	0.23	0.066	0.625	15	70	70	12

The parameters for cells are similar to (Tan and Gao, 2018). The parameter values related to energy consumption/replenishment are selected based on the data presented in Sec. 4.4.2.

In Scenario #3, we utilize real-world traffic data given in Zhang et al. (2023). As illustrated in Fig. 4.5c, the mainline demand d_1 and on-ramp demand d_2 are the original data, while the on-ramp demand is set as $d_3 = 0.5d_2$. Other parameters are summarized in Table 4.2. We selected data from 6:00 AM to 8:00 PM (1680 time steps). To better illustrate the impact of congestion, we increase the values of the original data by 20%. This adjustment aligns the data more appropriately with the road parameters in our model (since those are not given in (Zhang et al., 2023). To simulate the uncertainty in real traffic scenarios, we introduced

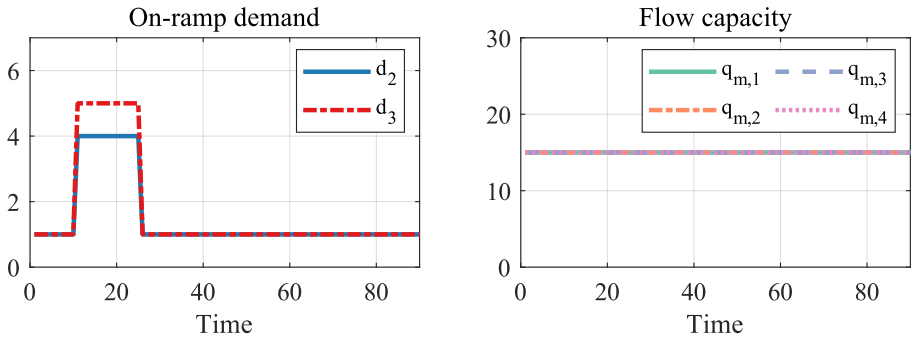

(a) Scenario #1

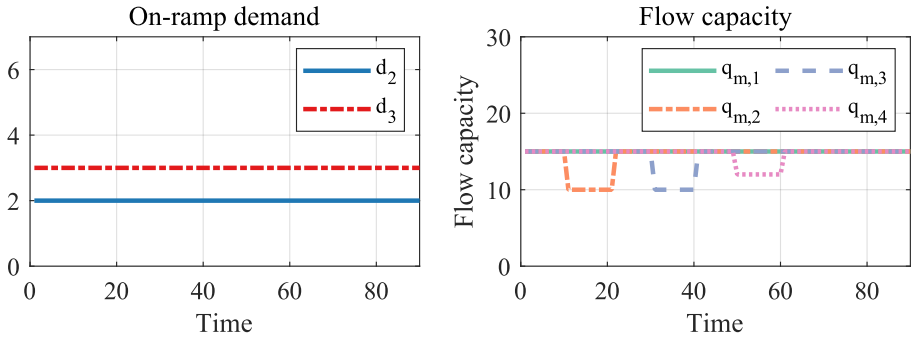

(b) Scenario #2

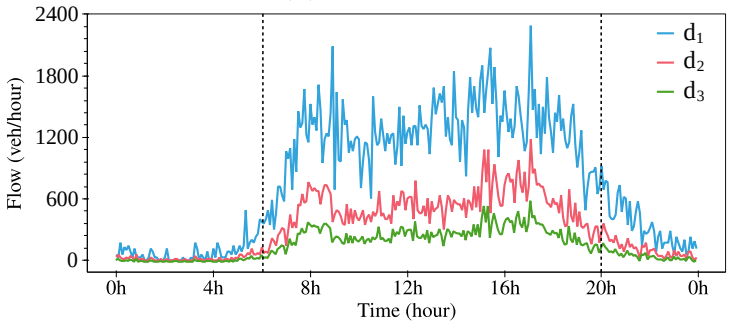

(c) Scenario #3

Figure 4.5: Three scenarios for numerical experiments

two sets of Gaussian noise with different levels into the system. We add $\boldsymbol{X}_1 \sim \mathcal{N}(0, \Sigma_1)$ and $\boldsymbol{X}_2 \sim \mathcal{N}(0, \Sigma_2)$ to on-ramp flows $\boldsymbol{r}$ and speed $\boldsymbol{v}$, respectively. The covariance matrices are set as $\Sigma_1 = 0.5^2\boldsymbol{I}$ and $\Sigma_2 = 0.02^2\boldsymbol{I}$ for noise level 1, and $\Sigma_1 = \boldsymbol{I}$ and $\Sigma_2 = 0.04^2\boldsymbol{I}$ for noise level 2, where $\boldsymbol{I}$ is the identity matrix with appropriate dimensions. Note that both $\boldsymbol{r}$ and $\boldsymbol{v}$ are truncated at zero to ensure positive values.

We further compare the performance of controllers with feedback structure (indexed by #2 and #3) to that of the controllers without feedback (indexed by $\#2^{\text{nf}}$ and$\#3^{\text{nf}}$) in terms of both the total cost (i.e., actual

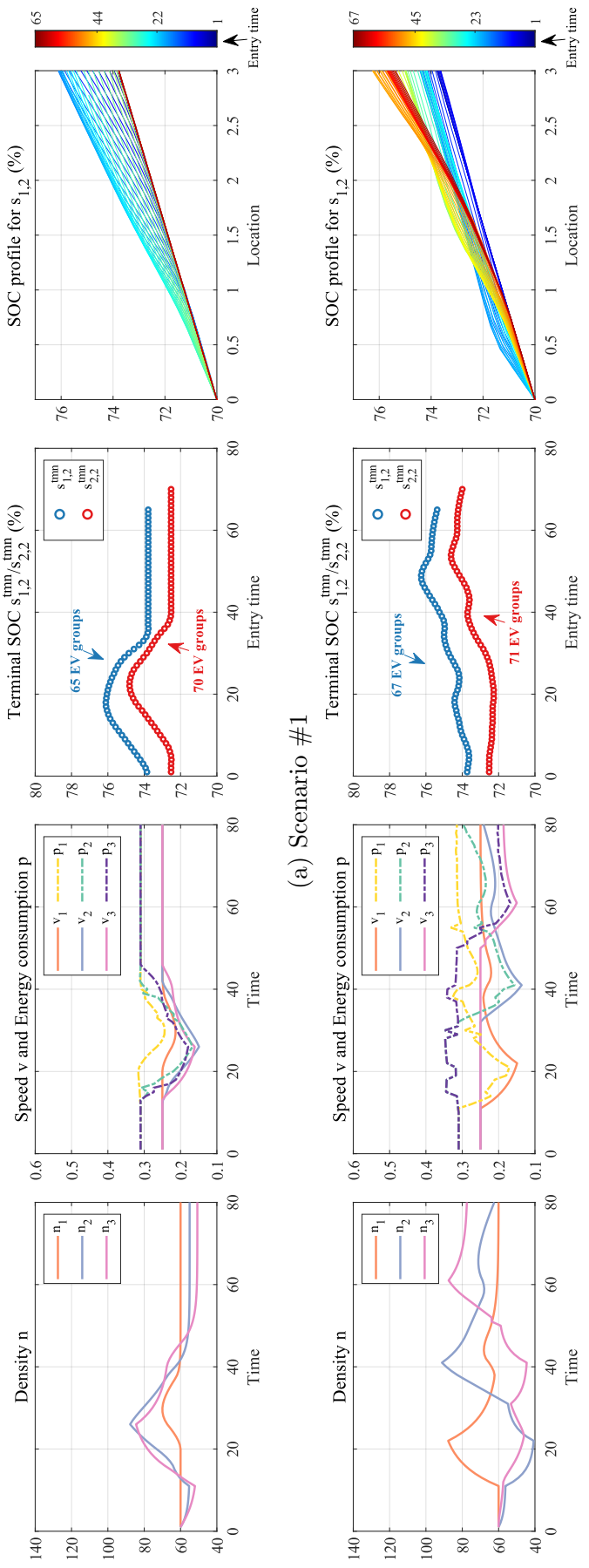

Figure 4.6: Evolution of cell-specific variables (Density, Speed, Energy consumption rate) and EV-specific variables (Terminal SOC, SOC profile). Since the EVs with the same origin share the same SOC profile except for the initial SOC level, we only take $\omega = 2$. In Scenario #1, there are 67 (for $s_{1,2}$) and 71 (for $s_{2,2}$) groups of EVs traversing the WCL. In Scenario #2, there are 65 (for $s_{1,2}$) and 70 (for $s_{2,2}$) groups of EVs traversing the WCL.

objective value) and the degree of constraint violation.

Considering the consistency with the objective function, we evaluate the performance of the controllers by two metrics: total tracking error (TTE) and total net energy replenishment (TER), which are defined as:

$$\mathrm{TTE} = \sum_{t=1}^{T_{tot}} \sum_{i=1}^{3} \|(n_i(t) - \psi n_c)\|_1 \tag{4.27}$$

$$\mathrm{TER} = \sum_{t=1}^{T_{tot}} \sum_{o=2}^{3} \sum_{\omega=1}^{2} \|(s_{o,\omega}^{tmn} - s_{o,\omega}^{ini})\|_1 \tag{4.28}$$

where $s_{o,\omega}^{ini}$ is the initial SOC of EVs corresponding to $s_{o,\omega}^{tmn}$. Generally, a small TTE and a large TER are desired.

We build the MILP problem by the YALMIP toolbox (Löfberg, 2004). The simulation is processed on a desktop (Intel CPU i9-12900K, RAM 64 G) to compute the optimal solution to the MILP in an online fashion using the GUROBI solver. Gurobi typically uses a combination of algorithms to solve MILP problems such as *Branch-and-Bound*, *Cutting planes*, and *Heuristics* algorithms. They work not just simultaneously but also in a synergistic manner. Branch-and-bound is the foundational framework for solving MILP. Gurobi uses this technique to systematically explore the set of possible solutions. It involves branching, which divides the problem into smaller sub-problems, and bounding, which uses linear programming (LP) relaxations to establish bounds on the optimal solution. The algorithm cuts off branches that cannot contain the optimal solution, significantly reducing the search space (Land and Doig, 2010). Alongside branch-and-bound, Gurobi integrates cutting planes, which are linear constraints added to the LP relaxation to exclude regions that do not contain feasible integer solutions but are part of the LP relaxation. These cuts help tighten the LP relaxation around the convex hull of feasible integer points, making the bounds tighter and speeding up convergence (Gomory, 1963). The

combination of the *Branch-and-Bound* method with the *Cutting planes* technique is indeed referred to as the *Branch-and-Cut* algorithm. In addition, Gurobi employs various heuristics at different stages of the solution process. Heuristics are used to quickly find feasible solutions early in the process, which can help guide the search (providing initial bounds and potential solutions). They can also be used to find better solutions while the branch-and-bound tree is being explored or after the exploration has concluded but before proving optimality.

It is also important to note that, before solving starts, Gurobi performs extensive pre-processing to simplify the problem. This includes removing redundant constraints, tightening bounds, and reducing variable ranges. Preprocessing can significantly decrease problem size and complexity, which enhances solver efficiency by reducing the number of variables and constraints handled during the branch-and-bound process. Besides, Gurobi can leverage modern multi-core processors to run these strategies in parallel when possible. For example, while one core may execute branch-and-bound on one part of the tree, another might explore a different part, and others might work on generating cutting planes or running heuristics. Therefore, these algorithms are orchestrated to work in an integrated fashion, where each complements the others. The coordination among them is key to Gurobi's ability to efficiently solve very large and complex MILP problems. This integrated approach allows Gurobi to exploit the strengths of each technique, minimizing weaknesses that might appear if they were used in isolation. Readers interested in more details about the algorithms used in the Gurobi Optimizer can refer to Gurobi Optimization, LLC (2024).

4.8 Results and discussions

4.8.1 SOC prediction

This section aims to demonstrate the impact of density changes on the EVs' SOC profile. We choose the no-control case (controller #3) in both scenarios as the example. Fig. 4.6 illustrates (1) the temporal evolution of cell-specific variables, encompassing density, speed, and energy consumption rate, throughout the simulation, and (2) EV-specific variables, including the terminal SOC and spatial evolution of SOC (hereafter called SOC profile). In the absence of control actions, EVs waiting in the on-ramp queue merge directly onto the road.

In Scenario #1, as depicted in Fig. 4.6a, the increased on-ramp flows lead to congestion in cells. Subsequently, as on-ramp demand dissipates, congestion dissipates. The speed and energy consumption rate within each cell exhibits a converse pattern of change in relation to density, aligning with the functional relationships depicted in Fig. 4.4c and 4.4d. The terminal SOC $\boldsymbol{s}^{tmn}$ varies significantly with their entry time. Due to congestion during time 10 to 40, EVs that enter the road during this period move relatively slowly, thereby consuming less energy and gaining more energy replenishment than their successors. The highest terminal SOC for $s_{1,2}^{tmn}$ and $s_{2,2}^{tmn}$ appear at entry times 20 and 24, with their corresponding net energy replenishment rates of 5.1% and 6.4%, respectively. The values are much higher than those in the free-flow state (enter the road after time 40), 2.7% and 3.9%. We also plot the SOC evolution of EVs against their location, as depicted in Fig. 4.6a, SOC profile for $s_{1,2}$. It can be seen clearly that the SOC profile for different entry times is quite different. Due to the congestion, the SOC for entry time $t \leq 40$ (represented by the blue and green bars) grows significantly faster than that for entry time $t > 40$

(represented by the yellow and red bars) through the simulation.

In Scenario #2, the sudden capacity drops lead to the sudden congestion in cells 1, 2, and 3, sequentially. In contrast to Scenario #1, the onset of congestion in the three cells peaks at different times, resulting in larger fluctuations in densities. It also leads to fluctuations in speed and, more obviously, in energy consumption rate due to the effect of acceleration (Notably, some slight fluctuations are attributed to approximation errors in the McCormick relaxation term. For instance, the fluctuations in p_3 from time 15 to 40 occur despite v_3 remaining constant). Consequently, as depicted in Fig. 4.6b, the terminal SOC of EVs exhibits a complex changing pattern, i.e., increases with the latter entry time but fluctuates in between. The highest terminal SOC for both $s_{1,2}^{tmn}$ and $s_{2,2}^{tmn}$ appears when the entry time is 48 and 52, with the net energy replenishment rates of 5.0% and 6.5%, respectively. The values are consistent with the observations in the SOC profile for $s_{1,2}$ (see Fig. 4.6b) that the orange bars (entry time is around 48) reach the highest terminal SOC. Moreover, it can be observed that the $s_{1,2}$ experiences the fastest increases within cell 3 (between locations 2 and 3), aligned with the fact that the onset of congestion in cell 3 begins at $t = 48$.

The above results show that our proposed predictive model is capable of capturing the relationship between SOC dynamics of EVs and traffic states (density, speed) of the WCL. Three main points are concluded: (1) EVs can gain more net energy replenishment when traveling in congested areas than in uncongested areas; (2) The additional net energy replenishment favored by congestion attributes to both the more energy replenishment (due to the longer charging time) and the less energy consumption (See the evolution of $\boldsymbol{p}$ depicted in Fig. 4.6a and 4.6b; (3) For an EV moving on a WCL, the amount of its net energy replenishment depends on the

temporal and spatial distribution of traffic congestion.

4.8.2 Ramp metering control under sample scenarios

This section compares the performance of the three controllers in the two traffic scenarios. Fig. 4.7 plots the final performance of the average computational time under various prediction horizons. It can be observed that in both scenarios, the performance of the two controllers arises in the prediction horizon until 6, after which the rise is negligible. It can also be seen that the computational time (seconds) for one control action increases approximately exponentially in the prediction horizon, though, it is much smaller than the time step $\Delta t = 30s$ used for the predictive model. hence, in the following, we adopt a prediction horizon of 6.

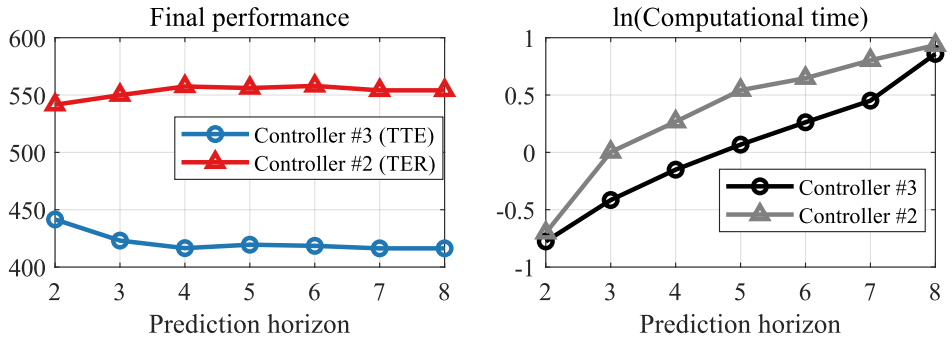

(a) Scenario #1

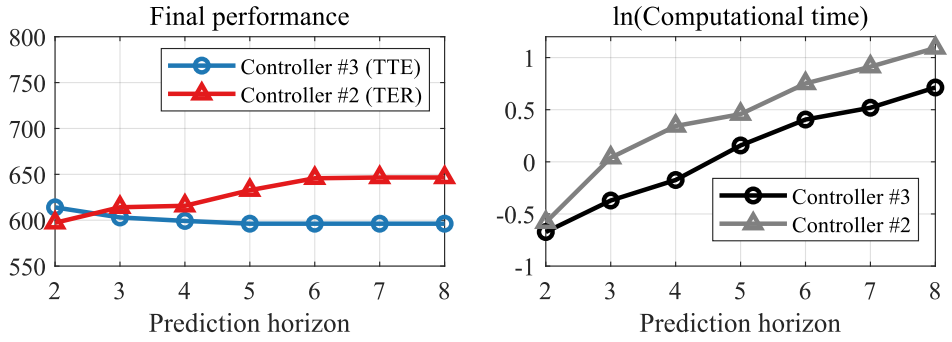

(b) Scenario #2

Figure 4.7: Performance and computational time under various prediction horizons

The simulation results are depicted in Fig. 4.8. The final performance of

the controllers is summarized in Table. 4.3. In general, controller #3 (TE) tends to let cell densities track the reference density (54) while controller #2 (CE) tends to extend the period of road congestion. Moreover, two notable control behaviors are observed during the onset and dissipation of congestion.

In Scenario #1. when the onset of congestion is observed ($t = 20$), Controller #2 (CE) tends to allow more on-ramp flows than Controller #3 (TE) to bring forward congestion (see r_2, r_3, n_2, n_3 in Fig. 4.8a and 4.8b). When the dissipation of congestion is observed ($t = 25$), Controller #2 tends to lower the ramp metering rate in advance for a short period (see r_2 from time 23 to 28). In the meantime, n_2 experiences a temporary decline. After that, the traffic accumulated in the on-ramp queue during this period is then released to compensate for a higher ramp metering rate (see r_2 from time 28 to 33) to extend the duration of congestion on the entire road. Similarly, in Scenario #2, when the onset of congestion is observed ($t = 30$ for n_2, $t = 45$ for n_3), Controller #2 tends to allow more on-ramp flows to bring forward congestion while Controller #3 tends to limit the on-ramp flows to ease congestion. As a result, EVs under Controller #2 experience more congested traffic on the WCL throughout the simulation, thereby having a higher terminal SOC, as shown in Fig. 4.8a and 4.8b.

Table 4.3: Performance of controllers under Scenarios #1 and #2

Scenario	Ctrl	Obj	TTE	TER
#1	#1	/	651.2	557.3
	#2(*)	CE	692.3 (672.2)	**565.6** (559.2)
	#3(*)	TE	**416.5** (492.3)	522.1 (527.3)
#2	#1	/	1095.3	614.3
	#2(*)	CE	1147.7 (1052.9)	**629.6** (603.5)
	#3(*)	TE	**596.2** (662.4)	562.5 (567.3)

The aberrations Ctrl and Obj stand for Controller and Objective, respectively. The numbers in bold are the best values of corresponding performance measures in each scenario.

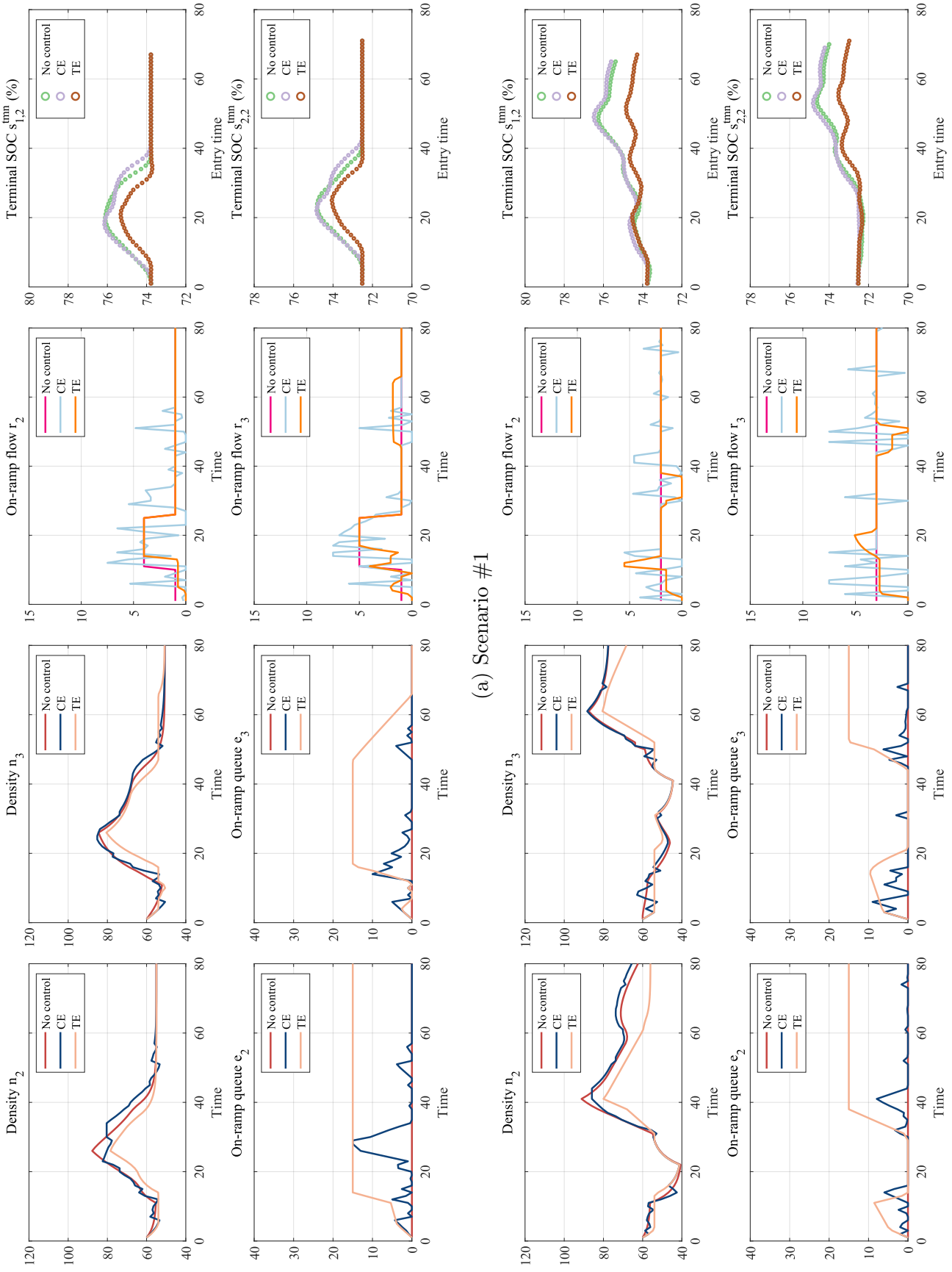

(a) Scenario #1

(b) Scenario #2

Figure 4.8: Evolution of cell-specific variables (Density $\boldsymbol{n}$, On-ramp queue $\boldsymbol{e}$, On-ramp flow $\boldsymbol{r}$) and EV-specific variables (Terminal SOC $\boldsymbol{s}^{tmn}$ for $\omega = 2$). The controlled input is $\boldsymbol{r}$. As mentioned in Sec. 4.7, no on-ramp is considered in cell 1 hence $e_1 = 0$

The final performance of the three controllers is shown in Table 4.3. It can be seen that Controller #3 (TE) achieves the best TE in both scenarios, with the lowest TTE of 416.5 and 596.2, respectively. The values are 39.8% and 48.1% smaller than those of Controller #2 (CE), respectively. Controller #2 achieves the best CE in both scenarios, with the highest TER of 565.6 and 629.6, respectively. The values are 8.3% and 11.9% higher than those of Controller #3, respectively. The performance of the no-control case falls between that of the other two controllers. These results demonstrate the inherent conflict between TE and CE, indicating that an increase in one leads to a decrease in the other. The conflict can also be observed in the comparison between the performance of Controller #2*/#3* and Controller #2/#3. Besides, it is notable that Controller #2* mainly satisfies the constraints of maximal travel time, while Controller #3 violates the constraints of target net energy replenishment. This violation implies that the control effect of ramp metering rate on EVs' SOC is constrained by the amount of on-ramp demand and a fixed speed limit.

To sum up, the ramp metering control problem on WCL yields distinct control results when comparing objectives of maximizing TE and CE. Three key findings are summarized as follows: (1) When the control objective is CE, the controller tends to extend the period of congestion; (2) The difference in the control effect between controller #3 (TE) and controller #2 (CE) mainly occurs during the onset and dissipation of congestion; (3) There exists an inherent conflict between TE and CE on a WCL. The degree of this conflict depends on various factors, including the charging power of the WCL, the power consumption of EVs, the free-flow speed, etc.

Table 4.4: Performance of controllers under Scenario #3

Noise	**Ctrl**	**Cost** ($\times 10^4$)		**Violation**	
		Ave.	Std.	%	Ave.
Level 1	#2	2.211	0.015	4.6	0.033
	$\#2^{nf}$	2.359	0.034	15.7	0.283
	#3	1.149	0.011	1.4	0.003
	$\#3^{nf}$	1.084	0.016	5.8	0.104
Level 2	#2	2.341	0.015	5.8	0.046
	$\#2^{nf}$	2.576	0.073	23.5	0.913
	#3	1.118	0.010	2.6	0.009
	$\#3^{nf}$	1.064	0.027	11.1	0.127

The violation refers to the average constraint violation for the on-ramp queue lengths, i.e., $\frac{1}{T \cdot N} \sum_{i=1}^{N} \sum_{t=1}^{T} \max(0, e_i(t) - e_i^{max})$. Ave. and Std. stand for the average and standard deviation over 10 replicate simulations. % is the percentage of periods where violations occur.

4.8.3 Ramp metering control under real traffic scenarios

This section compares the performance of controllers with and without feedback. As illustrated in Table 4.4, controllers with feedback outperform their nonfeedback counterparts by 5.1% to 9.1% in total cost. Moreover, they experience significantly fewer times of constraint violations and a lower average magnitude of violation for the on-ramp queue, $\boldsymbol{e}$. The results indicate that our MPC control model exhibits strong resistance to external disturbances. This is to say, even in the presence of errors in our predictive model, our MPC control model (with feedback structure) is still capable of yielding considerable control efficacy.

4.8.4 Insights for management and operations on the WCL

In DWC scenarios, the SOC profile of an EV primarily relies on its speed profile. In the context of ramp metering control, EVs' speed profile is affected by regulating the spatial and temporal distribution of on-ramp flows. However, the impact occurs during the periods of congestion onset and dissipation. Moreover, the impact of ramp metering rate on EVs' SOC is significantly constrained by fixed speed limits and uncontrolled on-ramp demands, which is a limitation of ramp metering control on WCLs. In practice, WCL operations necessitate a delicate balance between TE and CE, namely, prioritizing CE while alleviating traffic congestion. In this regard, the Variable Speed Limit (VSL) control is a superior strategy, which can better strike a balance between TE and CE by controlling the speed limit distribution on the WCL.

Moreover, an inherent conflict arises between TE and CE on a fully covered WCL due to the operational principles of electric motors and the distinctive nature of DWC. As mentioned in Sec. 4.8.2, maximizing CE leads to an extended period of congestion, with at most an 11.9% increase in CE and around a 48.1% decrease in TE, as illustrated in Table 5.3. However, it is important to note that these percentages are highly dependent on the values of the related parameters in a specific scenario. This implies that a DWC is more suitable for EV drivers who have a lower sensitivity to travel delay. Conversely, in a traffic scenario where both TE and CE are important, the WCL is better suited to be deployed in a multi-lane system, for example, a WCL can be deployed on the rightmost lane with a lower speed limit where other lanes are general-purpose lanes (He et al., 2017, 2018). This design has more potential to strike a balance between the two objectives, ensuring the effective operation of the WCL system.

4.9 Limitations and Future Work

In this section, we discuss the limitations of this study and suggest directions for future work. The limitations can be categorized into three aspects: (1) *Context*: This term refers to the specific assumptions about the traffic context examined in this study, such as the coverage of WCLs and whether EVs must charge on WCLs; (2) *Modeling*: This involves the methods used to model the traffic dynamics under the considered context; (3) *Algorithm*: This refers to the algorithm utilized to solve the optimization problem.

Regarding the context, as assumed in Sec. 4.4, the WCL is fully deployed on the road, and all EVs must charge on the WCLs whenever possible. We believe that full coverage of WCL is the primary approach for its deployment because more complex designs of WCLs, such as intermittent deployment (assumed in Chen et al. (2017) and Ngo et al. (2020)) and multi-lane deployment (assumed in He et al. (2018) and He et al. (2020)), require extensive discussion and careful design. Moreover, the macroscopic traffic flow model used in this study inherently assumes uniform road conditions. However, we recognize that some studies have pointed out the necessity of considering more complex designs for WCLs. For instance, He et al. (2018) and He et al. (2020) have argued that a fully covered WCL is impractical, as vehicles without the intention to charge might be delayed by those that are charging ahead of them. They suggest that WCLs would be more effectively implemented in a multi-lane system. Therefore, we propose that addressing ramp metering issues in the context of these complex WCL designs is a worthy endeavor. In such cases, variants of the CTM could be used to model traffic dynamics more accurately. Regarding the assumption that EVs must charge on the WCLs whenever possible, we believe it is difficult to relax this within the framework of a macroscopic traffic flow model. This is because whether or not an EV chooses to charge on the

WCL depends on individual vehicle attributes. The heterogeneity across different EVs conflicts with the basic assumption of macroscopic traffic flow theory that all vehicles exhibit uniform behavior. Instead, this could be addressed by adopting a microscopic traffic flow model. In such scenarios, a model-based control method like MPC may not be suitable. Rather, a model-free method such as reinforcement learning should be considered.

Regarding the modeling, this study exhibits three limitations. Firstly, uncertainties, including EV heterogeneity encompassing vehicle type, battery properties, initial SOC, and road conditions, are not explicitly considered in the control model. Future research should incorporate these uncertainties into the model as random variables. Methods such as robust optimization and chance-constrained programming are poised to address these stochastic optimization problems. Secondly, as WCLs have not been widely deployed, our model has not been validated and calibrated by real traffic data. The validation and calibration can be implemented once the real traffic data is available, as demonstrated in (Silgu et al., 2021a,b). In addition, utilizing data generated by a microscopic traffic simulator is a viable alternative. Thirdly, the proposed model, built upon the original CTM, cannot reproduce complex traffic phenomena such as capacity drops, traffic hysteresis, phantom jams, and flow patterns (Hoogendoorn and Bovy, 2001; Srivastava and Geroliminis, 2013; Celikoglu and Silgu, 2016). This limitation might lead to inaccuracies in SOC dynamics. Hence, our model can be enhanced by incorporating more formulations or adopting improved versions of the CTM (Celikoglu, 2014; Srivastava, 2016; Canudas-de Wit and Ferrara, 2018). Ideally, these formulations should be introduced in a mathematically convenient way to ensure computational feasibility. Furthermore, specialized traffic simulators for DWC scenarios, if available, can be employed to verify the validity and reliability of our model.

Regarding the algorithm, as discussed in Sec. 4.7, the MILP problem generated from hybrid MPC is solved using the Gurobi optimizer, in which well-established algorithms are adopted. We also examine the computational feasibility of these solutions, as depicted in Fig. 4.7. However, challenges arise when scaling to larger traffic systems (e.g., longer roads involving more cells in the CTM); under these conditions, the MILP problem may become intractable. To overcome this, developing an effective method to expedite the solution process is a potential research direction. In response, Chapter 5 introduces a tailored, efficient algorithm designed specifically to accelerate the resolution of MILP problems derived from hybrid MPC, promising significant improvements in computational performance.

In the following chapters, this thesis primarily focuses on two research directions. Chapter 5 explores a Variable Speed Limit (VSL) control strategy on WCLs. Although its coordination with ramp metering control is also a potential research direction, we leave it for future work (Hegyi et al., 2005; Silgu et al., 2021a). Chapter 6 investigates traffic management in a multi-lane system where a WCL is deployed on one specific lane to balance TE and CE. In this context, the lane-changing behaviors of Electric Vehicles (EVs) are crucial (Zhang and Ioannou, 2017; Yuan et al., 2022). Consequently, we propose a dynamic pricing problem in which the electricity price varies periodically to regulate TE and CE.

4.10 Conclusion

We have developed a ramp metering control model tailored for DWC scenarios considering optimal traffic and charging efficiencies. We incorporate the location and SOC dynamics of EVs into the CTM and formulate the entire model into a PWA system. By a hybrid MPC approach, the control

problem at each time stage is formulated into a MILP problem that can be solved in an online manner with well-established solvers. We conducted numerical experiments in two traffic scenarios on an 8-km WCL. The simulation results demonstrate both the efficacy and the limitation of ramp metering control on WCLs in terms of maximizing CE. Moreover, we reveal the inherent conflict between TE and CE. In both scenarios, the controller to maximize CE achieves 8.1% and 11.9% higher TE while sacrificing 39.8% and 48.1% CE, though, these values depend on various parameter values. These results give some insights to the traffic authorities and policymakers on the management and operations of WCLs. The limitations of this study are discussed in terms of the context, modeling, and algorithm, and avenues for related future research are proposed.

Chapter 5

Variable speed limit control on wireless charging lane considering optimal traffic and charging efficiencies

5.1 Introduction

The adoption of EVs has grown rapidly in recent years with the reinforcement of environmental awareness and the rapid development of battery technology. According to a report by Bloomberg (McKerracher, 2023), the global sales of EVs increased from 3.2 million in 2020 to more than 10 million in 2022 and are expected to continue to rise in the following year. Nevertheless, the problem of "range anxiety" due to the lack of public charging facilities and the long charging time still hamper the extensive use of EVs. To address this problem, EV manufacturers and research institutions have invested heavily in upgrading battery technology. Meanwhile,

they have developed more advanced charging modes. For instance, DWC, also known as charging-while-driving or charging-in-motion, is considered an ideal charging solution. With the support of charging facilities installed beneath the road surface, hereafter called WCLs, EVs can receive energy wirelessly while driving (Ahmad et al., 2017; Panchal et al., 2018). By far, DWC technology has been implemented and tested by many institutions; some pioneers are the University of California, Berkeley; Korea Advanced Institute of Science and Technology, and Bombardier Transportation. It is envisioned that DWC has great potential to revolutionize the way EVs are powered and charged. The problem of "range anxiety" is expected to be alleviated or even eliminated if WCLs can be deployed massively on the traffic network (Jansuwan et al., 2021).

Over the past decade, transportation issues in the DWC scenario have garnered significant attention in academia; real-time traffic control problems, however, have been hardly studied. One reason is that most ongoing DWC projects are still in their early experimental stages. Hence, the research community is devoting more attention to transportation planning issues, such as optimal allocation problems of WCLs. Another reason is the lack of a dynamic traffic model, specifically with regard to the SOC. In traditional traffic scenarios, the primary purpose of traffic control is to facilitate traffic efficiency that can be evaluated by conventional traffic flow characteristic parameters (e.g., flow and density). Whereas in the DWC scenario, since the road also provides an extra function of charging service, charging efficiency should be considered an essential aspect of control purpose (Li et al., 2019), which can be evaluated by the total energy transferred to EVs, namely, the total increment of the EVs' SOC. Unfortunately, the traditional macroscopic traffic flow models (e.g. the CTM) merely formulate the relationships among traffic flow characteristics such as density, flow, and average traffic speed. EVs' SOC has not been taken into consideration. As

a result, the existing models are insufficient to meet the requirements of real-time traffic control problems in the DWC scenario.

This thesis specifically focuses on addressing the real-time traffic control problems in the DWC scenario. In Chapter 2, we elaborated on the difficulties of modeling EVs' SOC and indicated that the key is to formulate the dependence of consumption/charging rate on dynamic traffic state (density and speed). Additionally, incorporating the location of EVs as an auxiliary variable is essential. They presented a high-level discrete-time dynamic system model to provide a more precise illustration, although a concrete implementation method was not provided. The first implementation of the model was proposed in Chapter 4, focusing on a ramp metering control problem on a freeway where a WCL is deployed along the entire road. They incorporated EVs' SOC into the CTM by formulating its dependence on the existing traffic flow parameters in a mathematically convenient way. Based on the proposed model, they designed several control models to explore control strategies considering both traffic efficiency and charging efficiency. These control models differ in terms of control objectives and system constraints. The underlying idea is that ramp metering can indirectly impact average traffic speed by controlling the congestion level, thereby influencing the SOC profile of EVs.

However, as demonstrated in Chapter 4, the effect of ramp metering control on optimizing the CE is significantly constrained by fixed speed limits and uncontrolled on-ramp demands, which is a limitation of ramp metering control on WCLs. In this regard, VSL control is expected to be a more effective approach since EVs' consumption/charging rate is highly dependent on their real-time speed (Liu et al., 2024).

This study addresses the research gap in real-time traffic control problems for the DWC scenario by considering a VSL control problem. The remain-

der of the chapter is organized as follows. In Section 5.2 we present a review of relevant literature and outline the contributions of this study. In Section 5.4, we present the modeling approach, including the system predictive model, the control model, and a simple-yet-effective algorithm (*LKNMS*) for HMPC. This is followed by a series of numerical examples in Section 5.5, where the simulation results are analyzed and discussed. Finally, in Section 5.7, we present the conclusions, limitations of this study, and avenues for future research.

5.2 Related work

This section presents a literature review of past studies related to this study, which comprises three sub-sections: (1) Operations issues on WCLs; (2) VSL control on the freeway; (3) HMPC with the CTM. Next, we highlight the contribution of this study in light of existing literature.

5.2.1 Operations issues on WCLs

Research on operations issues is still nascent. Given that the definition of operations issues is typically broad, in this study, we specifically define operations issues as modeling and analysis that can aid in assessing or improving the operational efficiency of WCLs. Within these operations issues, studies primarily focus on two key aspects: (1) evaluating the charging efficiency performance of WCLs, and (2) examining the impact of WCL presence on traffic efficiency.

The charging efficiency of WCLs has been extensively investigated in the literature using various traffic modeling and simulation techniques. Deflorio et al. (2015b) proposed a mesoscopic model to assess the performance

of WCLs used in a freight distribution scenario. They considered a three-lane road system where a discrete WCL deployed on its rightmost side. The charging EVs are divided into two groups according to their SOC level: "emergence" for a low SOC and "normal" for a moderate SOC, with different defined speeds, respectively. The simulation results showed that, in a heavy traffic scenario, the maximum power required by EVs increases by more than 50% compared to light traffic due to a lower average speed. Based on the same model assumptions, their subsequent work, Deflorio and Castello (2017), proposed a traffic simulation model designed to measure and characterize traffic performance, SOC variations of the fleet, and the energy demand of energy suppliers. All vehicles are assumed to drive in complete cooperation, which entails advanced driver assistance systems controlling their speeds and lane choices. Deflorio et al. (2016b) also adopted a similar model used in Deflorio et al. (2015b) to estimate both the daily energy demand of DWC EVs and the economic benefit of WCLs installed on motorways. The simulation result concluded that WCLs might be suitable for motorways connecting two nearby cities with a high volume of EVs commuting between their centers. The economic benefits are considerable if EVs drive at a low speed. The performance of WCLs deployed on different road stretches is compared in García-Vázquez et al. (2017). The work compared the performance of WCLs in highways, motorways, and urban stretches based on real-world traffic data. The numerical results showed that the increment of EVs' SOC per kilometer in urban stretches is significantly higher than that on highways because of a lower speed limit (50km/h). On motorways, however, it sees a slight decrease owing to a higher average speed (110km/h). The result indicated that it may be necessary to add a slow-speed additional lane on the highway and motorway to provide adequate charging time. Jansuwan et al. (2021) proposed an assessment framework for a more advanced transportation system consid-

ering DWC based on a microscopic approach. In the scenario, EVs are powered by WCLs and can automatically form platoons that can interact cooperatively. The simulation results demonstrated a substantial potential of DWC for significantly extending the maximum range of an EV. As an illustration, the range could be nearly doubled even under a comparatively low charging efficiency (55%) while driving at 65 mph.

The effect of WCL on traffic efficiency is only considered in a limited number of papers. He et al. (2018) explored the impacts of WCLs on travel time and energy consumption in a two-lane road system composed of one WCL and one conventional lane. They suggested that WCLs should be implemented in a multi-lane system, on which EVs should maintain a lower speed than that on GPLs. This is consistent with the model assumptions in Deflorio et al. (2015b, 2016b); Deflorio and Castello (2017). Considering that charging behavior inevitably impacts traffic behavior, such as speed and lane-changing maneuvers, they integrated it into the driving behavior model and refined the energy consumption model. Their simulation results revealed that the presence of WCLs could decrease road capacity by 8-17% and increase EV energy consumption by 3-14% due to frequent lane-changing maneuvers exhibited by EVs.

The literature review above yields the following key points: (1) Despite variations in the model assumptions and parameter settings, these studies demonstrated the great potential of DWC for EVs' range extension in various traffic scenarios; (2) The energy replenishment of EVs shows a significant increase at a low driving speed. This is because, within a specific range, driving at a low speed results in more charging time and leads to a lower energy consumption rate. However, this is always accompanied by a lower speed limit or heavy traffic conditions. Therefore, a trade-off exists between traffic and charging efficiencies, which should be considered and

explored in real-time traffic control problems on WCLs. Tan et al. (2022) first discussed the difficulties of real-time traffic control problems on WCLs. They stated that the main difficulty lies in designing tractable integration of EVs' SOC into the existing dynamic traffic model, the key of which is to formulate its dependence on dynamic traffic state (density and speed) in a mathematically convenient way. They further proposed a high-level discrete-time dynamic system model in which EVs are grouped according to their entry time. However, specific details on modeling need to be established and scrutinized when applying to a specific traffic scenario. The first concrete implementation of the model is presented in Chapter 4, which is also the first to address real-time traffic control problems on WCLs. As mentioned earlier, their basic consideration is that ramp metering can indirectly affect average traffic speed by controlling the degree of congestion, thereby further affecting EVs' SOC profile. A more direct way is to control the speed limit on the WCL, though it requires a more advanced transportation system, as it involves the use of sensors and cameras to monitor traffic conditions and adjust speed limits in real time.

5.2.2 VSL control on freeway

Variable Speed Limit (VSL) control is a common traffic control approach that adjusts the speed limit on a highway or motorway according to real-time traffic and weather conditions. The speed limit is usually displayed on variable message signs (VMS) installed at motorways for real-time updates. At present, VSL control has been widely applied around the world for traffic management of highway or motorway traffic to enhance traffic safety and reduce congestion. This section provides a concise overview of the existing literature on VSL control, specifically focusing on the use of the CTM for modeling and algorithm development.

Hadiuzzaman and Qiu (2013) proposed a VSL control approach for freeways based on the modified CTM and model predictive control. In that work, the microscopic simulation model is built based on VISSIM; the VSL control model is established using nonlinear Godunov fluxes in C++ program. The two models interact with a COM application interface. Muralidharan and Horowitz (2015) considered a coordinated ramp metering-VSL problem on freeways. With assumptions added and relaxation techniques adopted, they converted the nonlinear optimization problem derived from the MPC controller into a set of linear optimization problems. Han et al. (2017b) proposed an extended CTM for VSL control embedded in a linear-quadratic MPC approach. The model maintains the linear property of the traditional discrete first-order while considering capacity drop and the propagation of traffic jam waves. The model's accuracy is calibrated and validated in their subsequent work, Han et al. (2017a), using real-world traffic data and a speed limit control algorithm (SPECIALIST). VSL control in more advanced traffic environments is investigated in Chen et al. (2020); Mao et al. (2022). Chen et al. (2020) explored the VSL control problem for autonomous vehicles. They established a multi-class CTM that can calculate flows of both compliant and non-compliant vehicles between road segments. Since the optimization problem derived from the model is non-convex, a heuristic VSL algorithm is proposed to control speed limits to reduce the total energy consumption of vehicles. Mao et al. (2022) proposed a VSL control strategy to improve traffic efficiency in the connected environment. An extended CTM is adopted together with a non-linear MPC controller accelerated by a genetic algorithm.

The above-mentioned studies modify the CTM in different ways according to their specific requirements. Most adopted model predictive control as the control measure due to its ability to explicitly handle constraints on states and inputs. However, due to the nonlinearity of traffic flow dynamics,

the control problem at each time step is typically a nonlinear optimization problem that is computationally expensive and time-consuming to find the global optimum. Hence, these studies tend to establish an approximate linear model or a relaxed linear problem using various linearization techniques, despite some sacrifice of the abundance of the system dynamics and precision of the optimal solution. In contrast, Csikós and Kulcsár (2017) proposed a VSL design for motorway networks based on a mode-dependent CTM. In this work, the polyhedral CTM description framework in Thai and Bayen (2014) is extended to VSL control. The derived model is classified as a parameter-dependent piecewise affine (PWA) system in which the system dynamics on each partition is triggered by the control signal. By analyzing and exploiting the reachability of the PWA system, the online optimization problem is formulated into a mixed integer nonlinear optimization problem.

5.2.3 HMPC with the CTM

Hybrid Model Predictive Control (HMPC) is a control strategy that combines the principles of Model Predictive Control (MPC) with the ability to handle hybrid systems. In the context of control systems, a hybrid system is a dynamic system that combines both continuous dynamics and discrete events or behaviors. PWA systems are a broad class of hybrid systems that exhibit different linear behaviors in different regions or modes of operation, wherein the state-space representation of the system is divided into multiple regions. Within each region, the dynamics can be described by an affine model (linear dynamics with a constant term). When MPC is applied to a hybrid system, the discrete behaviors exhibited by the system can be represented by logic constraints with additional integer variables and auxiliary variables introduced. Then, the control problem at each time step can be formulated as a mixed-integer program (MIP) problem. The framework

is depicted in Fig. 5.1. Such control model formulation effectively takes advantage of the nature of hybrid systems. More importantly, it maintains the two major advantages of MPC: 1) Explicit consideration of constraints on system states, inputs, and outputs; and 2) Robustness to disturbances and uncertainties.

HMPC has been utilized in specific traffic control problems involving the Cell Transmission Model (CTM) and has demonstrated favorable control outcomes Hajiahmadi et al. (2015); Koehler et al. (2016); Tan and Gao (2018). Due to the relationship between flow and density, the CTM can be easily formulated into a PWA system. For instance, Koehler et al. (2016) developed a stable hybrid MPC strategy for freeway ramp metering. In the work, the CTM is formulated into a PWA system. The control problem is a mixed-integer quadratic program (MIQP). Tan and Gao (2018) developed a hybrid MPC strategy for dynamic tolling of managed lane systems. They formulated the CTM into a PWA system with polyhedral representation. The control problem is a mixed-integer linear program (MILP), which can be solved by various mature, efficient, and robust solutions.

Despite the advantages of HMPC, it faces a significant drawback in terms of computational complexity because the scale of the MIP problem escalates with the number of both dimensions of a hybrid system and the prediction horizon. A small-scale MIP problem can be solved efficiently in real-time using well-established algorithms, such as the branch and bound algorithm, which can find the globally optimal solution without exhaustively enumerating all possible combinations of binary variables. However, as the number of dimensions or the prediction horizon increases, the complexity of the MIP problem grows considerably (due to the combinatorial explosion caused by the escalating number of integer variables and constraints). Then, the computational burden can become substantial, making it challenging to

implement in real-time applications.

To solve this problem, explicit (hybrid) MPC was proposed to reduce the online computational cost by transferring it offline (Borrelli et al., 2006; Alessio and Bemporad, 2009). In practice, however, as the computational cost of offline computation and storage is extremely high, the applicability of explicit MPC is also limited to a low-dimensional hybrid system. More approaches have been explored and developed to soften the computational burden of HMPC with acceptable sub-optimal solutions obtained. For example, Axehill et al. (2014) proposed a parametric branch and bound approach that can reduce the storage requirements and the online computational effort. Marcucci and Tedrake (2020) proposed a warm-start algorithm to accelerate a mixed-integer quadratic program (MIQP) in HMPC. Their basic idea is that HMPC generates nearly identical optimization problems at each time step, the computations of which can be reused to accelerate (warm start) solving procedure. Their experimental results show that the proposed algorithm can significantly reduce the combinatorial complexity of the hybrid MPC problem with a negligible computational cost. Masti et al. (2020) proposed a Semi-Explicit HMPC method. First, machine learning techniques (specifically, the random forest method and decision tree) are employed to learn a predictor for optimal binary solutions using the available dataset. By assigning the predicted binary solutions generated by the predictor, the original MILP problem at each control stage degenerates into a linear programming (LP) problem. The practical application of this method was demonstrated in a microgrid power dispatching problem. The results indicated a substantial reduction in computational load with an acceptable feasibility level. However, it's important to highlight that the training process for the predictive model requires manual parameter extraction, which emphasizes the necessity of a comprehensive understanding of the underlying MILP problem. Zhu and

Martius (2020) also used machine learning techniques to approximate the explicit HMPC law. Different from the idea of Masti et al. (2020) where the ML techniques are adopted to directly learn the mapping between the optimal mode sequence and the system state x_0 (and other parameters), they use ML to find a feasible mode sequence of a given x_0 instead. Here, the feasible mode sequence is obtained by the mode sequence of the nearest neighbor of x_0 in a given dataset (each data sample consists of a $x0$ and its feasible mode sequence). The quality of data samples can be further improved by finding a better corresponding mode sequence (the most ideal one is the optimal sequence), to improve the solution optimality of the proposed algorithm. Notably, this approach is simple yet effective, making it readily implementable for practitioners. These algorithms are pro-

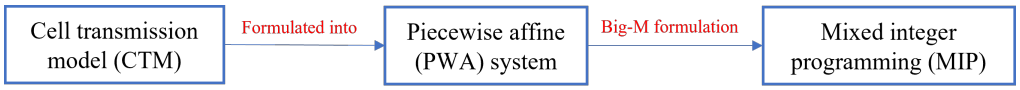

Figure 5.1: CTM-HMPC framework

posed to accelerate HMPC in different ways and achieve good performance. They all consider a low-dimensional MLD system, except Zhu and Martius (2020), which considers a low-dimensional PWA system (with only two states). However, the traffic model proposed in this study will be a high-dimensional PWA system (generated by the CTM) where the dimension grows exponentially with the number of cells. The algorithms mentioned above might not be particularly well-suited to the model employed in this study. Different from these algorithms, an algorithm proposed in Csikós and Kulcsár (2017) aims to lighten the computational burden by exploiting one-step polyhedral adjacency (defined in Thai and Bayen (2014)) of CTM modes. Let N_m be the dimension of the system mode vector. They then assume that only one mode of the system mode vector can change in one time step while others $N_m - 1$ modes remain the same. Based on this assumption, the reachable modes during the prediction horizon for a

given initial system state $x0$ can be significantly reduced, resulting in a much smaller MILP problem. However, this method is not applicable to some traffic scenarios, e.g., traffic accidents, where the traffic density may change abruptly. Second, it relies on the reachability analysis of system modes, which means the method is tailored to a given PWA system, which calls for a deep understanding of its dynamics. Hence, such a method can not be directly applied to another system.

Given the previous review, we aim to propose a new algorithm tailored to our system (more specifically, a high-dimensional PWA system). Motivated by Masti et al. (2020); Zhu and Martius (2020), we use the K-nearest neighbors (KNN) algorithm to accelerate solving the HMPC problem. The basic principle of the algorithm is that KNN can help greatly reduce the scale of the MIP problem at each time step. This algorithm will be designed to be simple yet effective and easy to implement.

5.2.4 Contributions

This study makes the following contributions.

- To the best of our knowledge, we are pioneers in considering the VSL problem on WCL. The study addresses a significant research gap in real-time traffic control problems in the DWC scenario.
- Building upon the work of Csikós and Kulcsár (2017); Tan et al. (2022) and Chapter 4, we propose a system predictive model that incorporates both the VSL and EVs' SOC into the CTM in a mathematically convenient way. The entire model is formulated into a PWA system through reasonable parameter design and linearization techniques. We then propose a control model based on a HMPC approach tailored to our system predictive model.

- We propose a simple-yet-effective algorithm to accelerate the MILP problem for HMPC, called after *learning from K-nearest neighbors mode sequences (LKNMS)*. The algorithm can greatly reduce the scale of MILP by exploiting the historical solution information and hence accelerate the solving procedure, making it applicable to real-time control tasks. Moreover, it has the potential to generalize to other high-dimensional PWA systems.

5.3 Problem statement

In this study, we consider a VSL control problem on WCLs in the context of an advanced intelligent transportation system (ITS). The WCL is deployed on a highway segment dedicated to providing charging service for the DWC EVs. VMS is installed along the entire road to regulate the travel speeds of EVs. The ITS can gather real-time data on both traffic and charging demands from EVs, enabling the formulation of the VSL control strategy accordingly. For example, when EVs entering the WCL tend to charge as much as possible while aiming to complete their journey within a specified time interval, the VSL control problem is to maximize the charging efficiency while considering travel time constraints. In this way, the traffic operator can adjust the WCL's speed limits in alignment with EVs' preferences and requirements.

5.4 MODELLING

This section describes the proposed system predictive model and the control model. The overall modelling framework is depicted in Fig. 5.2.

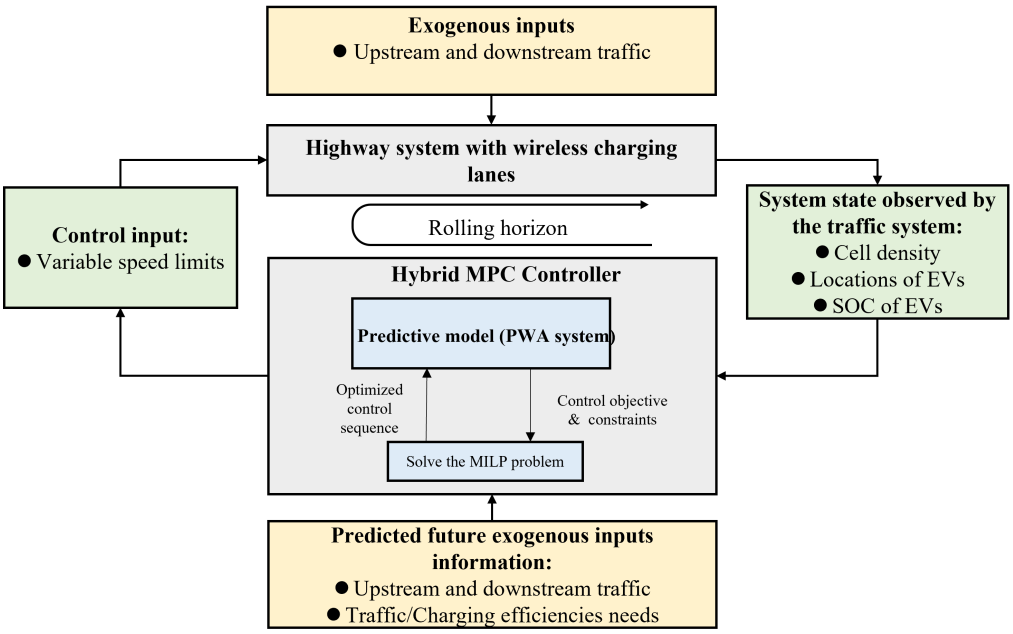

Figure 5.2: Modelling framework for study 2

5.4.1 System predictive model

In this section, we propose an extended CTM that can describe the evolution of both traffic flow characteristics and EVs' SOC. We inherit the model formulations used in Csikós and Kulcsár (2017) and Chapter 4 and extend them to the VSL scenario. We describe the traffic flow dynamics using the Godunov discretization scheme, similar to Csikós and Kulcsár (2017). Additionally, we describe the EVs' SOC in groups, similar to Chapter 4. The entire model is formulated as a well-posed PWA system in a mathematically convenient way through appropriate parameter settings and linearization techniques.

Traffic flow dynamics

The law of conversation based on the Godunov discretization scheme is described as follows:

$$\rho_i(k+1) = \rho_i(k) - \frac{\Delta t}{\Delta l}(G(\rho_i(k), \rho_{i+1}(k)) - G(\rho_{i-1}(k), \rho_i(k))) \tag{5.1}$$

where Δt and Δl represent the discrete time step and discrete space step. $G(\rho_i, \rho_{i+1})$ denotes the Godunov flux between segment i and segment $i+1$. For simplicity, we hereafter denote Godunov flux as q_i, hence $q_i = G(\rho_i, \rho_{i+1})$. We also assume both Δt and Δl are equal to 1. Then we have:

$$\rho_i(k+1) = \rho_i(k) - q_{i-1}(k) + q_i(k) \tag{5.2}$$

where q_i can be expressed as the minimum of the sending flow of segment i, q_i^s and the receiving flow of segment $i+1$, q_i^r:

$$q_i = \min[q_i^s, q_{i+1}^d] \tag{5.3}$$

Here q_i^s and q_i^r can be described as the supply flow of an upstream segment and the demand of a downstream segment:

$$q_i^s = \begin{cases} v_{f,i}\rho_i & if\ \rho_i \le \rho_{c,i} \\ q_{c,i} & if\ \rho_i > \rho_{c,i} \end{cases} \qquad q_i^r = \begin{cases} q_{c,i} & if\ \rho_i \le \rho_{c,i} \\ w(\rho_{J,i} - \rho) & if\ \rho_i > \rho_{c,i} \end{cases} \tag{5.4}$$

where $v_{f,i}$ denotes the speed limit; $\rho_{c,i}$ and $q_{c,i}$ denote the critical density and the capacity flow of segment i, which are defined as:

$$\rho_{c,i} = \frac{\rho_{J,i} w}{w + v_{f,i}} \tag{5.5}$$

$$q_{c,i} = \rho_{c,i} v_{f,i} = \frac{\rho_{J,i} w v_{f,i}}{w + v_{f,i}} \tag{5.6}$$

Notably, $\rho_{c,i}, q_{c,i}$ are nonlinear functions of $v_{f,i}$, however, they can be approximated as PWA functions by piecewise linear interpolation method.

We hereafter denote the approximate variables as $\hat{\rho}_{c,i}, \hat{q}_{c,i}$, defined as:

$$\rho_{c,i} = f_i^{PWA,\rho_c}(v_{f,i}) \tag{5.7}$$

$$q_{c,i} = f_i^{PWA,q_c}(v_{f,i}) \tag{5.8}$$

An example of PWA approximations Fig. 5.3 shows some examples of $\hat{\rho}_{c,i}, \hat{q}_{c,i}$, where v_f ranges from 0.3 to 0.5.

Table 5.1: Parameters

Symbols	Definitions	Units
Parameters		
Δt	Length of time step	sec
N	Number of segments	/
e	Charging rate of EVs travelling within segment i	percent
w_i	Congestion wave speed of segment i	segment
T_{tot}	Total simulation time	period
$\rho_{c,i}$	Critical density of segment i	veh/segment
$\rho_{J,i}$	Jam density of segment i	veh/segment
τ_m	Maximum possible travel time under consideration	/
Variables		
$v_{f,i}$	Variable speed limit of segment i	segment/period
ρ_i	Density of segment i	veh/segment
l_j	Location of EVs that have travelled j period	/
s_j	SOC of EVs that have travelled j period	percent
q_i	Number of vehicles flowing from segment i to segment $i+1$	veh
q_i^s	Sending flows of segment i	veh
q_i^r	Receiving flows of segment i	veh
v_i	Average speed of traffic within segment i	segment/period
v_j^{EV}	Speed of the jth group of EVs	segment/period
p_i	Consumption rate of EVs travelling within segment i	percent
p_j^{EV}	Consumption rate of jth group of EVs	percent
η	Total net energy replenishment of EVs	percent
π_i	McCormick relaxation term for bilinear term $v_{f,i}\rho_i$	veh

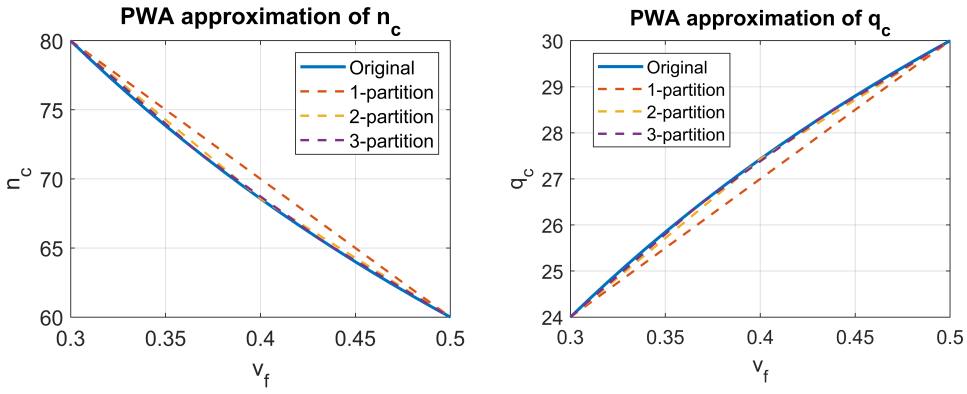

Figure 5.3: PWA approximation of n_c and q_c

It is also notable that the term $v_{f,i}\rho_i$ in Eq. (5.4) is bilinear. We therefore replace it with a relaxation term π_i using the McCormick relaxation technique. The bilinear term $v_{f,i}\rho_i$ can be replaced by a relaxation term π_i by adding the following four sets of constraints:

$$\begin{aligned}
\pi_i &\leq v_{f,i}^L \rho_i + v_{f,i}\rho_i^U - v_{f,i}^L \rho_i^U \\
\pi_i &\leq v_{f,i}^U \rho_i + v_{f,i}\rho_i^L - v_{f,i}^U \rho_i^L \\
\pi_i &\geq v_{f,i}^U \rho_i + v_{f,i}\rho_i^U - v_{f,i}^U \rho_i^U \\
\pi_i &\geq v_{f,i}^L \rho_i + v_{f,i}\rho_i^L - v_{f,i}^L \rho_i^L
\end{aligned} \tag{5.9}$$

where $v_{f,i}^L, v_{f,i}^U, \rho_i^L, \rho_i^U$ denote the lower and upper bound values of vsl_i and ρ_i, respectively. A tighter relaxation can be achieved by a piecewise McCormick relaxation (Castro, 2015) by dividing the domain of given variables into partitions to get their tighter bounds. In this study, we adopt piecewise McCormick relaxation with bivariate partitioning. Let $a \in \{1, ..., A\}$ and $b \in \{1, ..., B\}$ denote the number of predefined partition for vsl_i and ρ_i, respectively. Let binary variable δ_i^{ab} indicate the active partition for variables $v_{f,i}$ (bounded by $v_{f,i}^{L_a}$ and $v_{f,i}^{U_a}$) and n_i (bounded by $n_i^{L_b}$ and $n_i^{U_b}$), hence:

$$[\delta_i^{ab} = 1] \leftrightarrow [vsl_i \in [v_{f,i}^{L_a}, v_{f,i}^{U_a}], \rho_i(k) \in [n_i^{L_b}, n_i^{U_b}]] \tag{5.10}$$

This is implemented by:

$$
\begin{aligned}
\pi_i &\leq \sum_{a=1}^{A}\sum_{b=1}^{B} v_{f,i}^{L_a}\hat{\rho}_i^{ab} + \hat{v}_{f,i}^{ab}\rho_i^{U_b} - v_i^{L_a}\rho_i^{U_b}\delta^{ab} \\
\pi_i &\leq \sum_{a=1}^{A}\sum_{b=1}^{B} v_{f,i}^{U_a}\hat{\rho}_i^{ab} + \hat{v}_{f,i}^{ab}\rho_i^{L_b} - v_{f,i}^{U_a}\rho_i^{L_b}\delta^{ab} \\
\pi_i &\geq \sum_{a=1}^{A}\sum_{b=1}^{B} v_{f,i}^{U_a}\hat{\rho}_i^{ab} + \hat{v}_{f,i}^{ab}\rho^{U_b} - v_{f,i}^{U_a}\rho^{U_b}\delta^{ab} \\
\pi_i &\geq \sum_{a=1}^{A}\sum_{b=1}^{B} v_{f,i}^{L_a}\hat{\rho}_i^{ab} + \hat{v}_{f,i}^{ab}\rho^{L_a} - v_{f,i}^{L_a}\rho^{L_b}\delta^{ab} \\
v_{f,i} &= \sum_{a=1}^{A}\sum_{b=1}^{B} \hat{v}_{f,i}^{ab} \\
\rho_i &= \sum_{a=1}^{A}\sum_{b=1}^{B} \hat{\rho}_i^{ab} \\
1 &= \sum_{a=1}^{A}\sum_{b=1}^{B} \delta^{ab} \\
v_{f,i}^{L_a}\delta^{ab} &\leq \hat{v}_{f,i}^{ab} \leq v_{f,i}^{U_a}\delta^{ab} \\
\rho_i^{L_a}\delta^{ab} &\leq \hat{\rho}_{f,i}^{ab} \leq \rho_i^{U_a}\delta^{ab}
\end{aligned}
\tag{5.11}
$$

Then Eq.(5.4) can be rewritten as:

$$
q_i^s = \begin{cases} \pi_i & if\ \rho_i \leq \hat{\rho}_{c,i} \\ \hat{q}_{c,i} & if\ \rho_i > \hat{\rho}_{c,i} \end{cases} \qquad \hat{q}_i^r = \begin{cases} q_{c,i} & if\ \rho_i \leq \hat{\rho}_{c,i} \\ w(\rho_{J,i} - \rho) & if\ \rho_i > \hat{\rho}_{c,i} \end{cases} \tag{5.12}
$$

Note that the actual operating speed limit may not precisely match the commanded speed limit signal. This phenomenon is accounted for by introducing a scaling factor to the commanded speed limit values, as elucidated in Remark 1 of Csikós and Kulcsár (2017). In this study, we assume that this scaling factor is set to 1.

Dynamics of EVs' location and SOC

In our model, EVs are grouped and indexed by their entry time j, for $j = 1, ..., \tau_m$ where τ_m denotes the maximum possible travel time on the road segment under consideration. Then the location and SOC of jth EV group are updated as follows:

$$l_{j+1}(k+1) = l_j(k) + v_j^{EV}(k) \tag{5.13}$$

$$s_{j+1}(k+1) = s_j(k) - p_j^{EV}(k) + e \tag{5.14}$$

where e is the charging rate that is assumed to be a constant; v_j^{EV} and p_j^{EV} denote the speed and the change of SOC of jth group of EVs. Their values depend on which segment the EVs are located in: defined as:

$$v_j^{EV}(k) = v_i(k) \ for \ i - 1 \leq l_j(k) < i \tag{5.15}$$

$$p_j^{EV}(k) = p_i(k) \ for \ i - 1 \leq l_j(k) < i \tag{5.16}$$

where v_i and p_i are the speed and the consumption rate of EVs within segment i. Here we derive v_i and p_i in a way similar to Chapter 4, both of which can be expressed as a function of density ρ_i and speed limit $v_{f,i}$. We use a triangular fundamental diagram to describe the intracellular flow of segment i. Then v_i is expressed by a function of both $v_{f,i}$ and ρ_i. As depicted in Fig. 5.4a, when the density of segment i is below its critical density, v_i equals to the speed limit $v_{f,i}$. Whereas, when the density of segment i exceeds its critical density, v_i can be expressed as a nonlinear function of ρ_i, which can be approximately expressed as a PWA function by piecewise linear interpolation technique. Then we have:

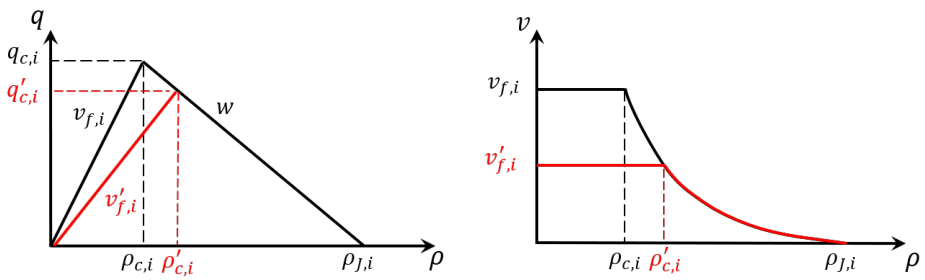

(a) Flow-Density (b) Speed-Density

Figure 5.4: Modifying effect of VSL on the speed

$$v_i = \begin{cases} v_{f,i} & if\ \rho_i \leq q_{c,i} \\ f_i^{PWA,v}(\rho_i) & if\ \rho_i > q_{c,i} \end{cases} \quad p_i = \begin{cases} v_{f,i} & if\ \rho_i \leq q_{c,i} \\ f_i^{PWA,p}(\rho_i) & if\ \rho_i > q_{c,i} \end{cases} \tag{5.17}$$

where $f_i^{PWA,v}, f_i^{PWA,p}$ are the PWA approximation functions for speed and consumption rate, respectively. For detailed equations, please refer to Chapter 4.

Dynamics of total net energy replenishment

The total net energy replenishment refers to the total increase of EVs' SOC, denoted as $\eta(k)$. It is an important indicator of charging efficiency. Hence, it is defined as:

$$\eta(k) = \sum_{j=1}^{\tau_m} e_j^{EV}(k) \quad if\ l_j(k) < N \tag{5.18}$$

PWA system

The system state is collected in the vector $\boldsymbol{x} = [\boldsymbol{\rho}, \boldsymbol{l}, \boldsymbol{s}]^{\mathrm{T}}$, where $\boldsymbol{\rho} = [\rho_1, ..., \rho_N]$, $\boldsymbol{l} = [\rho_1, ..., \rho_{\tau_m}]$, $\boldsymbol{s} = [s_1, ..., s_{\tau_m}]$ The control input is collected in the vector $\boldsymbol{u} = [\boldsymbol{\pi}, \boldsymbol{v}_f]^{\mathrm{T}}$, where $\boldsymbol{\pi} = [\pi_1, ..., \pi_N]$, $\boldsymbol{v}_f = [v_{f,1}, ..., v_{f,N}]$ The boundary conditions of the system are considered as exogenous inputs, col-

lected in the vector $\boldsymbol{d} = [\rho_0, \rho_{N+1}]$.

5.4.2 Control model

In this section, we design four controllers with different aims. Controller #1 and #3 are designed to maximize traffic efficiency, while controllers #2 and #4 are designed to maximize charging efficiency. In addition, controllers #3 and #4 also ensure a certain level of charging efficiency and traffic efficiency. respectively. Based on the concept of hybrid MPC, the control problem at time k is a MILP problem. The control result is the optimal control sequence $\boldsymbol{v}_f(k), \boldsymbol{v}_f(k+1), ..., \boldsymbol{v}_f(k+P-1)$. For controller #1 and #3, the optimization problem at time k is formalized as:

$$\min_{\boldsymbol{u}_k \ldots \boldsymbol{u}_{k+P-1} \in \mathbb{R}^V} J_1(k) = \sum_{p=1}^{P} \|Q(\boldsymbol{\rho}(k+p|k) - \boldsymbol{\rho}_c(k+p))\|_1 + \|\kappa(\boldsymbol{v}_f(k+p|k) - \boldsymbol{v}_f(k+p-1|k))\|_1 + \xi g^+ \tag{5.19}$$

s.t.

$$(5.2)(5.3)(5.4)\ (5.7)(5.8)\ (5.12)\ (5.11)(5.13)(5.15)(5.17)(5.18) \tag{5.19a}$$

$$\boldsymbol{x}^{min} \leq \boldsymbol{x}(k+p|k) \leq \boldsymbol{x}^{max} \qquad k = 1, ..., P \tag{5.19b}$$

$$\boldsymbol{u}^{min}(k+p) \leq \boldsymbol{u}(k+p) \leq \boldsymbol{u}^{max}(k+p) \qquad for\ k = 1, ..., P-1 \tag{5.19c}$$

$$\Delta\boldsymbol{u}^{min} \leq \boldsymbol{u}(k+p) - \boldsymbol{u}(k+p-1) \leq \Delta\boldsymbol{u}^{max} \qquad k = 1, ..., P-1 \tag{5.19d}$$

$$\rho_0(k+p|k) = d^1(k) \qquad k = 1, ..., P \tag{5.19e}$$

$$\rho_{N+1}(k+p|k) = d^2(k) \qquad k = 1, ..., P \tag{5.19f}$$

$$\eta(k+p|k) + g^+ \geq \eta^{min} \qquad k = 1, ..., P \tag{5.19g}$$

$$g^+ \geq 0 \tag{5.19h}$$

where Q and κ are the pre-selected weightings.

(5.19a) are system dynamics.

(5.19b) are the state constraints. The upper bound of $\boldsymbol{\rho}$ is $\boldsymbol{\rho}_J$ while its lower bound is $\mathbf{0}$. The upper bound of $\boldsymbol{l}$ and $\boldsymbol{s}$ are assigned their maximum possible values. Note that a lower limit on SOC can be added for practical needs.

(5.19c) are the constraints on control input $\boldsymbol{u}$. Here, they refer to the upper and lower bounds of $\boldsymbol{v}_f$.

(5.19d) are the constraints on the delta changes of $\boldsymbol{v}_f$. Here, they refer to the upper and lower bounds of $\boldsymbol{v}_f$. Their values depend on the need for

safety and stability of traffic flow Tan and Gao (2018).

(5.19e) and (5.19f) are the boundary conditions of the system, whose values are assigned exogenous input $\boldsymbol{d}$.

(5.19g) limits the minimum charging efficiency at each stage. η^{min} is a constant. g^+ is a relaxation term that is non-negative (5.19h). ξ is a pre-determined large positive value. Hence, (5.19g) is a soft constraint.

For controller #2 and #4, the optimization problem at time k is formalized as follows:

$$\min_{\boldsymbol{u}_k \dots \boldsymbol{u}_{k+P-1} \in \mathbb{R}^V} J_2(k) = \sum_{p=1}^{P} -\eta(k+p|k) + \|\kappa(\boldsymbol{v}_f(k+p|k) - \boldsymbol{v}_f(k+p-1|k)\|_1 + \xi g^+ \tag{5.20}$$

s.t.

$$(5.2)(5.3)(5.4)(5.7)(5.8)(5.12)\ (5.11)(5.13)(5.15)(5.17)(5.18) \tag{5.20a}$$

$$\boldsymbol{x}^{min} - g^+ \leq \boldsymbol{x}(k+p|k) \leq \boldsymbol{x}^{max} \qquad for\ k = 1, ..., P \tag{5.20b}$$

$$\boldsymbol{u}^{min}(k+p) \leq \boldsymbol{u}(k+p) \leq \boldsymbol{u}^{max}(k+p) \qquad for\ k = 1, ..., P-1 \tag{5.20c}$$

$$\Delta\boldsymbol{u}^{min} \leq \boldsymbol{u}(k+p) - \boldsymbol{u}(k+p-1) \leq \Delta\boldsymbol{u}^{max} \qquad for\ k = 1, ..., P-1 \tag{5.20d}$$

$$\rho_0(k+p|k) = d^1(k) \qquad for\ k = 1, ..., P \tag{5.20e}$$

$$\rho_{N+1}(k+p|k) = d^2(k) \qquad for\ k = 1, ..., P \tag{5.20f}$$

$$g^+ \geq 0 \tag{5.20g}$$

where Q and κ are the pre-selected weightings.

(5.20a) are dynamics the system. (5.20b) are the state constraints. Apart from the constraints in (5.19b), the state constraints also contain the lowest limit on l_j where j is the maximal travel time to ensure a certain level of traffic efficiency. Note that (5.19b) is a soft constraint with the relaxation term g^+ introduced, similar to (5.19g). (5.20c)(5.20d) (5.20e) are identical to (5.19c)(5.19d)(5.19e).

5.4.3 Approximate HMPC by learning from K-nearest neighbors mode sequences (LKNMS)

As mentioned earlier, the primary challenge of our HMPC problem is associated with the exponential growth of the scale of the MILP problem as the dimension of the hybrid system increases. In the worst case, the solver must exhaustively enumerate all possible combinations of integer variables and solve that many LP problems, rendering the task computationally intractable. However, we observe that the set of states in a high-dimensional PWA system (each state corresponding to an integer variable if the PWA system is well-posed) that can be reached from a given initial state is constrained. This observation implies that, by accurately predicting the reachable states before solving a given MILP problem, it is easy to eliminate the inactive integer variables and their associated logical constraints. Consequently, this reduction in the size of the MILP formulation leads to a considerably more concise MILP problem, effectively mitigating the computational burden. Hence, our idea can be briefly summarized as follows: "Remove the predicted inactive integer variables before solving the MILP at each time step by leveraging historical data on integer solution configurations." As mentioned in Sec. 5.2.3, Zhu and Martius (2020) aims to find

a feasible mode sequence (integer variables configuration) from the nearest neighbor of the given x_0. Our algorithm aims to obtain a set of inactive integer variables from K nearest neighbors of the given x_0. The algorithm identifies the K-nearest neighbors $\{d_1, d_2, \ldots, d_K\}$ of the initial state $\mathbf{x}_0$ using the Euclidean distance metric. The Euclidean distance between the current state $\mathbf{x}_0$ and a historical state $\mathbf{x}_i$ is given by:

$$d(x_0, x_i) = \sqrt{\sum_{j=1}^{n} (x_{0,j} - x_{i,j})^2},$$

The detailed algorithm is explained in Alg. 1. For the remainder of the chapter, we refer to the proposed algorithm as *approximate HMPC by learning from K-nearest-neighbors mode sequences (LKNMS).*

5.5 Numerical example

5.5.1 Simulation setup

Algorithm 1: LKNMS Algorithm

Input: Data set $\mathbf{D}, \mathbf{M}$, initial state $\mathbf{x}_0$, number of neighbors K
Output: Optimal control sequence $\mathbf{u}$

Find K nearest neighbors $d_1, ..., d_K$;
Obtain the element-wise sum of the integer solutions of these neighbors $m_{x_0} = \sum_{i=1}^{K} m_i$;
Extract all the unactivated integer variables ;
Delete the constraints of the original MILP that corresponds to the unactivated integer variables ;
Solve the simplified MILP problem ;
if *Exists a feasible solution* **then**
    Obtain the optimal solution $\mathbf{u}$;
    Apply $\mathbf{u}_0$ into the system
else
    Use more neighbors (bigger K), go back to Step 1
end

In this section, we conduct a simulation study of the proposed control model for a numerical experiment. We consider a 10.7-km WCL that is divided into 4 identical cells (so $N = 4$). For the McCormick relaxation terms, we use two partitions for both ρ_i and $v_{f,i}$ (so $A = B = 2$). The bounds of each partition and other detailed parameter values of the controllers are depicted in Table. 5.2. We design 3 scenarios as follows. In Scenario #1, the system initiates with low traffic volumes; upstream demand is low, and downstream conditions remain uncongested. In Scenario #2, the system starts with moderate traffic levels; upstream demand is still low, but downstream experiences congestion from time 5 to 10. In Scenario #3, the system initiates with light traffic; downstream remains uncongested, but the flow capacity of segment 3 decreases by one-third between times 5 and 10. We evaluate the overall performance of the controllers by four metrics: total time spent (TTS), total travel distance (TTD), network average speed (NAS), and total net energy replenishment (TER). The four metrics are similar to that used in Csikós and Kulcsár (2017) and Chapter 4.

- *Total time spent (TTS)*:

$$TTS = \sum_{k=1}^{T} \sum_{i=1}^{N} \rho_i(k) \tag{5.21}$$

- *Total travel distance (TTD)*:

$$TTD = \sum_{k=1}^{T} \sum_{i=1}^{N} q_i(k) \tag{5.22}$$

- *Network average speed (NAS)* $\bar{v}$:

$$NAS = \frac{TTD}{TTT} \tag{5.23}$$

- *Total net energy replenishment (TER)*:

$$TER = \sum_{k=1}^{T} \eta(k) \tag{5.24}$$

5.5.2 Approximate HMPC by learning from K-nearest-neighbors mode sequences

Dataset Generation

To facilitate the proposed LKNMS algorithm, we generate datasets denoted as D, M:

$$D = \{d_i \mid i = 1, ..., 1000\} \tag{5.25}$$

$$M = \{m_i \mid i = 1, ..., 1000\} \tag{5.26}$$

where D is the set of initial states, d_i; M is the set of integer solutions, m_i, corresponding to d_i. For a general high-dimensional PWA system whose state space is a convex polytope, uniformly distributed samples are needed, which can be generated by the Markov chain Monte Carlo (MCMC) method. An efficient and simple MCMC sampler for a convex polyhedron is the hit-and-run (HAR) sampler. We refer interested readers to Smith (1996) for a detailed theoretical introduction. Moreover, a more efficient and faster MCMC sampling algorithm is proposed in Corte and Montiel (2021). The algorithm is termed "Matrix Hit and Run" (MHAR) since it takes advantage of matrix multiplication routines that require less computational and memory resources than a normal HAR sampler, especially when sampling in a high-dimensional polytope. However, in our case, the state vector elements are correlated, which means that uniform sampling may generate unrealistic samples. Therefore, we generate 1000 time-series

data samples that consist of 30 individual simulations. Each simulation lasts for about 33 periods and begins with an initial state of light traffic. Each initial state $\boldsymbol{x}(0)$ is composed of two elements: (1) $\boldsymbol{\rho}(0)$, a 4×1 vector randomly sampled within the range of $[50, 60]$; and (2) $\boldsymbol{l}(0)$ and $\boldsymbol{s}(0)$, which are generated according to $\boldsymbol{\rho}(0)$ (assume light traffic conditions).

Performance Evaluation

We conducted an extra simulation study to evaluate the performance of the LKNMS approach. The initial value of K is selected to be 30. We compare the performance of the naive HMPC approach and the approximate HMPC by LKNMS approach under Scenario #1 in terms of three aspects:

- Optimization Performance: involves 1) Cost, i.e., objective function value; and 2) reduction in the number of integer variables involved in MILP.
- Computational Efficiency: involves 1) the solving time of the MILP at each time step; and 2) the time spent on neighbor searches.
- Feasibility: involves handling different scenarios and avoiding infeasible solutions.

Table 5.2: Parameter used in numerical examples

Δt	T_{tot}	$\rho_{c,i}$	$\rho_{J,i}$	w	N	e	τ_m
60	30	60	160	0.3	4	1	14
$v_{f,i}^{L_1}$	$v_{f,i}^{U_1}$	$v_{f,i}^{L_2}$	$v_{f,i}^{U_2}$	$\rho_i^{L_1}$	$\rho_i^{U_1}$	$\rho_i^{L_2}$	$\rho_i^{U_2}$
0.3	0.4	0.4	0.5	0	60	60	160

In our model, $v_{f,i}^{U_2}$ corresponds to 80 km/h

5.5.3 Results and Discussions

Simulation result with the normal HMPC

We use the YAMLIP toolbox to build the MILP problem in MATLAB. We use Gorubi 10.0.1 solver to compute the optimal solution to the MILP in an online fashion. The simulation is processed on a server (Intel Xeon Gold 6342 CPU @2.80 GHz, 96 processors, RAM 512 G). We simulate the closed-loop performance of the proposed four controllers for each scenario. The control results $\{v_{f,i}\}$ are shown in Fig. 5.5. The density profile is shown in Fig. 5.7. The overall performance in (1) traffic efficiency, evaluated by NAS, and (2) charging efficiency, evaluated by TER, is depicted in Fig. 5.6 and Table. 5.3. It can be observed that, in all scenarios, Controller #1 exhibits the highest TER but the lowest NAS, conversely, controller #2 exhibits the lowest TER but the highest NAS. Controllers #3 and #4 exhibit similar performance, both displaying intermediate levels of TER and NAS. The biggest difference between the two metrics occurs in scenario #1 where both the initial traffic volumes and traffic demand are low.

In Scenario #1, the traffic on the road is light throughout the simulation. As shown in Fig. 5.5, controller #1 tends to maintain the highest speed limit (0.5) while controller #2 tends to impose the lowest speed limit (0.3), to maximize the energy replenishment of EVs. Therefore, the density profile for controller #1 remains low. By contrast, the reduction in speed limits of all segments imposed by controller #2 results in a forward-propagating congestion wave and eventually stabilizes at a relatively high level. Similar to controller #1 and #2, controllers #3 and #4 also yield opposite results. In the beginning, they both impose lower speed limits. However, controller #3 eventually imposes progressively increasing (from segment 1 to 4) speed limits. By contrast, Controller #4 imposes progressively decreasing speed

limits instead. They also result in contrasting density distribution trends in spatial dimensions (Note that the speed limit values can vary by at most 0.05 between adjacent segments). This difference is caused by the design of the control model. Constraints can be made more stringent in cases where there is a high demand for traffic safety and stability, for example, by employing a smaller value for speed limit variation. Fig. 5.6 illustrates the overall performance of the four controllers in terms of TER and NAS. Controller #1 exhibits the highest TER but the lowest NAS, conversely, controller #2 exhibits the lowest TER but the highest NAS. Controllers #3 and #4 exhibit similar performance, both displaying intermediate levels of TER and NAS.

In Scenario #2, a transient congestion event arises downstream. As illustrated in Fig. 5.5, controller #1 tends to mitigate the shockwave by imposing varying levels of VSL signals across different segments in both spatial and temporal domains. This result is consistent with the observation in Sec 5.1 in Csikós and Kulcsár (2017). The control results of controller #2 and #4 closely resemble those observed in Scenario #1. Controller #3, however, yields a distinct VSL result. It tends to uniformly decrease the speed limits across all segments (with some fluctuations in between), ultimately stabilizing at a relatively low value. Accordingly, as depicted in Fig. 5.7, its density profile is nearly evenly distributed, which differs from that of controller #4. In terms of TER and NAS performance, they closely resemble that in scenario #1.

In scenario #3, the flow capacity of segment 3 experiences a sudden drop for a short period. Note that it is assumed that the controllers can observe the capacity drop. As illustrated in Fig. 5.5, although the capacity drop can be treated as another form of downstream congestion, the decreasing speed limits imposed by controller #1 emerge upstream, opposite to those

in scenario #2. This is because the initial traffic volume on the road differs in the two scenarios. The control results of the other three controllers closely resemble those in scenario #2. Notably, the controller #3 imposes more fluctuated speed limits. Analyzing the density profile, as depicted in Fig. 5.7, we observe distinct congestion dynamics under different controllers. Under the influence of Controller #1, congestion resulting from the capacity drop is rapidly mitigated and nearly dissipates by time 27. Controller #2, in stark contrast, substantially increases density over time. Controller #3 and #4 fall in between, resulting in a moderate congestion level.

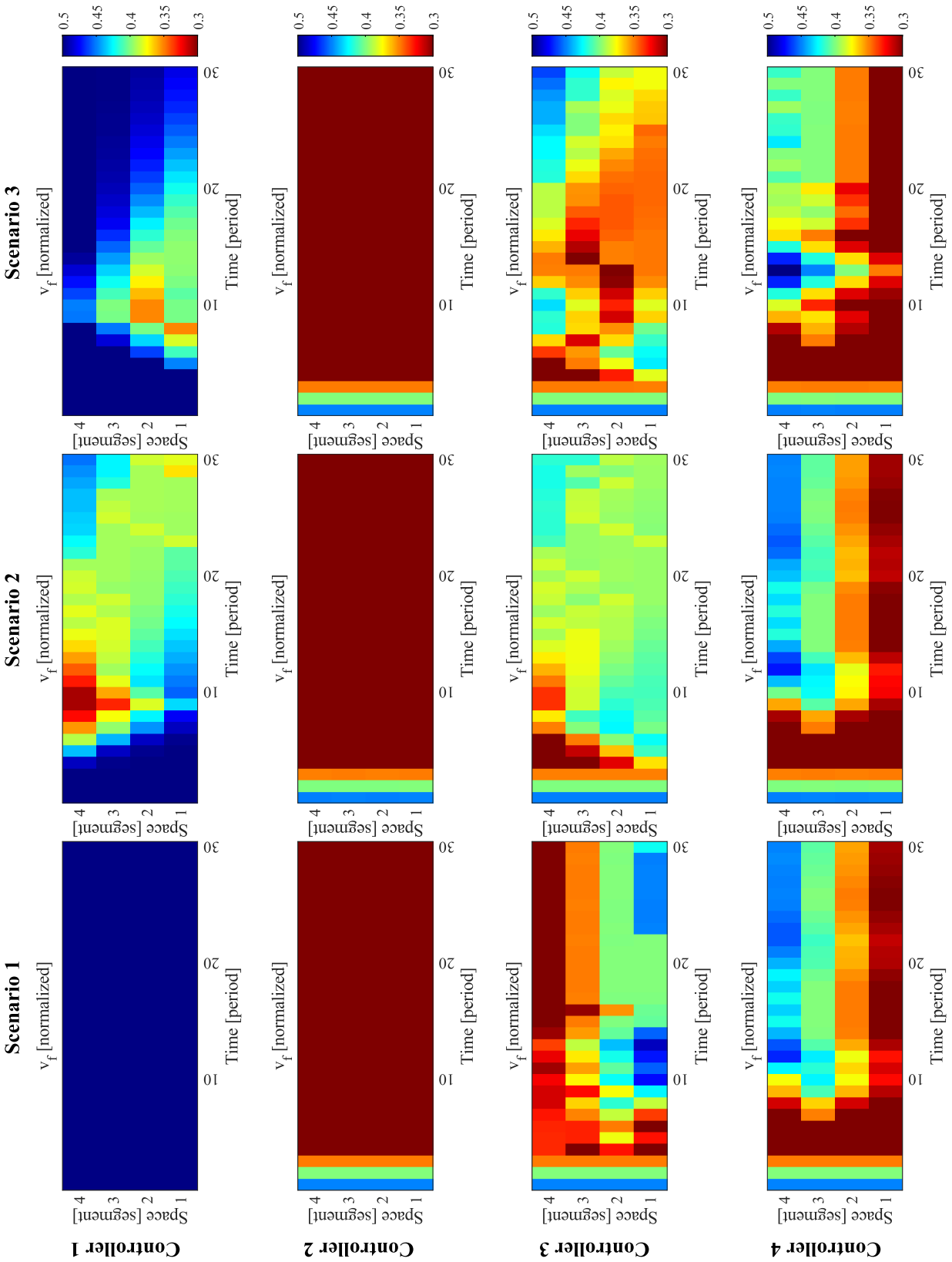

Figure 5.5: VSL control result

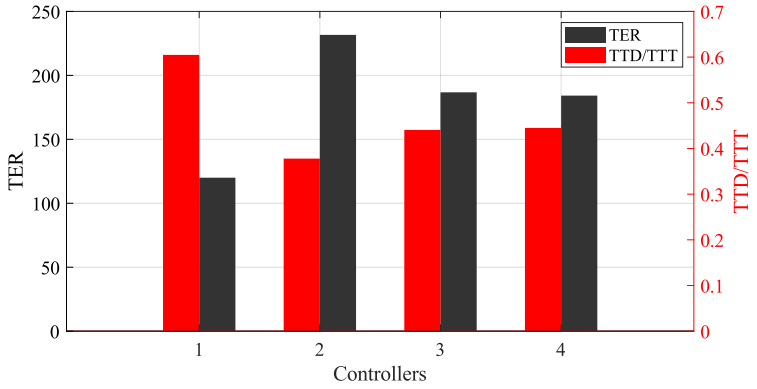

(a) Scenario 1

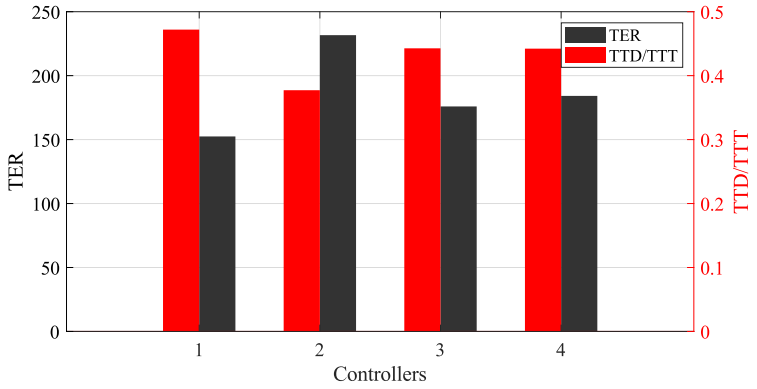

(b) Scenario 2

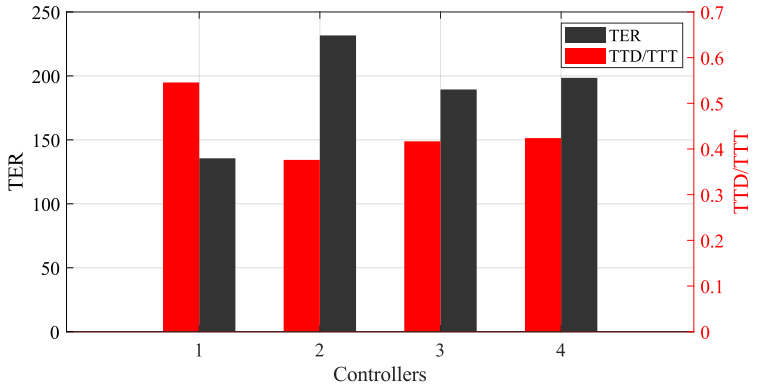

(c) Scenario 3

Figure 5.6: Performance in terms of TER and TTD/TTT

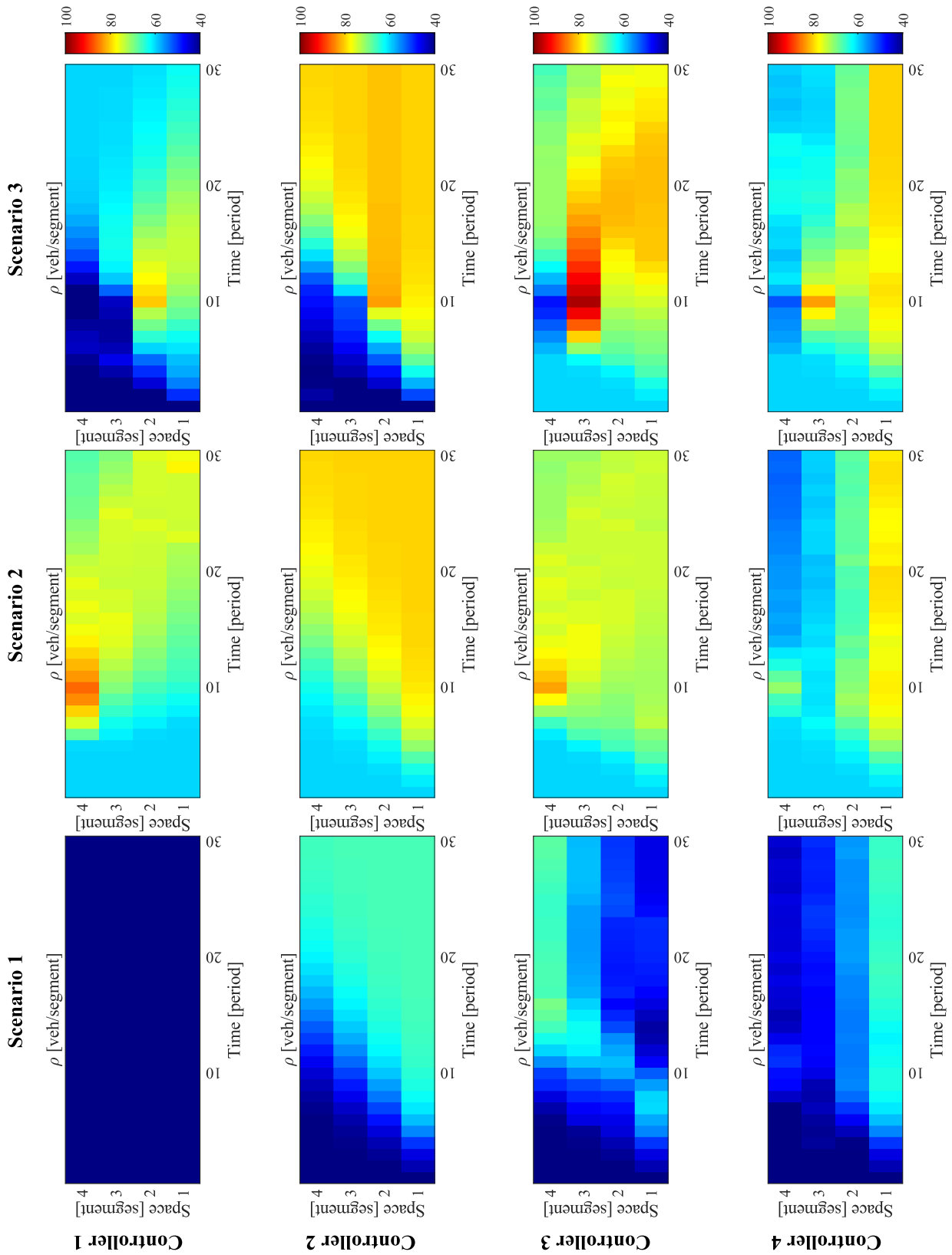

Figure 5.7: Density profile

Table 5.3: Performance of controllers

Scenario	Controller	TER	TTT	TTD	NAS
1	1	120.00	4960.03	3000.04	0.60
	2	231.65	7237.00	2733.92	0.38
	3	186.74	6536.03	2879.52	0.44
	4	184.17	6349.13	2825.23	0.44
2	1	152.46	8696.77	4104.66	0.47
	2	231.65	9134.01	3445.46	0.38
	3	175.92	8881.36	3931.90	0.44
	4	184.16	8097.14	3580.57	0.44
3	1	135.57	7318.75	3993.23	0.55
	2	231.65	8619.65	3242.39	0.38
	3	189.39	9061.05	3776.60	0.42
	4	198.48	8383.54	3553.16	0.42

5.6 Results for LKNMS

5.6.1 Performance of LKNMS

Regarding optimization performance, Fig. 5.8c illustrates a significant reduction in the number of integer variables in the MILP problem achieved by the *LKNMS* algorithm. As depicted in Table 5.4, this reduction rate reaches $60 \sim 67\%$. Fig. 5.8b compares the closed-loop cost between *LKNMS* and the naive HMPC approach. Overall, the optimality gap remains small throughout the entire simulation process, with an average value of $7\%, 1\%, 0\%$ for $K = 30, 50, 70$, respectively. The largest gap is recorded at 29% at time step 7 when $K = 30$, however, the gap disappears when K is increased to

70.

Regarding computational efficiency, Fig. 5.8a compares the solving time for the MILP problem between the naive HMPC and *LKNMS* approaches. It is evident that *LKNMS* substantially reduces the solving time compared to the naive HMPC. However, it is worth noting that there is a slight increase in solving time as the number of neighbors (K) increases. This trend is consistent with the findings depicted in Fig. 5.8c, which illustrates a significant reduction in the number of integer variables in the MILP problem achieved by the *LKNMS* algorithm. Particularly noteworthy is the pronounced reduction observed from time 7 to 9, corresponding to the onset of congestion. Further discussion on this phenomenon will be provided. Fig. 5.8d compares the time spent on neighbor searches for three different values of K. Overall, the search time required for KNN is significantly shorter than the solving time for the MILP problem (in milliseconds). However, it is noteworthy that the computational time increases slightly with larger values of K. Moreover, variations in search time across different time steps, such as times 1 and 5, can be attributed to the data distribution characteristics of a given dataset.

The performance in terms of feasibility is depicted in Fig. 5.8b where it is evident that the simplified MILP is only infeasible at time 10 (becomes feasible when K is increased to 70) and time 26 (becomes feasible when K is increased to 50). Hence, the *LKNMS* algorithm successfully avoids all the infeasible models in this case. This result validates the effectiveness of the infeasibility avoidance design of the proposed *LKNMS* algorithm (See Alg. 1, step 10).

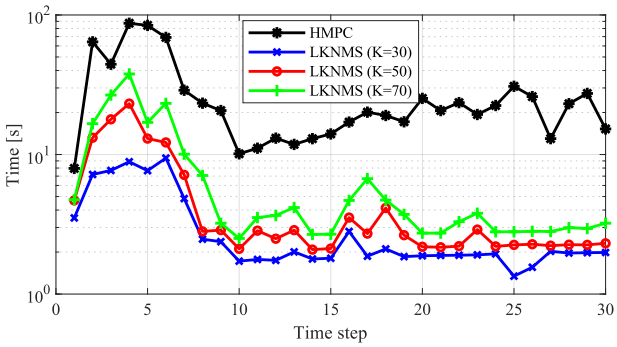

(a) Elapsed runtimes (the y-axis is in log-scale)

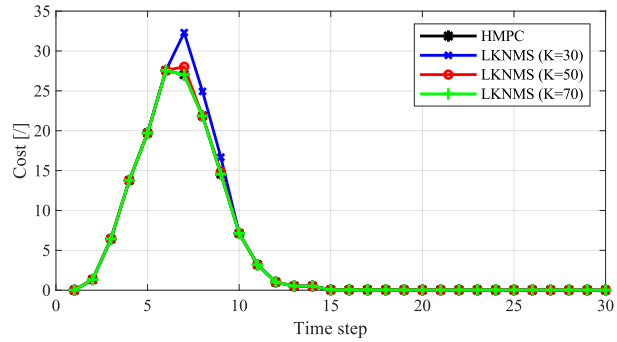

(b) Cost

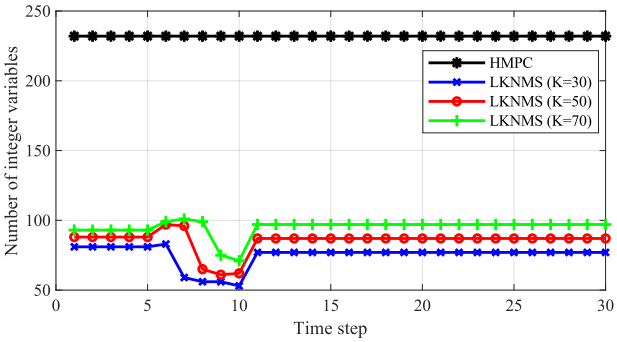

(c) Number of integer variables involved in MILP

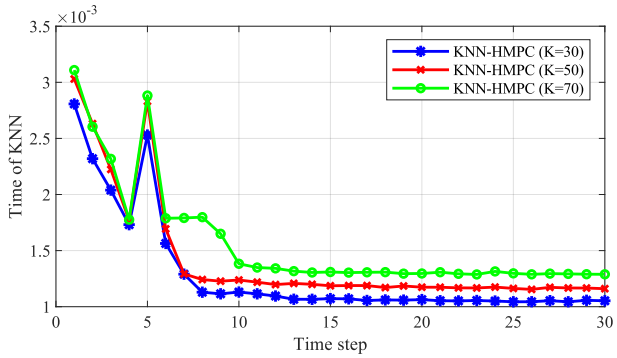

(d) Time spent for KNN

Figure 5.8: Modifying effect of VSL on the speed

	Elapsed runtimes [s]	Cost	Number of integer variables	Searching time [ms]	% Infeasibility
HMPC	27.44	4.84	232	/	/
LKNMS ($K = 30$)	3.13 (-89%)	5.19 (+7%)	76 (-67%)	1.3	6.6
LKNMS ($K = 50$)	4.99 (-82%)	4.88 (+1%)	84 (-64%)	1.4	3.3
LKNMS ($K = 70$)	7.28 (-73%)	4.84 (+0%)	93 (-60%)	1.6	0.0

Table 5.4: Performance of LKNMS

5.6.2 Limitations of LKNMS

- Dependence on Data Set: The efficacy of the *LKNMS* algorithm is intrinsically linked to the quality of the dataset employed. This quality encompasses both the volume and the uniformity of data distribution within the dataset. In an ideal scenario, a dataset with enough uniformly distributed data points enables the algorithm to simplify the original MILP problem significantly and efficiently. However, challenges arise in cases where the dataset is sparse or unrepresentative of the system's future states. Under such circumstances, the algorithm's performance might be substantially weakened (yield more infeasible solutions or execute more loops). Therefore, the generation of a robust dataset is pivotal for the successful implementation of this algorithm. Effective dataset generation can be facilitated through strategic random sampling within a pre-defined polytope, as delineated in Sec. 5.5.2.

- Dependence on K and ΔK: The selection of the initial K value and its subsequent increment, denoted as ΔK, is subject to user discretion and

has a profound impact on the algorithm's efficiency. An overly narrow K or ΔK may result in infeasible solutions and necessitate additional iterations in the *LKNMS* process, thereby escalating computational demands. Conversely, an excessively large K or ΔK can circumvent infeasible solutions, but at the cost of enlarging the (albeit simplified) MILP problem, subsequently requiring greater computational resources for resolution. Furthermore, the optimal K value is not static; it varies depending on the data distribution surrounding a specific system state. This variability suggests that developing an adaptive methodology for determining K and ΔK for a given system state, x_0, could be a significant direction for future research and development.

5.6.3 Insights for traffic operators

Understanding the impact of VSL on charging efficiency is crucial for the effective management of WCLs. In general, VSL control strategies aimed at maximizing charging efficiency tend to enforce lower speed limits across the road, whereas those prioritizing traffic efficiency are characterized by higher speed limits. In scenarios where both objectives are considered, VSL control strategies demonstrate fluctuations across both temporal and spatial dimensions (see Fig. 5.5), which adjust in response to evolving traffic conditions. As demonstrated in Table. 5.3, the prioritization of either traffic efficiency or charging efficiency yields distinct results. The most significant difference is observed in light traffic conditions (Scenario #1), where VSL control aimed at maximizing charging efficiency results in a substantial increase in TER by 93% but a reduction in NAS by 37% compared to that aimed at maximizing traffic efficiency. However, these variances in percentages become smaller under conditions of heavier traffic (Scenarios #2 and #3).

VSL control is more effective than RM control in enhancing charging efficiency for EVs. As mentioned in Chapter 4, the influence of RM control on EVs' SOC is markedly limited due to fixed speed limits and unregulated on-ramp demand. In contrast, VSL exerts a more direct and noticeable impact on EVs' SOC by dynamically modulating their speeds, thus directly influencing the energy replenishment rate. This capability positions VSL control as a superior method in optimizing EV charging efficiency compared to RM control.

However, VSL control is comparatively more challenging to implement. In our study, the effectiveness of VSL control is evaluated under the assumption that actual operating speeds precisely align with the commanded speed limit signals (where the scaling factor is equal to 1). However, achieving such precise alignment in real-world scenarios is challenging. Enhancing accuracy necessitates significant investments in advanced traffic monitoring technologies, including loop detectors, cameras, and sensors. With these technologies, a more refined VSL control can be actualized. A future scenario envisaged involves EVs receiving VSL commands via sophisticated vehicular communication systems, allowing for automatic speed adjustments by autopilot systems. This, however, requires elevated technical capabilities.

From a traffic management perspective, it is proposed that WCLs are best suited to contexts where a highly intelligent traffic system can support VSL control. The integration of advanced technologies with VSL control not only optimizes charging efficiency but also aligns with the evolving landscape of smart traffic management systems.

5.7 Conclusions and future work

In this study, we have developed a VSL control model tailored for DWC scenarios considering optimal traffic and charging efficiencies. Building upon prior research, we propose a system predictive model by incorporating the SOC of EVs into the CTM. Through thoughtful parameter design, the entire model is formulated as a high-dimensional PWA system. By a HMPC approach, the control problem at each time stage is formulated into a MILP problem. To evaluate the effectiveness of our models, we conduct a series of numerical examples on a 10.7-km WCL. Simulation results reveal the great effect of speed limit adjustments on the SOC profiles of EVs. Furthermore, our control strategies have demonstrated their ability to strike a delicate balance between traffic flow and charging efficiency according to EVs' requirements. These findings offer valuable insights for traffic operators and policymakers regarding the management of WCLs.

Given the exponential growth of the scale of MILP with the length of the WCL, we propose an innovative learning-based algorithm, *LKNMS*, specifically designed to accelerate the MILP problems for HMPC. The proposed algorithm is engineered to be both straightforward, effective, and easy to implement, which leverages historical solutions information and the properties of PWA systems. Simulation results show that the *LKNMS* can significantly reduce the scale of MILP and shorten the computational time of its solving procedure without deteriorating closed-loop performance. Furthermore, the algorithm holds the potential for further refinement and extension to other HMPC problems, particularly those involving high-dimensional PWA systems.

This study has several limitations. First, it assumes that the actual operating speed on WCLs aligns with the commanded speed limit. In reality,

however, some EVs may violate speed restrictions, introducing behavioral uncertainty that is not explicitly addressed in the model. Second, the model does not account for the complexities and uncertainties arising from driver behavior. While our focus was on addressing real-time traffic management issues on WCLs and demonstrating the feasibility and effectiveness of VSL in enhancing CE, the model was deliberately kept fundamental. Nevertheless, the complexities and uncertainties of driver behavior should be explored in future research and incorporated into the model in a mathematically tractable way. This is particularly challenging for real-time management, as overly complex control models can slow down optimization, undermining the ability to meet real-time requirements. Uncertainties related to EV heterogeneity, such as variations in vehicle type, battery properties, initial SOC, and road conditions can be modeled as random variables using methods like robust optimization or chance-constrained programming that could better address the stochastic nature of real-world traffic systems.

Our future work involves the following aspects: 1) considering the combination of multiple real-time traffic control strategies, for example, coordinated ramp metering and variable speed limit control, which is a traffic management and control strategy commonly used in highway systems; 2) refining the proposed algorithm in terms of the selection of hyper-parameters such as K, ΔK, distance measures.

Chapter 6

Dynamic pricing for wireless charging lane management based on deep reinforcement learning

6.1 Introduction

With growing environmental awareness, EVs have become mainstream in transportation due to their lower emissions (McKerracher, 2023). However, their limited driving range remains a significant obstacle to their full potential. To overcome this challenge, alongside traditional plug-in charging, advanced EV charging methods have been developed, such as static wireless charging, battery swapping, and DWC. Among these, DWC stands out as the most promising method. It allows EVs to charge while in motion, using facilities embedded under the road surface, known as WCLs (Ahmad et al., 2017; Panchal et al., 2018). So far, DWC technology has been researched

in many countries, including the United States, China, Germany, Sweden, and Korea. However, most of the research on DWC remains experimental and has not yet been widely implemented in existing traffic systems (Jansuwan et al., 2021).

Recognizing the significant potential of DWC, transportation management issues within the DWC context have increasingly attracted academic attention. By far, these issues have been categorized into four aspects: (1) Development and features of DWC technology, (2) Optimal allocation of WCLs, (3) EV energy consumption analysis in WCL context, and (4) Billing and pricing for EVs on WCLs (see Chapter 2). In particular, real-time traffic management issues have not been thoroughly studied. In Chapters 4 and 5 of this thesis, we explore a ramp metering control problem and a variable speed limit (VSL) control problem on WCLs, respectively. Both studies assume that the WCL is fully deployed on the road. The conclusions of these studies reveal the inherent conflict between traffic efficiency (TE) and charging efficiency (CE) on a fully covered WCL, demonstrating the limitations of such traffic designs in promoting operational efficiency. Some studies, such as those by He et al. (2017) and He et al. (2018), also highlight this issue and suggest that WCLs should be deployed in a multi-lane system. This is because, in scenarios where WCLs are deployed on a single-lane system, EVs aiming to charge would have to decelerate, causing potential delays for non-charging vehicles. By contrast, in scenarios where WCLs are deployed on a multi-lane system, EVs with charging needs can move on the WCL at a relatively slower speed, while EVs without charging needs can use the GPL. Such traffic design can avoid the inherent conflict between TE and CE in traffic systems with WCLs. However, real-time traffic management in a multi-lane system with WCLs has not been addressed. In the multi-lane system with WCLs, as illustrated in the previous chapters, the goal of real-time management is to optimize both TE and CE.

Hence, its key lies in dynamically adjusting traffic assignments across different lanes by adapting to traffic demand. This study explores a dynamic pricing problem in a double-lane system consisting of one GPL and one WCL.

A dynamic pricing problem on highways is a strategy where toll prices or charging fees are adjusted in real time based on current traffic conditions, demand, or other relevant factors. This approach aims to manage congestion, optimize traffic flow, and maximize road usage efficiency by incentivizing drivers to make lane choices that align with overall system goals. Studies have shown that dynamic pricing effectively reduces congestion and improves traffic distribution by making certain lanes or routes more or less attractive depending on real-time conditions (Saharan et al., 2020).

Our basic consideration is that the charging price can influence EVs' lane choices, thereby affecting the traffic and charging efficiency of the system. Therefore, a dynamic pricing strategy is essential to enhance these efficiencies. Given the heterogeneity of EV attributes, the traffic dynamics should be modeled at a micro-level where each EV acts as an autonomous agent. To this end, we employ an Agent-based Model (ABM) to establish the traffic dynamics in *NetLogo* environment. Due to the complexity of ABM, a reinforcement learning method, a deep Q-learning algorithm, is utilized to derive a dynamic pricing strategy.

The primary contributions of this study are twofold: (a) we pioneer the exploration of dynamic pricing problems in a multi-lane system with WCLs, thereby filling a significant gap in this field; (b) we propose a novel framework that combines ABM tailored to a multi-lane system with WCLs and deep reinforcement learning to derive dynamic pricing strategies. This framework can be applied or extended to other real-time traffic manage-

ment on WCLs.

The rest of the chapter is organized as follows: Section 6.2 reviews the related works. Section 6.3 states the problem considered in this study Section 6.4 describes the research methodology employed in this study, introducing *NetLogo* and DRL. Section 6.5 describes the traffic model and deep Q-learning algorithms adopted in this study. Section 6.6 conducts the numerical experiments. Section 6.7 presents simulation results and discussion. Section 6.8 provides the conclusion of this study and points out its limitations and future research directions.

6.2 Related work

This section presents a brief review of the existing literature related to our study, specifically focusing on three aspects: (1) Pricing problem in traffic systems with WCLs, especially focusing on the scale of the traffic system and the aim of dynamic pricing; (2) Studies on the multi-lane systems with WCLs, especially focusing on the establishment of traffic models and energy consumption models employed within these studies. Besides, the impact of the integration of WCLs into existing traffic infrastructures on traffic flow dynamics and charging efficiency is concerned; (3) Studies that apply DRL algorithms in dynamic pricing problems on highways. Our review concentrates on the types of DRL algorithms applied, the route choice models, and the design of state and reward functions.

Several studies have addressed the pricing problems in traffic systems with WCLs. They all consider a static pricing problem on a traffic-network scale. The aim is to reduce costs and promote traffic efficiency. He et al. (2013) explored a static pricing problem on WCLs from a government agency's perspective. The goal is to optimize both transportation and power net-

works. This study aimed to validate the efficacy of two pricing models, the first and second best, in enhancing social welfare. The first-best model endeavors to minimize the combined costs of power generation and travel by implementing locational marginal pricing, whereas the second-best model focuses solely on the transportation network, aiming to reduce travel time and energy consumption while ensuring fiscal sustainability. Similarly, Wang et al. (2020) also considers a static pricing problem in a network traffic system and introduces an intriguing charging pricing and vehicle scheduling algorithm based on a double-layer game model. In the lower layer, each EV behaves in self-interest, striving to minimize detours and reduce electricity costs while securing adequate power for travel. The upper layer encapsulates the interaction between WCLs and EVs, where EVs seek to lower charging costs and WCLs aim to maximize profits from electricity sales. This study demonstrates that the proposed double-layer game model can achieve a balanced outcome benefiting both EVs and WCL operators. Similar to He et al. (2013), Esfahani et al. (2022) also addresses an optimal pricing problem in a DWC scenario, considering both transportation and power networks. However, their focus was on a more advanced scenario where the WCLs are bidirectional, formulating a bi-level optimization problem to determine the optimal buying price for electricity at each charging link, based on the assumption that the selling price is set by the Locational Marginal Price (LMP). The effectiveness of this bidirectional charging model in mitigating peak loads and reducing EV charging costs was substantiated through three numerical examples. It is evident that the existing research concentrates on network-level pricing problems, presuming complete coverage of WCLs on a link. And all of them consider a static pricing problem. A dynamic pricing problem on a multi-lane system with WCLs on a road level has not been addressed.

A few studies address the multi-lane system with deployed WCLs. He

et al. (2017) develops a car-following model to simulate the driving behaviors of EVs on double-lane systems where the WCL is partially deployed on one lane. This model particularly focuses on the car-following and lane-changing behaviors induced by the presence of WCLs, offering insights into the adjustments drivers make to utilize charging facilities, which in turn affect overall traffic dynamics and safety. Notably, the authors make some basic assumptions about the traffic rules. For example, the parameters of all EVs are assumed to be identical. EVs that need charging must choose the WCL, whereas those that do not require charging can also travel on the WCL. Building on the foundational models and basic assumptions of He et al. (2017), a subsequent study, He et al. (2018), extends the theoretical framework to quantitatively measure the impacts of WCLs on travel time and energy consumption. This study not only refines the energy consumption models specific to EVs but also calibrates these models against empirical data, thus validating the theoretical predictions. The results indicate a notable decrease in road capacity (8% to 17%) and an increase in energy consumption (3% to 14%) under varying traffic densities, underscoring the practical implications of integrating WCLs into existing infrastructures.

Several studies have applied DRL algorithms to dynamic pricing problems on highways. Pandey et al. (2020) explore a dynamic pricing model designed to optimize the use of express lanes. The DRL algorithm utilized here is an Actor-Critic (A2C) algorithm, which is adept at handling continuous state and action spaces, making it particularly suitable for the dynamic and complex environment of highway traffic. The state representation in this model includes variables such as current traffic density, time of day, and historical usage patterns of the lanes, while the reward function is designed to maximize revenue and minimize travel time. Abdalrahman and Zhuang (2020) extends the application of DRL to manage dynamic pricing in EV charging stations. This study employs a multi-agent

framework where each charging station operates as an independent agent utilizing a variant of the Q-learning algorithm. The state space for each agent includes the number of EVs waiting, the state of charge of each EV, and the current electricity price, whereas the reward function is constructed to maximize profit while ensuring customer satisfaction by reducing waiting times and charging costs. Cui et al. (2023) applies DRL algorithms for dynamic pricing at EV fast charging stations, focusing on optimizing station profit and enhancing user satisfaction. The study effectively integrates traffic flow predictions and EV charging demands into a dynamic pricing model that adjusts in real-time to traffic and usage conditions. The study establish the vehicle–road learning environment using the Markov decision process (MDP) and employs the Deep Deterministic Policy Gradient (DDPG) algorithm, which is a policy-based reinforcement learning method, particularly suited for continuous action spaces such as pricing strategies. The state space in the DRL framework includes the current load at the charging stations, the availability of the chargers, the real-time traffic conditions around the stations, and the predicted demand for charging. These variables help the system to understand the current scenario at both the traffic and energy distribution levels. The reward function is designed to maximize the profitability of charging stations while balancing the electrical grid's demands and user satisfaction.

6.3 Problem Statement

We consider a dynamic pricing problem in a double-lane system dedicated to providing charging service for DWC EVs. The system consists of one GPL and one WCL. The speed limit on the WCL is set a bit lower than that on the GPL to extend the charging duration for EVs (He et al., 2017). In

this study we assume $v^{wcl} = 0.9v^{gpl}$. *NetLogo* establishes the entire system as an ABM in which an EV is treated as an agent that has attributes including location, current travel speed, SOC, minimum SOC level, etc. The traffic rules in this system are assumed as follows:

- In the lane-changing zone (see Fig. 6.1), each EV can choose one lane. Its lane choice depends mainly on three factors: the current SOC, the observed travel speeds on each lane, and the charging price.
- Once an EV enters the GPL or WCL, lane-changing behavior is restricted unless its SOC drops below the minimum or exceeds the maximum threshold. Violations incur penalties, enforced by advanced ITS.
- EVs entering the WCL must charge their battery until their SOC reaches its maximum SOC level.
- The charging price is modeled as a discrete variable and can be changed at regular intervals, e.g., every three minutes.

We develop an ABM tailored to the double-lane system in the context of the DWC scenario in *NetLogo*, as depicted in Fig. 6.1. Since the traffic and charging demands change over time, it is crucial for traffic operators to dynamically adjust the charging prices to influence EVs' lane choices and optimize traffic distribution between the two lanes. The goal is to enhance the operational efficiency of the system. In this study, we focus on both traffic efficiency and charging efficiency from the perspective of traffic operators. Detailed definitions of these efficiencies will be provided in the following section. Considering the complexity of the ABM, a model-based control

Figure 6.1: A schematic diagram of a 2-lane road system.

method is deemed unsuitable for implementing a dynamic pricing strategy. Instead, a model-free approach based on a deep Q-learning algorithm is derived for the dynamic pricing strategy. Additionally, a straightforward method using the classification and regression tree (CART) algorithm is established as a benchmark approach. We conduct a series of numerical experiments and a case study to demonstrate the effectiveness of the proposed algorithm. The challenges lie in two aspects: (a) the establishment of the ABM tailored to the double-lane system, which involves integrating traffic dynamics and the lane-choice model; (b) the design of the deep Q-learning algorithm, particularly the formulation of the system state and reward function.

6.4 Research Methodology

The methodology framework of the interaction between our ABM and the deep Q-learning algorithm is depicted in Fig. 6.2. It can be seen that the ABM (that is, the environment of the Deep Q-learning algorithm) is coded in *NetLogo* by extending the existing model "Traffic 2 lanes" in the *NetLogo* Library (Wilensky and Payette, 1998), which has been used in a number of traffic problems. For example, Triastanto and Utama (2019) extends the model to explore the ways to overcome traffic congestion on toll roads. Mitrovic et al. (2019) develops a new traffic simulation environment in *NetLogo* to explore an intersection control task. In this study, we incorporate the rules of the double-lane system, depicted in Fig. 6.1, and SOC dynamics of EVs into the model. Since the deep Q-learning algorithm is coded in *Python*, we adopt the *pyNetLogo* library to build the bridge between the algorithm and the environment (Jaxa-Rozen and Kwakkel, 2018). The *pyNetLogo* library provides a seamless interface enabling Python to interact

with *NetLogo*. By integrating this library, we are equipped with capabilities to dynamically load models, execute *NetLogo*-specific commands, and extract data from reporter variables. Such functionalities are instrumental for the training of our deep Q-learning algorithm in an online fashion. In the following, the Ne and DRL are introduced.

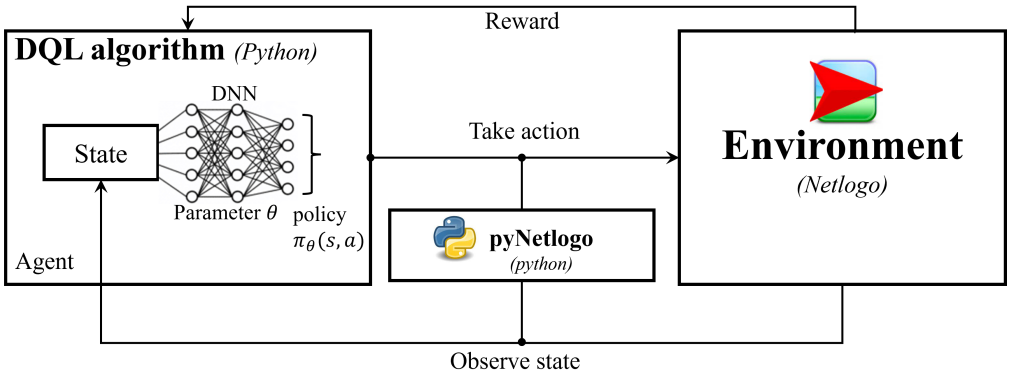

Figure 6.2: Methodology framework

6.4.1 NetLogo

NetLogo is a powerful programming language for the ABM, which is designed and authored by Uri Wilensky, director of Northwestern University's Center for Connected Learning and Computer-Based Modeling in 1999 (Wilensky, 1999). ABM, as the core of *NetLogo*'s functionality, is a computational method that enables autonomous agents to be modeled and analyzed in a shared environment. These agents have distinct behaviors and attributes, which, when allowed to interact under a set of rules, may lead to the emergence of complex, system-level phenomena (Railsback and Grimm, 2019). *NetLogo* is tailored to this approach, providing a rich set of built-in commands and the flexibility to simulate the actions and interactions of autonomous agents in both natural and social phenomena.

One of the primary advantages of *NetLogo* is its accessibility. The environment provides a user-friendly interface coupled with a low learning curve,

which democratizes the ability to construct sophisticated models (Sklar, 2007). Its built-in library of sample models covers various domains, from biology and physics to economics and social science (Gilbert, 2019). Moreover, *NetLogo* supports the exploration of simulation parameters through its "BehaviorSpace" tool, which is useful for conducting systematic simulation experiments (Lytinen and Railsback, 2012). This capability allows researchers to automate the exploration of parameter spaces, running numerous simulations with varying inputs to analyze outcomes and patterns. In recent years, *NetLogo* has been instrumental in numerous research studies. It has facilitated insights into complex adaptive systems and contributed to the understanding of phenomena such as the spread of infectious diseases (Bi et al., 2019a), and the behavior of social networks (Ross et al., 2019). It has also been frequently applied in various traffic problems (Mostafizi et al., 2021; Kponyo et al., 2016; Wang et al., 2022b; Mitrovic et al., 2019)

Unlike traditional traffic simulators like VISSIM and SUMO, which are (not agent-based but) more focused on simulating traffic flow based on vehicles, *NetLogo* emphasizes the behavior and interaction of individual agents. This approach can provide deeper insights into the dynamics of complex systems, such as traffic networks, where individual EV behaviors significantly influence the overall traffic patterns or the heterogeneity among different agents can not be ignored. Readers interested in more agent-based traffic simulators can refer to Nguyen et al. (2021). In the traffic scenario explored in this study, an EV's lane choice is influenced by multiple attributes, including its location, SOC, charging prices, and observed travel speeds. The heterogeneity of the agents' attributes is central to the traffic scenario analyzed in this study and should be taken into account in our approach. Consequently, we employ *NetLogo* to simulate the traffic dynamics of a double-lane system.

6.4.2 Deep reinforcement learning (DRL)

Reinforcement Learning (RL) is a paradigm of machine learning where an agent learns to make decisions by performing actions in an environment to achieve a goal. The agent receives feedback in the form of rewards or penalties, guiding it toward effective strategies. The process involves learning what actions to take in different states to maximize a cumulative reward (Sutton and Barto, 2018). The key components of any RL problem include:

- **State**: The current situation or observation of the environment. The states are the inputs to the agent that help it decide the action to take. In complex scenarios, states can be high-dimensional data such as images or sensor readings.
- **Environment**: Everything the agent interacts with and learns from. It provides the agent with states, and in response to the agent's actions, it presents new states and rewards.
- **Agent**: The learner or decision-maker in RL. An agent makes decisions based on observations from the environment, seeking to achieve a goal or maximize its reward.
- **Action**: An action that the agent can take in the environment based on its observation. Actions affect the future state of the environment and ultimately the reward the agent receives.
- **Reward**: Feedback from the environment. Rewards can be positive (reinforcing the action) or negative (discouraging the action). The agent's objective is to maximize the cumulative reward over time.
- **Policy**: A strategy or rule that guides the agent's decision-making process in each state. The policy maps states to actions and determines the

behavior of the agent. It can be deterministic, where a specific action is chosen for a given state, or stochastic, where a probability distribution over actions is used. The goal in RL is often to learn an optimal policy that maximizes the expected cumulative reward.

Based on the knowledge of the environment, the learning strategy, and the learning objective, RL can be categorized as follows:

- **Model-Free vs. Model-Based** Model-free learning methods do not attempt to understand or model the environment. Instead, they directly learn the optimal policy or value function based on the information provided by the environment. Common model-free approaches include Policy Optimization, where the aim is to directly learn the policy that maps states to actions, and Q-Learning, which focuses on learning the value of taking a certain action in a given state (Sutton and Barto, 2018).

  Model-based learning, on the other hand, involves learning a model of the environment and using it to predict future states and rewards. This approach can lead to more efficient learning by simulating future events and evaluating the best course of action (Ha and Schmidhuber, 2018). Model-Based strategies are particularly useful for planning, as they allow the agent to consider the consequences of actions before taking them.

- **Policy-Based vs. Value-Based** Policy-based learning directly parameterizes and optimizes the policy, outputting probabilities for each action. These methods can handle both discrete and continuous action spaces and are characterized by their ability to learn stochastic policies. Policy Gradients are a common policy-based approach (Williams, 1992). Value-based learning focuses on learning the value of each action in a given state and selecting the action with the highest value. These methods are typically applied to discrete action spaces. Q-learning and its deep learning

variant, the Deep Q Network (DQN), along with Sarsa, are well-known value-based methods (Rummery and Niranjan, 1994).

In particular, actor-critic methods combine the advantages of policy-based and value-based approaches. The actor component is responsible for selecting actions (policy), while the critic evaluates the action by computing the value function. This combination accelerates the learning process by using the critic's evaluations to update the actor's policy. Examples include A2C (Advantage Actor-Critic), A3C (Asynchronous Advantage Actor-Critic), and DDPG (Deep Deterministic Policy Gradient).

- **On-Policy vs. Off-Policy**

  On-policy RL algorithms are the algorithms that evaluate and update the same policy that is carried out by the agent for action selection. In other words, the target policy is consistent with the behavior policy. Some typical examples of On-Policy algorithms are Policy Gradient, Sarsa, etc (Sutton et al., 1999). Such on-policy algorithms make the learning process more transparent; however, they may face challenges in exploration, as they must balance exploration with the exploitation of the current policy, which can slow down learning in complex environments (Osband et al., 2016).

  Off-policy RL allows the agent to learn about one policy while following another, providing greater flexibility and efficiency in learning. Q-learning and DQN are typical examples of off-policy methods, where a behavior policy different from the target policy is used to explore the environment (Mnih et al., 2015).

It should be noted that, in the context of Policy-Based reinforcement learning methods, the term "policy" explicitly refers to the strategy that an agent employs to execute actions based on the current state. These method-

ologies typically involve the formulation and refinement of a parameterized policy function that directly maps states to a probability distribution over actions. The principal objective within Policy-Based approaches is to directly optimize this policy function to maximize the cumulative rewards, rendering the "policy" as the focal point of learning and optimization endeavors. Conversely, within On-Policy learning frameworks, the "policy" encompasses both the strategy utilized for decision making (i.e., action selection) and the policy subject to evaluation and optimization. This implies that in On-Policy learning, the agent derives learning from the policy it presently adheres to, signifying that the behavior policy (employed for action selection) and the target policy (undergoing learning and optimization) are identical.

However, traditional RL methods face challenges in handling high-dimensional state spaces, limiting their applicability in complex scenarios. The advent of Deep Learning has revolutionized RL, leading to the emergence of Deep Reinforcement Learning (DRL). DRL combines the RL decision making framework with the powerful functions approximation capabilities of deep neural networks, enabling agents to learn in environments with high-dimensional input and achieve remarkable performance (Mnih et al., 2015). In DRL, neural networks serve as function approximators, interpreting complex input data such as images or sensor readings. Deep learning helps in extracting features and patterns essential for decision-making. A critical aspect of DRL is the balance between exploration (trying new actions) and exploitation (leveraging known information), crucial to the agent's learning process (Lillicrap et al., 2015). Therefore, DRL merges the decision-making framework of RL with the representational capabilities of deep learning. This synthesis enables agents to learn optimal policies in complex environments, especially where the state and action spaces are highly dimensional and not easily tractable by traditional RL methods

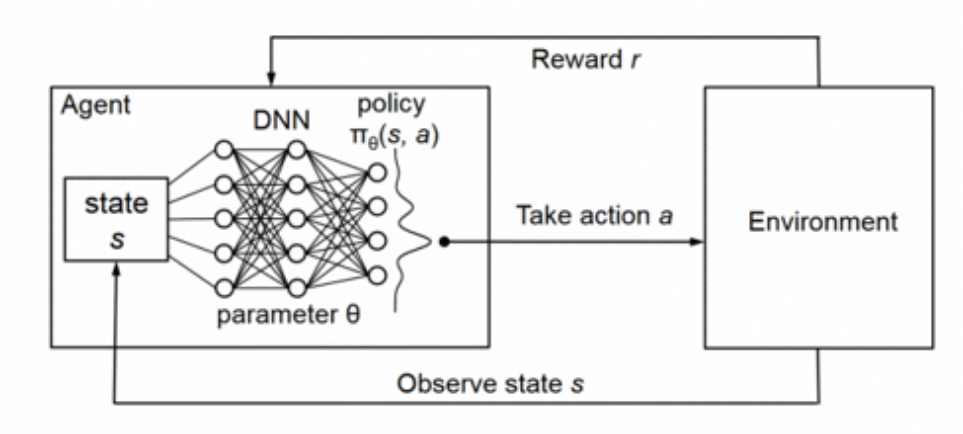

Figure 6.3: A schematic diagram of deep reinforcement learning

(Mnih et al., 2015).

By far, DRL has achieved notable success in various domains, from playing complex games such as Go and Chess to robotics, autonomous vehicles, and personalized recommendations. Notable achievements include AlphaGo defeating a world champion in Go and advanced control systems in robotics (Silver et al., 2016). Despite its success, DRL faces challenges like sample inefficiency, the need for large amounts of data, and difficulties in generalizing learned policies. Future directions may focus on improving efficiency, generalization, and developing more robust and interpretable DRL models.

6.5 Modelling and Algorithms

This section introduces the basic elements of the ABM and the Deep Q-learning algorithm we adopt.

6.5.1 Agent-based model (ABM)

The ABM employed for the double-lane road system comprises two types of agents. The first type of agent encompasses the road infrastructure,

specifically the GPL and the WCL. The second type of agent is the EV, which is capable of making autonomous decisions and interacting with both the GPL/WCL (i.e., gain energy) and other EVs. The attributes (global variables and EV attributes) of these agents are defined in Table. 6.1.

Table 6.1: List of Variables

Notations	Definitions	Units	Type
Global variables			
e^+	Charging power on the WCL	kW	New
p	Charging price on the WCL	\$/kWh	New
v^{gpl}	Speed limit on GPL	km/h	New
v^{wcl}	Speed limit on GPL	km/h	New
$Throughput$	Total throughput	veh	New
$Energy$	Total Energy	kWh	New
EV attributes			
e_i^-	Energy consumption of the i-th EV	kW	New
v_i^{max}	Maximum travel speed the i-th EV	km/h	Old
v_i	Current travel speed of the i-th EV	km/h	Old
$\bar{v}_i^{gpl}$	Observed travel speed on the GPL by the i-th EV	km/h	New
$\bar{v}_i^{wcl}$	Observed travel speed on the WCL by the i-th EV	km/h	New
a_i	Acceleration the i-th EV	m/s^2	Old
s_i	SOC of the i-th EV	percent	New
s_i^{min}	Minimum SOC level of the i-th EV	percent	New
s_i^{max}	Maximum SOC level of the i-th EV	percent	New
s^{ini}	The mean value of initial SOC of incoming EVs	percent	New
Δs^{ini}	The standard deviation of initial SOC of incoming EVs	percent	New
l_i^x, l_i^y	Location of the i-th EV	km	New
y^*	Target lane of the i-th EV	/	New
v_i^{lat}	Lateral speed of the i-th EV	km/h	Old

Global variables

In our ABM, global variables include speed limits on GPL, speed limits on WCL, charging power, charging price, total throughput, and total energy. Their definitions and notations are as follows.

- **Speed limit on GPL** (v^{gpl}): This denotes the maximum speed at which an EV is allowed to travel on the GPL. In our model, it is defined as a constant. Its unit is km/h.
- **Speed limit on WCL** (v^{wcl}): This denotes the maximum speed at which an EV is allowed to travel on the WCL. Generally, v^{wcl} is set slightly lower than v^{gpl} to allow EVs more time to charge (He et al., 2017).
- **Charging power** (e): This denotes the power available at the WCLs, assumed constant over time and uniform along the lane, measured in kilowatts (kW).
- **Charging price** (p): This refers to the cost of charging per kilowatt-hour on the WCL, communicated in real-time to all EVs to facilitate informed lane choices. We assume that p is a discrete variable, priced at \$/kWh.
- **Total throughput** ($Throughput$): This denotes the cumulative number of vehicles that pass a specific point, such as the entrance of the road, within a given time interval, measured in vehicles per hour (veh/h).
- **Total energy** ($Energy$): This denotes the total energy delivered to vehicles via the WCL, calculated as the sum of the energy received by each vehicle, measured in kilowatt-hours (kWh).

Note that only $Throughput$ and $Energy$ are statistical accumulators that

can change over time, while the other four attributes are assumed to be time invariant.

EV Attributes

Each EV has a set of attributes as follows:

- **Maximum travel speed** (v_i^{max}): This attribute specifies the upper limit of the speed of an EV, normalized to the range $[0, 1]$. In our model, its value is defined as a constant, which is generally bigger than v^{gpl} and v^{wcl}.

- **Current travel speed** (v_i): This attribute describes the instantaneous speed of the EV. Its value is constrained within a normalized range of 0 (stationary) to 1 (maximum travel speed).

- **Observed travel speed** ($\bar{v}_i^{gpl}$,$\bar{v}_i^{wcl}$): This attribute captures the speed of EVs within a lane as observed by an individual EV. It is quantified as the average speed of EVs along a specified observable distance (e.g., 100 meters) ahead of the observing EV. In this model, we assume it to be the average speed of vehicles across the entire lane, which is disseminated to all vehicles in real time through advanced vehicle communication systems Its value is normalized to the range $[0, 1]$.

- **Acceleration** (a_i): This attribute describes the change of an EV's speed within one time interval. In our model, their values are defined as constants.

- **SOC** (s_i): The SOC is a crucial attribute for operations and management on WCLs, indicating the current energy level of the EV's battery. The value is constrained within a normalized range of 0 (completely depleted) to 1 (fully charged).

- **Minimum SOC level** (s_i^{min}): This threshold represents the critical SOC below which an EV risks imminent power depletion, potentially leading to operational failure and reduced battery lifespan. In our model, an EV is allowed to change to the WCL whenever its SOC level drops below this point.

- **Maximum SOC level** (s_i^{max}): This threshold signifies the optimal SOC at which an EV's battery is considered fully charged without exceeding the manufacturer's recommended limits to prevent overcharging. In our model, an EV is allowed to change to the GPL whenever its SOC level drops below this point.

- **Location** (l^x, l^y): The EV's location in the context of the *NetLogo* model is captured by a two-dimensional coordinate l^x, l^y, where l^x represents the longitudinal axis along the road while l^y denotes the lateral position across lanes.

- **Target location** (l^{y*}): This attribute is denoted as the y-axis value of the target location of an EV (corresponding to the target lane). In our double-lane system, the GPL and the WCL can be expressed as $l^{y*} = 0$ and $l^{y*} = 1$, respectively.

- **Lateral speed** (v_i^{lat}): This attribute signifies the speed at which an EV executes a lane-changing behavior. In our model, this parameter is defined as a constant.

Exogenous input

In our model, traffic demand is an exogenous input to the double-lane system. Recognizing that EVs might choose their lanes before reaching the designated lane-changing zone, we assume that EVs appear on their

selected lane when they enter the zone if there is available capacity; otherwise, they are compelled to the other lane. This assumption reflects the dynamic interaction between traffic demand and lane availability, ensuring a realistic representation of traffic demand. We also assume that the arrival of EVs into the system within a fixed interval of time (equal to the minimum time interval between two charging price signals, denoted τ) satisfies a Poisson distribution (Zhu et al., 2022). In this case, the time intervals between consecutive events (an EV enters the system) can be described using an exponential distribution. Then the inter-arrival times follow an exponential distribution whose probability density function is given by:

$$f(t) = de^{-dt} \tag{6.1}$$

where the constant rate d represents the vehicles that enter the system per minute, t represents the time interval between consecutive vehicle arrivals. Taking $d = 6$ as an example, the (6.1) can be plotted as:

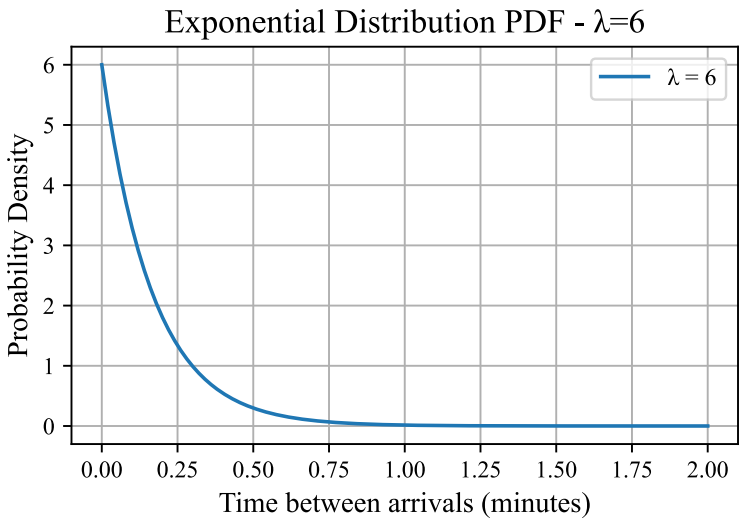

Figure 6.4: The time interval between consecutive vehicle arrivals $d = 6$

In *NetLogo*, random interarrival times are generated from the exponential distribution with the specified rate d. The arrival time for each vehicle is then calculated by the cumulative sum of these random intervals. This

process effectively models the stochastic nature of traffic flow into the specified road segment over the given time frame. Note that we simulate a non-homogeneous Poisson process where the rate d changes over time (here we assume it changes every 3 minutes) which is approximated by a piecewise constant function. Besides, we assume that the initial SOC of incoming EVs s^{ini} within a given time frame follows a Gaussian distribution, with a mean (μ) and a standard deviation (σ). This assumption is consistent with one of the findings yielded in (Hu et al., 2019) that the SOC distribution of EVs at the beginning of charging events is similar to a Gaussian distribution, with an average initial SOC of around 41%.

Scale

In the *NetLogo* traffic model, an explicit scale is not defined. Instead, a normalized scale is adopted, wherein the roadway is comprised of numerous 1×1 patches, with each vehicle occupying one patch. By assuming that the length of an EV spans four meters, it is inferred that one patch equates to four meters in real-world dimensions. Consequently, this allows for the extrapolation of other parameters, such as speed, on a similar basis. For example, a normalized speed of 0.5 used in *NetLogo* corresponds to 80km/h in reality.

Lane-choice model

The probability of lane choices of EVs can be estimated by a discrete choice model (DCM), which is a powerful tool used in econometrics and behavioral research to model the decision-making process of individuals faced with multiple alternatives. It was initially proposed by McFadden (1972) based on random utility theory. The theory assumes that individuals make

decisions based on the total utility of available options, which consists of an observable deterministic component related to choice attributes and an unobservable stochastic component that captures individual preferences and random fluctuations. This theory explains why individuals may choose differently under similar conditions and vary their choices over time, highlighting the role of both deterministic influences and stochastic elements in decision-making (Train, 2009). In this study, we assume a logit model, which is widely used in predicting drivers' lane choice among a set of alternatives (Lou et al., 2011; Tan and Gao, 2018; Li et al., 2022). Note that although our logit model applies to two alternative settings as in our double-lane system, it can be extended to multi-lane systems using a multinomial logit model.

The multinomial logit model for the double-lane system is established in the following. First, we specify two separate utility functions, U_{gpl} and U_{wcl} for the two lanes. Each utility function in our model is assumed to be a linear combination of explanatory variables that affect the EVs' lane choice. In the context of issues related to the pricing of EV charging, explanatory variables usually include at least SOC, travel time, and charging cost. Since the WCLs have not been commercialized on a large scale, the charging choice in the context of WCLs can not be well investigated, though, there are studies investigating the charging choice under other scenarios. For instance, Ge and MacKenzie (2022) analyzed the factors that influence EVs' charging choice among charging stations using the data from an interactive stated choice experiment. The result shows that the utility of charging choice is negatively correlated with a set of variables including SOC, charging time, and charging price. Similarly, in our model, we assume that the utility of choosing the GPL for the i-th EV is only influenced by travel time, denoted as $T^{gpl}_{travel,i}$, calculated as the travel time to traverse the selected lane; the utility of choosing the WCL is assumed to be influenced

by the charging time, $T^{wcl}_{charging,i}$ (calculated as the time to charge on the WCL, i.e., the time to traverse the WCL), SOC (the current SOC of the i-th EV, denoted as s_i), and charging cost (calculated as the total cost of the EV to charge on the WCL, denoted as $C_{charging,i}$). Then the utility functions can be expressed as:

$$U^{gpl}_i = \beta_T \times T^{gpl}_{travel,i} + \beta_0 + \epsilon^{gpl}_i \tag{6.2}$$

$$U^{wcl}_i = \beta_s \times s_i + \beta_T \times T^{wcl}_{travel,i} + \beta_C \times C_{charging,i} + \epsilon^{wcl}_i \tag{6.3}$$

where the coefficients β_s, β_T, and β_C represent the marginal utilities of SOC, travel time, and charging cost, respectively. $\epsilon^{gpl}_i, \epsilon^{wcl}_i$ are random error terms, which independently and identically follow a Gumbel distribution. β_0 is a constant term used to calibrate the utility function. s_i in the both utility functions is the SOC of i-th EV at the time it makes lane-choice; $T^{gpl}_{travel,i}$, $T^{wcl}_{charging,i}$, and $C_{charging,i}$ are defined as:

$$T^{gpl}_{travel,i} = \frac{L_{sys}}{\bar{v}^{gpl}_i} \tag{6.4}$$

$$T^{wcl}_{charging,i} = \frac{L_{sys}}{\bar{v}^{wcl}_i} \tag{6.5}$$

$$C_{charging,i} = \frac{L_{sys}}{\bar{v}^{wcl}_i} \times e^{+} \times p_{charging} \tag{6.6}$$

where L_{sys} represents the length of the double-lane system. In the equations, we utilize the observed speeds, $\bar{v}^{gpl}_i$ and $\bar{v}^{wcl}_i$, to calculate the expected travel times for the i-th EV traversing the GPL and the WCL, respectively. This calculation is considered reliable in most contexts, provided that the traffic flow speed remains relatively stable over short intervals. The marginal utilities $\beta_s, \beta_T, \beta_C$ are all negative, indicating that the utility of choosing a lane of an EV decreases with the increase of its SOC, travel/charging time, and charging cost.

Following the traffic rules mentioned in Sec. 6.3, we assume that β_s is a

piecewise function by dividing the SOC into three ranges, which is similar to the model used in (Zhou et al., 2019):

$$\beta_s = \begin{cases} \infty & \text{if } 0 \leq s_i < s_i^{min} \\ \beta_s' & \text{if } s_i^{min} \leq s_i \leq s_i^{max} \\ -\infty & \text{if } s_i^{max} < s_i \leq 1 \end{cases} \tag{6.7}$$

This piecewise β_s satisfies the traffic rule that an EV whose SOC is below its minimum SOC level will choose the WCL; while an EV whose SOC exceeds its maximum SOC level will choose the GPL. Then the choice probability of i-th EV for each lane at time t, denoted as $P_{wcl}(t)$, can be expressed as:

$$P_i^{gpl} = \frac{exp(U_i^{gpl})}{exp(U_i^{wcl}) + exp(U_i^{gpl})} \tag{6.8}$$

$$P_i^{wcl} = \frac{exp(U_i^{wcl})}{exp(U_i^{wcl}) + exp(U_i^{gpl})} \tag{6.9}$$

The selection of marginal utilities $\beta_s, \beta_T, \beta_C$ is crucial for the utility functions. In our model, we aim to derive a set of appropriate values for these utilities in Sec. 6.6.1 based on the results from Ge and MacKenzie (2022).

EV driving behavior

The behavior of an EV is characterized by the dynamics of its attributes. Among the attributes mentioned in Sec. 6.5.1, maximum travel speed and acceleration/deceleration are constant, while others are variable. For the

i-th EV, its acceleration at time t is calculated as:

$$a_i(t) = \begin{cases} a_{acc,i} & \text{accelerate, if there are no blocking cars ahead and} \\ & v_i(t) < v^{wcl} \cdot 1_{\{l^{y*}(t)=1\}} + v^{gpl} \cdot 1_{\{l^{y*}(t)=-1\}} \\ 0 & \text{maintain } v_i(t), \text{ if there are no blocking cars ahead and} \\ & v_i(t) = v^{wcl} \cdot 1_{\{l^{y*}(t)=1\}} + v^{gpl} \cdot 1_{\{l^{y*}(t)=-1\}} \\ a_{dec,i} & \text{decelerate, if there are blocking cars ahead} \end{cases} \tag{6.10}$$

where $a_{acc,i}$ and $a_{acc,i}$ are constants, representing the acceleration magnitude for EV i when there are no blocking cars ahead and the deceleration magnitude for EV i when there are blocking cars ahead, respectively. Their values can vary slightly across different EVs. 1_c is the indicator function that equals 1 if condition c is satisfied and 0 otherwise.

Then its speed, v_i location along the road, x_i, lateral movement, y_i, can be expressed as:

$$v_i(t+1) = v_i(t) + a_i(t) \tag{6.11}$$

$$l_i^x(t+1) = l_i^x(t) + v_i(t) \tag{6.12}$$

$$l_i^y(t+1) = l_i^y(t) + v_i^{lat}(t) \tag{6.13}$$

where v^{lat} represents the lateral speed of EVs. In this model, we assume it to be a constant value for all EVs.

As mentioned in Sec. 6.5.1, the observed travel speeds of EV i on the two lanes, $\bar{v}_i^{gpl}$, and $\bar{v}_i^{wcl}$ are defined as the average speed of vehicles on the entire lane. Let $\{\bar{v}_j^{gpl}\}, j \in \{1, ..., J^{gpl}(t)\}$ and $\{\bar{v}_j^{wcl}\}, j \in \{1, ..., J^{wcl}(t)\}$ denote the set of speeds of these observed vehicles on the GPL and WCL,

respectively, then we have:

$$\bar{v}_i^{gpl}(t) = \begin{cases} \frac{1}{J^{gpl}(t)} \Sigma_{j=1}^{J^{gpl}(t)} \bar{v}_j^{gpl} & \text{if there are observable EVs ahead} \\ v^{gpl} & \text{if there are no observable EVs ahead} \end{cases} \tag{6.14}$$

$$\bar{v}_i^{wcl}(t) = \begin{cases} \frac{1}{J^{wcl}(t)} \Sigma_{j=1}^{J^{wcl}(t)} \bar{v}_j^{wcl} & \text{if there are observable EVs ahead} \\ v^{wcl} & \text{if there are no observable EVs ahead} \end{cases} \tag{6.15}$$

where $J(t)$ is the total number of vehicles on the lane on which EV i is moving at time t.

Its SOC, s_i, is updated as:

$$s_i(t+1) = \begin{cases} s_i(t) + e^+ - e_i^-(t) & \text{if the EV is on the WCL, e.g., } l_i^y(t) = -1 \\ s_i(t) - e_i^-(t) & \text{otherwise} \end{cases} \tag{6.16}$$

where e^+ is the charging power of the WCL, which is assumed as a constant. $e_i^-(t)$ is the energy consumption of i-th EV at time t. Based on the analysis of the laboratory tests from (Galvin, 2017), it can be expressed as a nonlinear function of its speed $v_i(t)$ and acceleration $a_i(t)$:

$$e_i^-(t) = f^e(v_i(t), a_i(t)) \tag{6.17}$$

As discussed in Section 6.5.1, the model for determining the lane choice probability of an EV as it first enters the system is represented by the random variable l_i^{y*}, with the probability defined as:

$$Pr(l_i^{y*} = -1) = P_i^{wcl} \tag{6.18}$$

$$Pr(l_i^{y*} = 1) = P_i^{gpl} \tag{6.19}$$

where $Pr()$ represents the probability function, which calculates the likelihood of an EV choosing a particular lane for its first entry. Here, l_i^{y*} equals -1 for the choice of the WCL and 1 for the GPL. P_i^{wcl} and P_i^{gpl} are the probabilities for choosing each lane, respectively.

As mentioned in Sec. 6.3, once an EV enters the GPL or the WCL, it is prohibited from changing lanes. Exceptionally, its SOC falls outside the range $[s_i^{min}, s_i^{max}]$, it can re-select its target lane using the probability model shown in (6.18).

6.5.2 Deep Q-learning algorithm

Background

First, we define a set of notations as follows:

- x: State
- a: Action
- r: Reward
- π: Policy
- γ: Discount Factor - Used to calculate the current value of future rewards, with a range of $[0, 1]$.
- $Q(x, a)$: Action-Value Function

- $Q^*(x, a)$: Optimal Action-Value Function - Denotes the maximum expected return achievable by any policy, given state s and action a.
- θ: Weights of a neural network.
- $L(\theta)$: Loss function with weights θ

Traditional Q-learning utilizes a Q-table to estimate the maximum expected rewards for an optimal action a for a given state x in a specific environment (Zhu and Ukkusuri, 2014; Li et al., 2017). Let $Q^*(x, a)$ be the optimal action-value function which denotes the maximum expected return achievable by any policy, given state x and action a. By the Bellman optimality equation, $Q^*(x, a)$ is defined as:

$$Q^*(x, a) = \mathbb{E}\left[r + \gamma \max_{a'} Q^*(x', a') \mid (x, a)\right] \tag{6.20}$$

This equation indicates that the optimal state-action value function, $Q^*(x, a)$, is equal to the immediate reward r obtained by taking action a in state x, plus the expected value of future rewards discounted by γ, which are attainable through executing the optimal action a' in the subsequent state x'. By the value iteration algorithm, this equation facilitates the approximation of the $Q^*(x, a)$, thereby converging towards the policy that maximizes the expected cumulative reward from any given state (Mnih et al., 2015). However, this tabular approach of traditional Q-learning faces significant challenges in environments with large or continuous state spaces, where the Q-table becomes impractically large and hence impossible to enumerate. Moreover, the tabular method struggles with generalizing from seen to unseen states, limiting its applicability in complex environments (Müller et al., 2015).

To overcome the challenges, Deep Q-learning extends the Q-learning framework by employing a deep neural network, known as a Q-network, to ap-

proximate the action-value function Mnih et al. (2013). The Q-network, parameterized by weights θ, takes the representation of a state x as input and outputs the estimated Q-values for all possible actions in that state. This approach allows Deep Q-learning to handle high-dimensional state spaces and generalize across states, making it feasible to manage complex environments. In this context, the optimal action-value function $Q^*(\boldsymbol{x}_t, a_t)$ represents the maximum expected return achievable, while the approximate action-value function $Q(\boldsymbol{x}_t, a_t; \theta)$, parameterized by θ, seeks to closely estimate this optimal function. The learning objective in Deep Q-learning is to iteratively adjust the parameters θ of the Q-network to minimize the discrepancy between the approximate and the optimal action-value functions. Training the Q-network involves adjusting the parameters θ to minimize the difference between the predicted Q-values and the target Q-values, which are computed using the Bellman equation. This is typically achieved through gradient descent, utilizing a loss function defined as:

$$L_t(\theta_t) = \mathbb{E}\left[(y_t - Q(\boldsymbol{x}_t, a_t; \theta_t))^2\right], \tag{6.21}$$

where $y_t = r_{t+1} + \gamma \max_{a'} Q(\boldsymbol{x}_{t+1}, a'; \theta_t)$ represents the target Q-value. Here, r_{t+1} is the reward received after taking action a_t in state $\boldsymbol{x}_t$, γ is the discount factor that balances the importance of immediate and future rewards. The expectation $\mathbb{E}[\cdot]$ is taken over the distribution of transitions $(\boldsymbol{x}_t, a_t, r_{t+1}, \boldsymbol{x}_{t+1})$ encountered under a policy derived from Q. By leveraging the representational power of deep neural networks, deep Q-learning can effectively approximate the optimal action-value function $Q^*(x, a)$ in environments with complex, high-dimensional state spaces. This overcomes the limitations of traditional Q-learning and enables the development of more sophisticated and capable reinforcement learning agents, capable of navigating and making decisions in complex environments. In the following, we define the basic elements of the deep Q-learning algorithm including state,

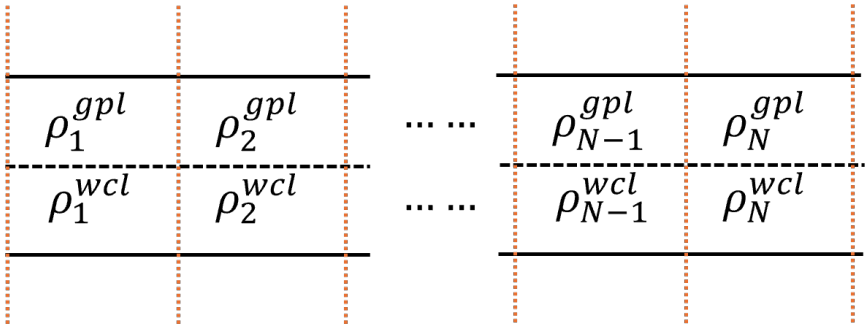

Figure 6.5: Road segments

action, and reward, and then introduce the training procedure.

State

The state of our Deep Q-learning algorithm contains both traffic states and the future traffic demand. For the representation of traffic states, we first divide the road system under consideration into N segments (in this study we assume that each segment is identical), as depicted in Fig. 6.5. Let $\boldsymbol{\rho}^{gpl}, \boldsymbol{\rho}^{wcl}$ be the vectors collected the normalized traffic densities on the GPL and the WCL, respectively. Then we have:

$$\boldsymbol{\rho}^{gpl} = [\rho_1^{gpl}, ..., \rho_N^{gpl}], \tag{6.22}$$

$$\boldsymbol{\rho}^{wcl} = [\rho_1^{wcl}, ..., \rho_N^{wcl}]. \tag{6.23}$$

Here the n-th normalized traffic density, $\rho_n^{gpl}/\rho_n^{wcl}$, $n = 1, ..., N$ is defined as

$$\rho_n^{gpl} = \frac{m_n^{gpl}}{m_{j,n}^{gpl}} \tag{6.24}$$

where m_n^{gpl}/m_n^{wcl} is the number of EVs located within the n-th segments; $m_{c,n}^{gpl}/m_{c,n}^{wcl}$ represents the maximum number of vehicles that can be accommodated on a road segment. Similarly, we use a vector $\boldsymbol{d} = [\frac{d_1}{d_{max}}, \ldots, \frac{d_{N_d}}{d_{max}}]$ to represent the future traffic demand over the next N_d periods of pricing signals. Here, d_i for $i = 1, \ldots, N_d$ is the average number of incoming ve-

hicles per minute within the i-th period in the future, which equals the d adopted in Sec. 6.5.1. d_{max} is the pre-defined maximum value of d_i. Let $\boldsymbol{x}$ be the system state of the Deep Q-learning algorithm, then $\boldsymbol{x}$ can be expressed as:

$$\boldsymbol{x} = [\boldsymbol{\rho}^{gpl}, \boldsymbol{\rho}^{wcl}, \boldsymbol{d}]. \tag{6.25}$$

To prepare the input for the Q-network, all elements in the state $\boldsymbol{x}$ have been normalized to fall within the range $[0, 1]$.

Action

The action within our DRL framework is charging price $p_{charging}$ (its unit is \$/kWh), which is a discrete variable belonging to the set $\mathscr{P} = \{0, 0.5, 1, 2, 3\}$, with each element representing a price level. The base price, set at $p_{charging} = 1$, represents the price under normal conditions. In our model, we adopt a fixed marginal utility for each price; however, in some cases, a piecewise marginal utility can be assumed, as demonstrated in (Wen et al., 2016).

Reward

The immediate reward in our DRL algorithm after taking action a in state x at time step t, denoted as r_t, depends on the objective of the dynamic charging, i.e., maximizing the total throughput and maximizing the total energy received by EVs. Meanwhile, we consider the congestion in each road segment as a penalty, C^{gpl}/C^{wcl}. For each segment, the penalty is defined as a negative value if its density exceeds its critical density, otherwise set to zero. Similar to the model adopted in (Wang et al., 2022a), we

utilize a variant of the sigmoid function, which can be expressed as:

$$C^{gpl} = \sum_{n=1}^{N} \frac{1}{1 + exp((m_n^{gpl} - m_{1,n})/k_{1,n})} \tag{6.26}$$

$$C^{wcl} = \sum_{n=1}^{N} \frac{1}{1 + exp((m_n^{wcl} - m_{2,n})/k_{2,n})} \tag{6.27}$$

where $m_{1,n}$, $m_{2,n}$, $k_{1,n}$, $k_{2,n}, n = 1, ..., N$ are the coefficients of the penalty function. These parameters determine the scaling and translation of the function which can be user-defined. (6.27) indicate that, with appropriate parameters selected, when $m_n^{gpl} \leq m_{c,n}^{gpl}$, the penalty is close to zero; when $m_n^{gpl} > m_{c,n}^{gpl}$, there is a penalty for traffic congestion. Hence, the reward at t step iteration is defined as the sum of the two objectives deducted by the penalty:

$$r_t = W_1 \times Throughput_t + W_2 \times Energy_t - W_3 \times Penalty_t \tag{6.28}$$

where $Penalty_t = C_t^{gpl} + C_t^{wcl}$; $Throughput_t$ is the total throughput within the time interval t, defined as the total number of vehicles that pass over the loop detector (see Fig. 6.5) installed at the entrance of the WCL; $Energy_t$ is the total energy received by EVs; W_i is the weight of different terms.

Q-network

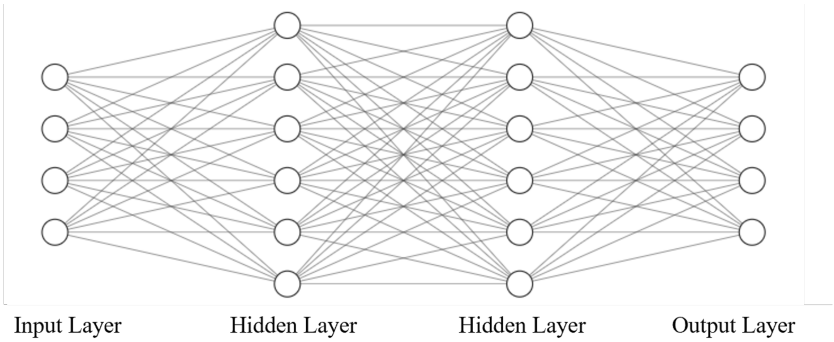

Figure 6.6: A schematic diagram of the Q-network (Fully connected neural network)

The Q-network, typically represented by a deep neural network, addresses this challenge by estimating the Q-values directly from the continuous state inputs. This network takes as input the state of the environment and outputs Q-values for all possible actions within that state. Its architecture is designed to capture complex patterns in high-dimensional spaces, facilitating the learning of optimal policies over continuous and complex state spaces without necessitating a discrete and enumerable state-action space. In our algorithm, the state vector $\boldsymbol{x}$ has been defined in (6.25), then the Q-network approximates the Q-value function $Q(\boldsymbol{x}, a)$. Our Q-network comprises a series of fully connected (FC) layers interspersed with non-linear activation functions. Here we adopt the Rectified Linear Unit (ReLU) as the activation function, which is the most commonly used and has proven effective in most tasks (Agarap, 2018). A schematic diagram of our Q-network is depicted in Fig. 6.6. In general, the input size of the network is equal to the dimension of the state, while the output size corresponds to the number of actions. Other hyperparameters of the network, such as the size of the hidden layers and the number of hidden layers, are user-defined and primarily depend on the scale of the state and the complexity of the environment. The mathematical representation of the Q-network is as follows:

1. The output of the first FC layer is given by:

$$h_1 = W_4 \times x + b_1 \tag{6.29}$$

where W_4 represents the weight matrix of the first FC layer, b_1 denotes the bias vector, s is the input state vector, and h_1 is the output of the layer.

2. The ReLU activation function is applied to h_1, producing:

$$a_1 = \max(0, h_1) \tag{6.30}$$

   The ReLU function introduces non-linearity by applying a threshold operation that sets all negative values in h_1 to zero, resulting in the activation vector a_1.

3. The second FC layer's output is:

$$h_2 = W_5 \times a_1 + b_2 \tag{6.31}$$

   where W_5 and b_2 represent the weight matrix and bias vector of the second FC layer, respectively, and h_2 as the output.

4. ReLU is applied again to h_2 to obtain:

$$a_2 = \max(0, h_2) \tag{6.32}$$

5. The final FC layer outputs the Q-values for the actions:

$$Q(x, a) = W_6 \times a_2 + b_3 \tag{6.33}$$

   Here, W_3 and b_3 are the weight matrix and bias vector of the last FC layer, respectively.

Training the Q-network involves adjusting its weights $(W_4, b_1, W_5, b_2, W_6, b_3)$ to minimize the difference between the predicted Q-values and the target Q-values, which are computed using the Bellman equation. The target Q-values are derived from the rewards obtained by taking actions in the environment, plus the discounted highest Q-value predicted for the next state. This process, known as temporal difference (TD) learning, itera-

tively improves the network's accuracy in estimating long-term rewards, steering the agent toward more strategic decision-making. The integration of deep learning with Q-learning not only enhances the capability of handling complex decision-making tasks but also broadens the applicability of reinforcement learning to a range of problems previously considered intractable with traditional methods.

Training

(1) Episodic Reinforcement Learning

In RL, the learning process is commonly divided into discrete episodes. Each episode begins with an initial state x_0 and concludes either when the system reaches a specific state or satisfies a pre-defined condition. Within the context of Deep Q-learning, episodes are instrumental not only in structuring the learning process but also as a vital component for stabilizing and enhancing the learning dynamics. Through iterative adjustments of its policy, based on the aggregated experience from multiple episodes, the agent gradually enhances its decision-making capabilities, aiming to maximize cumulative rewards. Moreover, episodic learning provides a pragmatic approach to managing complex environments by segmenting the learning process into manageable units, thus mitigating the challenges posed by long-term dependencies and sparse reward distributions.

In our algorithm, an episode terminates upon reaching a maximum step count. Hence, each episode constitutes a learning trajectory, defined as a sequence of states, actions, and rewards. During the learning process, the algorithm seeks to find a policy that maximizes the expected reward (discounted by γ) across the entire episode. Employing episodic frameworks facilitates learning by periodically refreshing the agent's experiences and

establishing clear boundaries for exploration, policy assessment, and learning. Such a strategy promotes the accumulation of experience, enhancing the algorithm's ability for pattern recognition and generalization across varied scenarios.

In certain RL tasks, particularly in some gaming tasks (e.g., Super Mario), each episode commences with a fixed initial state. In our algorithm, however, the initial state x_0 for each episode may vary, representing different initial traffic densities in the double-lane system. Consequently, x_0 is generated randomly. Further details are provided in Alg. 2.

(2) Exploration rate

In DRL, the use of a gradually decaying exploration rate is a strategic approach to balance the exploration-exploitation trade-off. This method involves initially allowing the agent to explore the environment freely by choosing actions with high randomness. Over time, as the agent learns more about the environment, the exploration rate is gradually reduced, encouraging the agent to exploit its accumulated knowledge to make more informed decisions. This strategy ensures that the agent does not become stuck in a local optimum early on by exploiting too aggressively, while also ensuring that it leverages its learned experiences to maximize rewards as it becomes more familiar with the environment. A common implementation of this strategy employs an epsilon-greedy policy, where the parameter ϵ (epsilon) represents the probability of selecting a random action, and decays over time according to a predefined schedule.

The decay of ϵ is modeled by the following formula, where ϵ^s, ϵ^f, and ϵ^d represent the initial exploration rate, final exploration rate, and the decay

factor, respectively:

$$\epsilon(t) = \epsilon^f + (\epsilon^s - \epsilon^f) \exp\left(-\frac{t}{\epsilon^d}\right)$$

Here, t represents the frame index or the number of iterations. This formula ensures that ϵ decreases exponentially from ϵ^s to ϵ^f, reducing as the agent gains more experience, thereby transitioning from exploration to exploitation.

(3) Experience replay

We adopt a Deep Q-learning algorithm with an experience replay mechanism. This mechanism involves storing the agent's experiences at each time step, denoted by a tuple, $(\boldsymbol{x}_t, a_t, r_t, x_{t+1})$, consisting of state $\boldsymbol{x}$, action a, reward r, and subsequent state $\boldsymbol{x}^{'}$, in a data repository known as the replay buffer. The experiences stored in the replay buffer encompass a wide variety of situations, including different states, actions, and outcomes, thereby encapsulating the diversity of the agent's interactions with the environment.

During the training process, the algorithm does not learn from consecutive experiences as they occur because it may lead to strong correlations between successive learning samples and thereby lead to inefficient learning. Instead, it randomly samples a minibatch of experiences from the replay buffer. This sampling strategy mitigates the issues of correlated data and non-stationary distributions, common in online reinforcement learning scenarios, by breaking the temporal correlations. Each minibatch of experiences is then used to update the neural network's parameters.

The update process involves calculating the loss between the predicted Q-values and the target Q-values for each experience in the minibatch. The

target Q-value is computed as the immediate reward plus the discounted maximum future reward, expected from the next state, as per the Bellman equation. This approach ensures a more stable and robust learning process by leveraging the diversity of experiences and smoothing over the data distribution changes. In essence, the experience replay mechanism not only enhances the data efficiency by reusing past experiences but also stabilizes the training process of the deep neural network within the Deep Q-learning framework.

Algorithm 2: Deep Q-Learning with Experience Replay

Input: γ: discount factor, α: learning rate, ϵ: exploration rate

Input: C: memory capacity for experience replay, M: minibatch size

Initialize replay memory $\mathbb{D}$ to capacity C

Initialize Q-network with random weights $\boldsymbol{\theta}$

for *episode* $= 1$ **to** E **do**

  Initialize state $\boldsymbol{x} = [\boldsymbol{\rho}^{gpl}, \boldsymbol{\rho}^{wcl}, \boldsymbol{d}]$ by resetting the *NetLogo* environment

  for $t = 1$ **to** T **do**

    Select a random action a_t with probability ϵ

    else select $a_t = \arg\max_x Q(\boldsymbol{x}_t, a; \boldsymbol{\theta})$

    Execute action a_t in environment

    Observe reward r_t and next state $\boldsymbol{x}_{t+1}$

    Store transition $(\boldsymbol{x}_t, a_t, r_t, \boldsymbol{x}_{t+1})$ in $\mathbb{D}$

    Sample random minibatch of transitions $(\boldsymbol{x}_j, a_j, r_j, \boldsymbol{x}_{j+1})$ from $\mathbb{D}$

    if x_{t+1} *is terminal* **then**

      Set $y_t = r_t$

    else

      Set $y_t = r_t + \gamma \max_{a_{t+1}} Q(\boldsymbol{x}_{t+1}, a_{t+1}; \boldsymbol{\theta})$

    end

    Perform a SGD update on $(y_t - Q(\boldsymbol{x}_t, a_t; \boldsymbol{\theta}))^2$ with respect to the Q-network parameters $\boldsymbol{\theta}$

    Update state: $\boldsymbol{x}_t = \boldsymbol{x}_{t+1}$

  end

end

6.5.3 Decision Tree Regression

Background

A decision tree is an efficient type of machine learning algorithm that is used for both classification and regression tasks (Breiman et al., 1984). As a type of supervised learning algorithm, they model decisions and their possible consequences as a tree structure, comprising nodes that represent questions or tests on features, and branches that correspond to outcomes of these tests. Among the foundational algorithms in this category, ID3 and CART have established significant precedents. ID3, developed by Quinlan, uses information gain to decide the best feature for splitting the data (Quinlan, 1986), whereas CART, introduced by Breiman et al., utilizes Gini impurity or mean squared error depending on whether the task is classification or regression, respectively. These methods have been extended in various forms, such as C4.5, which improves upon ID3 by handling both continuous and discrete attributes and employing more sophisticated pruning methods (Quinlan, 2014).

The construction of a decision tree involves selecting the best feature to split the data at each node based on a set of hyper-parameters that aims to partition the data into the most homogeneous subsets possible. The goal is to split the data into distinct subsets that contain instances with similar values (homogeneous samples). The construction of a decision tree involves several systematic steps to effectively model decision-making pathways. Here's how these trees are generally built:

1. **Feature Selection**:
    - **Objective**: The first step in building a decision tree is to select the best feature that will split the data into the most homogeneous

subsets possible. This is crucial as it determines the effectiveness of the classification or regression task.

- **Method**: This involves evaluating each feature and its corresponding splitting point to determine how well it separates the data into two subsets based on a specific metric, typically mean squared error (MSE) for regression trees. The MSE is calculated as:

$$\text{MSE} = \frac{1}{n}\sum_{i=1}(y_i - \hat{y}_i)^2$$

where y_i is the actual value and $\hat{y}_i$ is the predicted value within each subset; n is the number of data points in the subset.

- **Split Decision**: The algorithm selects the optimal splitting feature and the corresponding splitting point with which the combined MSE of the resulting two subsets is minimized.

2. **Tree Generation**:

- **Recursive Binary Splitting**: A decision tree is constructed using a method known as recursive binary splitting. This top-down approach starts from a root node and involves partitioning the data into subsets that are as pure as possible.

- **Nodes**:

  – **Decision Nodes**: These nodes perform a test on a specific feature, determining the path of branching. Each node in the tree acts as a test case for some condition on a single feature, thus splitting the dataset into two distinct subsets.

  – **Leaf Nodes**: These are the terminal nodes that represent the predicted output. For regression trees, this is typically the mean or median of the target values in the leaf.

3. **Decision Tree Pruning**:

- **Purpose**: To avoid overfitting, which can occur if the tree is overly complex and captures noise in the data rather than actual patterns.
- **Method**: Pruning involves removing parts of the tree that do not provide power to classify instances. This process can be based on criteria such as the minimum cost complexity pruning, where branches that have little statistical impact on the model performance are removed. It should be noted that the set of `max_depth`, which serves as a form of pre-pruning, also prevents the overfitting of the tree.

Common hyper-parameters include `max_depth`, the maximum depth of the tree, `min_samples_split`, the minimum number of samples required to split an internal node, and `min_samples_leaf`, the minimum number of samples a leaf node must contain.

The depth of a decision tree refers to the maximum length of a path from the root node to a leaf node, measured by the number of edges traversed. This depth is a critical parameter in the construction and performance of decision tree models as it influences both the complexity of the model and its ability to generalize. A deeper tree can model more intricate decision boundaries by incorporating a greater number of splits, thereby capturing finer details in the data. Conversely, a tree that is too deep is prone to overfitting, where the model captures noise instead of the underlying data distribution. Thus, controlling the depth of a decision tree is crucial for balancing between underfitting and overfitting, ensuring that the model remains robust and predictive across varied data scenarios. The `max_depth` parameter limits the total number of levels in the tree. Constraining the depth of the tree helps prevent overfitting, as deeper trees can learn more detailed data specifics, reflecting anomalies and noise in the training data. A lower value of `max_depth` can increase the bias but generally decrease

the variance, leading to a model that is less likely to capture noise in the data. `min_samples_split` is used to decide whether a node can be split further. It effectively controls the minimum size of the detectable patterns, thus acting as a means to regularize the tree. By setting this threshold, smaller groups in the data that may be anomalies or outliers will not cause further splits; hence, the tree will be less complex and more general. This is particularly useful in avoiding overfitting in scenarios where the model is trained on small datasets or datasets with significant noise. `min_samples_leaf`, on the other hand, ensures that each leaf, the terminal node of the tree, has a minimum number of samples. This parameter impacts the model at the most granular level—individual predictions. By requiring a minimum number of samples in each leaf, the tree averages more samples in its predictions, thereby increasing model stability and accuracy. It can also prevent the model from making overly confident decisions based on a small number of cases, thereby enhancing its generalization capabilities.

One of the key advantages of decision trees is their simplicity and transparency; they are easy to understand and interpret, making them especially valuable in sectors where understanding the decision-making process is as important as the accuracy of the predictions. Additionally, decision trees require no input feature scaling and can handle both numerical and categorical data, supporting their flexibility in dealing with various types of data. However, decision trees also have their limitations. They are prone to overfitting, especially when they grow too deep and complex. This can be mitigated by setting appropriate hyper-parameters such as `max_depth` and `min_samples_leaf` to prevent the tree from creating overly complex models based on the training data. Another disadvantage is their sensitivity to small changes in the data, which can lead to vastly different tree structures. This instability is a challenge, particularly in dynamic environments where data may change frequently.

In practice, decision trees can effectively handle diverse data types and scenarios but require careful setting of hyper-parameters and understanding of their strengths and weaknesses to ensure that the models generated are both accurate and robust, capable of generalizing well to new data.

Training

In this study, we develop a dynamic pricing strategy using the CART algorithm, primarily to establish a benchmark for evaluating our Deep Q-Learning (Deep Q-learning) algorithm, rather than to fully explore the potential of traditional machine learning techniques. Considering that the price p is a discrete variable, the dynamic pricing challenge could initially be approached as a classification task. However, such an approach fails to leverage the continuous value data of each price p, which is crucial for a nuanced understanding of pricing dynamics. To address this limitation, we employ the CART algorithm for a regression task to better utilize the quantitative information associated with each potential price. Our methodology unfolds in three steps:

1. **Data Generation**: Utilizing an Agent-Based Model (ABM), we generate a dataset (X, Y), where $X = [\boldsymbol{x}^{'}, a]$ comprises the feature vector. Here, $\boldsymbol{x}^{'} = [\boldsymbol{\rho}^{gpl}, \boldsymbol{\rho}^{wcl}, d_1]$ represents the state, specifically including only the immediate future traffic demand, distinct from the states used in Deep Q-learning. The action a is also included in X. The corresponding $Y = [r(\boldsymbol{x}^{'}, 0, \ldots, r(\boldsymbol{x}^{'}, 3)]$ consists of the rewards for each charging price p, illustrating the reward's dependency on the price.

2. **Decision tree training**: We apply the CART algorithm to map the relationship between X and Y (as defined in (6.28)), thereby

modeling how different charging prices influence the rewards. The purity of each node is measured using the MSE.

3. **Optimal Price Implementation**: The price yielding the highest reward is selected and implemented in the system, optimizing the charging strategy within the defined parameters.

Our aim is to test the efficacy of the deep Q-learning algorithm by comparing it against a straightforward, regression-based benchmark. The pseudocode of the algorithm is detailed in Alg. 3.

Algorithm 3: Modified CART

Input: Training data $\mathbb{D} = \{(X_1, Y_1), \ldots, (X_N, Y_N)\}$, Hyper-parameters: `max_depth`, `min_samples_split`, `min_samples_leaf`

Output: Decision tree

Initialize tree with a single node containing all points
Initialize `current_depth` $= 0$
Discretize continuous features in X using a suitable method (e.g., quantile bins)
while *termination criteria not met (`current_depth` $<$ `max_depth` and node samples $>$ `min_samples_split`)* **do**
    if *possible to split* **then**
        for *each candidate splitting point* **do**
            Compute the combined MSE of two subsets (left and right):

$$MSE = \frac{1}{|L|} \sum_{i \in L} (y_i - \bar{y}_L)^2 + \frac{1}{|R|} \sum_{jinR} (y_j - \bar{y}_R)^2$$

        end
        Choose the split with the lowest combined MSE
        Split the node into two child nodes based on this split
    else
        Mark node as a leaf
    end
end
return *Decision tree*

6.6 Numerical Experiments

6.6.1 Parameter settings for the lane-choice model

As detailed in Sec. 6.5.1, the marginal utilities $\beta_s, \beta_T, \beta_C$ in our logit model are informed by the results from (Ge and MacKenzie, 2022), where the corresponding values are -4.58, -0.242, and -0.01 for the variables s_i, $T_{charging,i}$, and $C_{charging,i}$ respectively. These variables represent SOC in percentage, charging time in hours, and charging cost in dollars. It is crucial to note that in the cited study, $T_{charging,i}$ and $C_{charging,i}$ denote the time and cost to fully charge an EV's battery. However, in the WCL context, it is not feasible for an EV to achieve a predetermined SOC since the charging duration is equivalent to the time taken to travel the entire WCL. Given this discrepancy in the definition of $T_{charging,i}$ and $C_{charging,i}$, we adapt the marginal utilities in our model by considering the relative values of different variables, rather than directly adopting the values from the cited reference. In our model, we assume that all EVs share the same battery capacity of 75 kWh; the actual power of WCL, e^+, is 15 kW. Other parameters are collected in Table.

First, since $T_{charging,i}$ and $C_{charging,i}$ are calculated in the same way, it can be inferred:

$$\frac{\beta_T}{\beta_C} = \frac{-0.242}{-0.01} \approx 24 \tag{6.34}$$

According to the coefficients of SOC and charging cost, the value of a 1% decrease in SOC is calculated as ($\frac{-4.58\%}{-0.01} = \$4.58$), indicating that a 1% reduction in SOC equates to a decrease of \$4.58 in the total charging cost when charging from the current SOC to full capacity. For simplicity, we assume that the current SOC of EVs is 41%, then the equivalent charging cost per kWh that corresponds to the same financial impact as a 1% SOC

decrease is calculated as $\frac{4.58}{(1-0.41)\times 75} \approx \$0.1$ /kWh. Then we have $1\% \times \beta_s = \frac{L_{sys}}{\bar{v}_i^{wcl}} \times e^+ \times 0.1 \times \beta_C$. Hence, the ratio of β_C to β_s can be calculated as:

$$\frac{\beta_C}{\beta_s} = \frac{1}{8.33} \tag{6.35}$$

Let $\beta_s = -4.58$. Based on equations (6.34) and (6.35), we calculate that $\beta_C = -0.55$ and $\beta_T = -13.24$. To emphasize the impact of charging price on lane choice, we increase the coefficient for β_C by 1.5 times, resulting in $\beta_C = -0.55 \times 1.5 = -0.825$. The relationship between the probability of choosing the WCL and the charging price $p_{charging}$, for an EV with a SOC of 41%, is illustrated in Fig. 6.7.

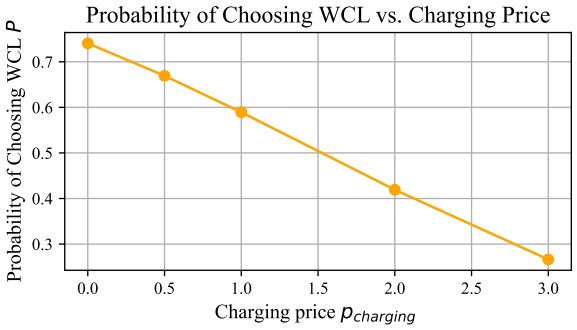

Figure 6.7: The relationship between the probability of choosing the WCL and the charging price, assuming an EV with a SOC of 41%.

However, it is important to note that these marginal utilities are only for reference. Accurate values should be derived from experimental analysis in the context of WCLs. Nonetheless, this is difficult to implement before the large-scale commercialization of WCLs.

6.6.2 Simulation for sample scenarios

In this section, we conduct a series of numerical experiments across twelve sample scenarios. In each scenario, we test the performance of every possible charging price. Hence, each scenario only lasts for one pricing interval.

The objectives of these experiments are threefold: (1) to demonstrate the effectiveness of our ABM developed in *NetLogo*, (2) to validate the design of the reward function as defined in Equation (6.28), and (3) to elucidate the performance disparities among various charging prices $p_{charging}$.

The initial conditions of the twelve scenarios are detailed in Table. 6.2, where $m_{tot}^{gpl} = \sum_{n=1}^{5} m_n^{gpl}$ and $m_{tot}^{wcl} = \sum_{n=1}^{5} m_n^{wcl}$ represent the total number of EVs on the GPL and on the WCL, respectively. In scenarios #1 to #4, the system begins with free-flow traffic, whereas scenarios #5 to #8 and #9 to #12 start with medium and heavy congestion, respectively. To facilitate a consistent comparison of different charging prices ($p_{charging}$), a uniform highway traffic demand of $d_1 = 60$ is maintained across all scenarios. This setup is designed to encompass a broad range of traffic conditions, providing a comprehensive analysis of the impacts of pricing strategies. The performance of each price setting ($p_{charging}$) within a scenario is determined by averaging the outcomes of ten repeated experiments, enhancing the reliability of our results.

6.6.3 Parameter settings for the Deep Q-learning algorithm

This section introduces the parameter settings for the Deep Q-learning algorithm. First, the parameters for the ABM used for the numerical experiments and the hyper-parameters for the Deep Q-learning algorithm are collected in Table. 6.3. During the process of Deep Q-learning training, in each episode, the system begins with a random initial state wherein the total number on the GPL and the WCL satisfy a uniform distribution: $\sum_{n=1}^{N} \rho_n^{gpl} \sim \mathcal{U}(\rho_{min}^{gpl}, \rho_{max}^{gpl})$, $\sum_{n=1}^{N} \rho_n^{wcl} \sim \mathcal{U}(\rho_{min}^{wcl}, \rho_{max}^{wcl})$. The variation in the initial state across different episodes helps enhance the algorithm's abil-

ity to address diverse traffic dynamics. Each episode lasts for 10 pricing intervals, namely, 30 minutes. Hence, T in Step 5 of Alg. 2 is set to be 10.

Table 6.2: Initial states for the numerical examples

No. of Scenario	Traffic State	m_{tot}^{gpl}[1](veh)	m_{tot}^{wcl}[2](veh)	d_1[3](veh/min)
#1	Free-flow	100	100	60
#2		100	200	60
#3		200	100	60
#4		200	200	60
#5	Congested (Medium)	200	400	60
#6		200	600	60
#7		400	200	60
#8		600	200	60
#9	Congested (Heavy)	400	400	60
#10		400	600	60
#11		600	400	60
#12		600	600	60

[1] Total number of EVs on the GPL.
[2] Total number of EVs on the WCL.
[3] Traffic demand in the next pricing interval

6.6.4 Parameter settings for the CART algorithm

In this section, we introduce the configuration of the training data and the hyper-parameter settings employed for the CART algorithm. The training dataset, constructed from the twelve illustrative scenarios discussed in Sec. 6.6.2 and outlined in Table 6.2, comprises 60 data points resulting from a combination of 12 scenarios and 5 distinct pricing levels. For each data point, traffic demands are selected from a set $d \in \{20, 30, 40, 50, 60\}$, generating 300 unique combinations. We believe that these 300 data points can cover most traffic scenarios. Regarding the hyper-parameters for the CART algorithm, we focus on three primary settings: `max_depth`, `max_samples_split`, and `min_samples_leaf`. These parameters are pivotal in tailoring the decision tree to the specific characteristics of our problem and the nature of the training data. Based on the foundational concepts discussed in

Table 6.3: Values of the double-lane system

Hyper-parameters	**Values**
Learning rate	0.0001
Discount factor[1]	0.99
Initial exploration rate[1] ϵ	1
Final exploration rate[1] ϵ	0.01
Batch size	32
Number of hidden layers	2
Size of a hidden layer	64
Gradient descent optimizer	Adam(Da, 2014)
Memory capacity	10000
Parameters	**Values**
e^+	15
p	{0.5, 1,1.5, 3,5 }
v^{gpl1}	22
v^{wcl1}	20
v_i^{max}	100
$a_{acc,i}{}^1$	3
$a_{dec,i}{}^1$	-4.5
s_i^{min}	20
s_i^{max}	80
v_i^{lat}	1

[1] The parameter settings are similar to Shi et al. (2023).

Section. 6.5.3, the parameters are set to 4, 10, and 5, respectively. These settings are chosen to optimize the balance between model complexity and generalization capability, ensuring robust performance across various traffic scenarios.

The model is evaluated using the testing subset. Predictions for the test features are generated and then compared against the actual results in the test data set. The MSE is used to evaluate the average squared difference between the predicted values and the actual values. A lower MSE value indicates higher model accuracy and better performance in capturing the underlying data patterns.

6.6.5 Simulation of Real Traffic Scenarios

In this subsection, we construct two real traffic scenarios that facilitate a comparative analysis between the Deep Q-learning algorithm and the CART algorithm. Each scenario spans 30 minutes, corresponding to 10 pricing intervals. In Scenario #1, the system initiates under conditions of light traffic, replicating a typical morning traffic scenario with low demand lasting 30 minutes. Conversely, Scenario #2 starts with heavy traffic, characterized by greater congestion on the WCL compared to the GPL, and maintains high traffic demand throughout the same duration.

We employ real-world traffic demand, d_1, as illustrated in Fig. 4.5 from 8:00 to 8:30 (here scale d_1 by 2.5 times), to model rush hours in the morning. The traffic demand data is sampled every 3 minutes, aligning with the pricing interval. In the *NetLogo* environment, the arrival pattern of incoming EVs is modeled according to a Poisson distribution, as delineated in Sec. 6.5.1.

In each scenario, both the Deep Q-learning and CART algorithms generate 10 pricing signals. To underscore the impact of charging prices on traffic flow and charging efficiencies, we also evaluate the performance of a constant pricing strategy (here we adopt the base price, \$1/kWh). The efficacy of the three strategies is compared in terms of total throughput, total energy received by EVs, and the penalties for congestion, consistent with the reward function defined in (6.28).

6.7 Results and Discussions

6.7.1 Results for sample scenarios

Fig. 6.8 displays the results of the first four numerical experiments conducted under an initial state of free-flow traffic. Among these experiments, it is observed that the lowest charging price results in the best reward. The reasons are intuitive. Firstly, it can be observed that the total throughput *Throughput* in different $p_{charging}$ is almost the same in all four experiments. This is because the light initial traffic conditions allow incoming EVs to enter the double-lane system without experiencing congestion, regardless of how traffic demand is allocated between the two lanes. It can also be observed that the penalty for traffic congestion in each experiment remains at a low level (< 0.04) in the four scenarios. Hence, the total energy *Energy* dominates the reward according to (6.28). The lowest charging price $p_{charging} = 0$ results in more EVs choosing the WCL compared to other prices, thereby yielding the highest *Energy*.

Fig. 6.9 and Fig. 6.10 display the results of the first four numerical experiments conducted under initial states of medium and heavy traffic, respectively. In scenarios #7, #8, and #11, where the GPL is more congested than the WCL, a lower price results in more EVs choosing the WCL, which not only eases the congestion on the GPL (indicated by a lower *Penalty*) but also increases the total throughput and improves the total energy received by EVs. Consequently, the lowest price $p_{charging} = \$0$ exhibits the best reward. Conversely, in scenarios #5, #6, and #10, where the WCL is more congested than the GPL, a higher price leads to more EVs choosing the GPL, effectively easing the congestion on the GPL (lower *Penalty*) and increasing the total throughput. Although a lower price still exhibits a higher *Energy*, in the context of congestion, *Penalty* and

Throughput dominate. Consequently, the best rewards are achieved at $p_{charging} = \$2, \$3, \$2$ in these scenarios, respectively. In scenarios #9 and #12, where the congestion on both lanes is about the same, a medium price (\$1/kWh) performs best considering the trade-off between *Throughput*, *Energy*, and *Penalty*.

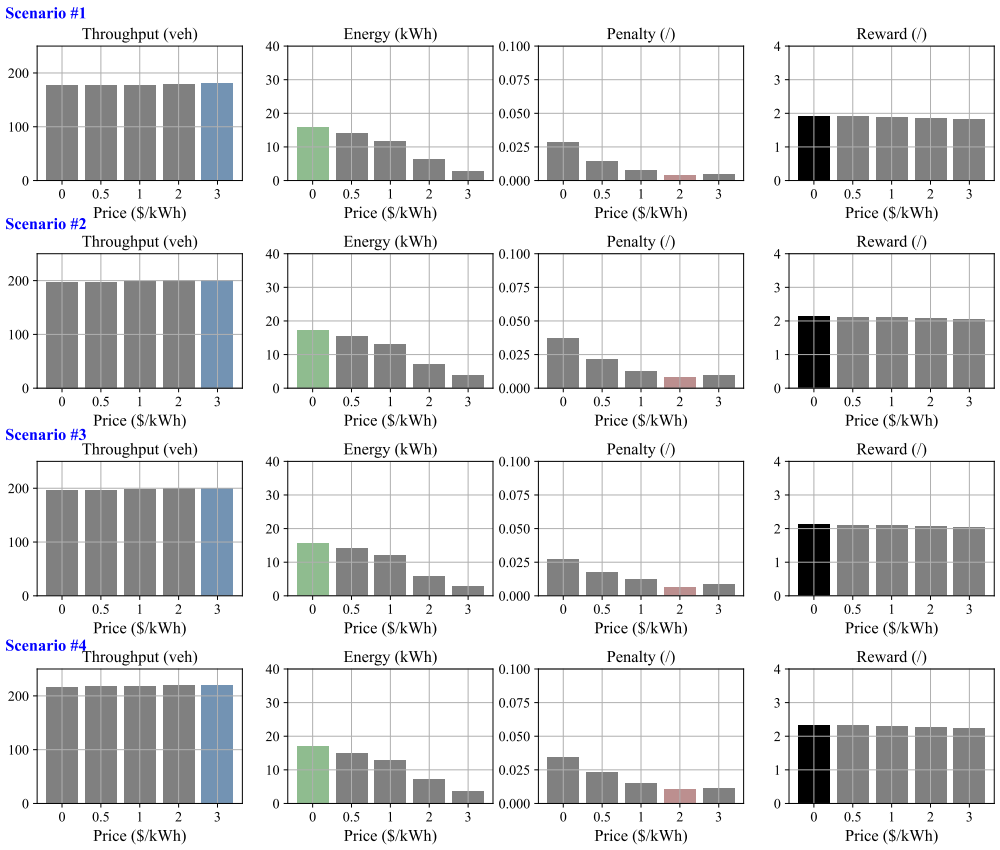

Figure 6.8: Results for sample scenarios 1 to 4, characterized by an initial state of free-flow traffic

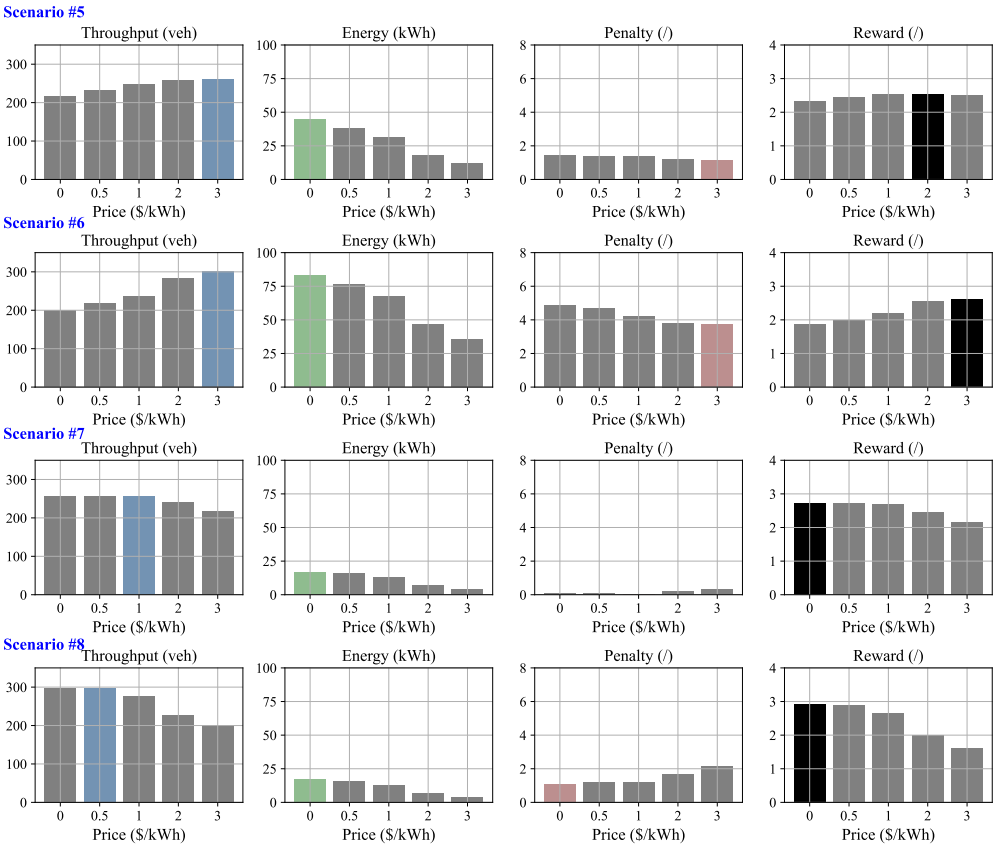

Figure 6.9: Results for sample scenarios 5 to 8, characterized by an initial state of congested (medium) traffic

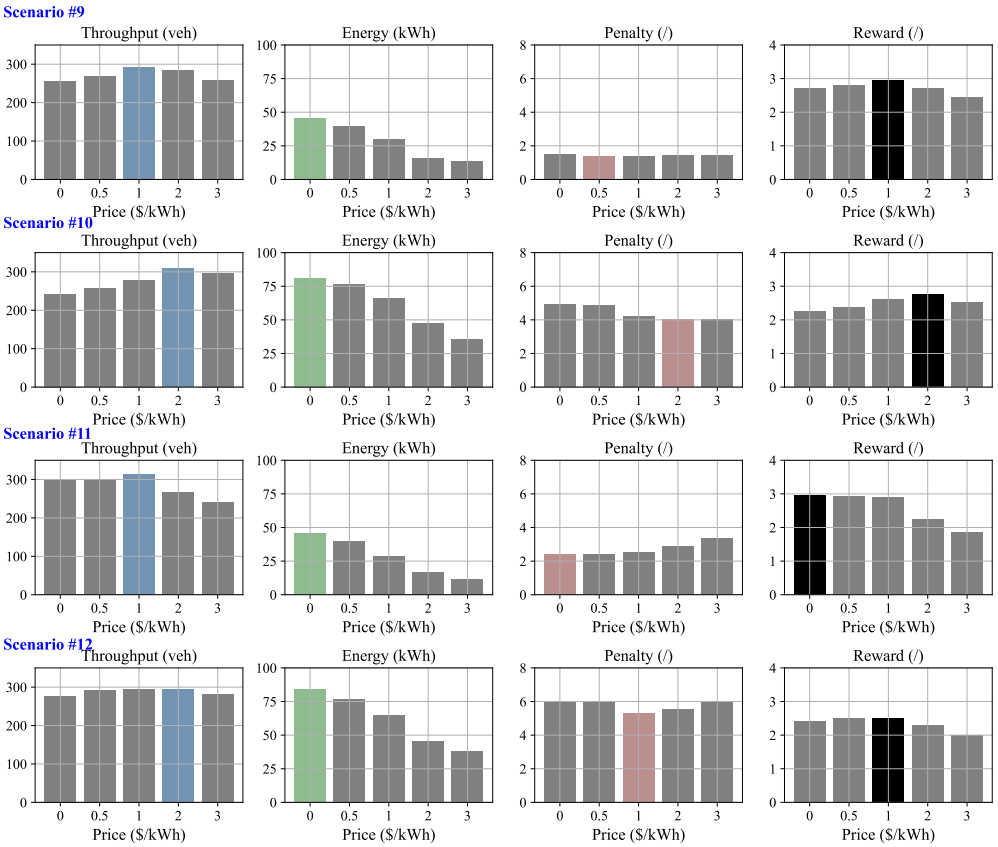

Figure 6.10: Results for sample scenarios 9 to 12, characterized by an initial state of congested (medium) traffic

6.7.2 Learning Performance of the Decision Tree Algorithm

The performance of the Decision Tree Regression model was evaluated using both the Mean Squared Error (MSE) and the coefficient of determination (R^2). These metrics collectively provide a comprehensive view of the model's predictive accuracy and its ability to explain the variability in the target variable.

The MSE provides a measure of the average of the squares of the errors, indicating how closely the model's predictions match the actual values:

$$\text{MSE} = \frac{1}{n}\sum_{i=1}^{n}(Y_i - \hat{Y}_i)^2$$

In addition, R^2 is calculated to assess the proportion of variance in the dependent variable that is predictable from the independent variables:

$$R^2 = 1 - \frac{\text{Sum of Squares of Residuals}}{\text{Total Sum of Squares}} = 1 - \frac{\sum_{i=1}^{n}(Y_i - \hat{Y}_i)^2}{\sum_{i=1}^{n}(Y_i - \bar{Y})^2}$$

where $\bar{Y}$ is the mean of the observed data y_i.

The model achieved an MSE of 0.054, indicating a strong predictive accuracy with minor deviations from the actual values. Additionally, the R^2 value obtained was 0.85, suggesting that 85% of the variance in the dependent variable is explainable by the independent variables. This high R^2 value corroborates the model's effectiveness in capturing and quantifying the underlying data patterns. The combination of a low MSE and a high R^2 demonstrates not only the model's ability to produce accurate predictions but also its capacity to explain a significant proportion of the variance in the data.

6.7.3 Learning performance of Deep Q-learning

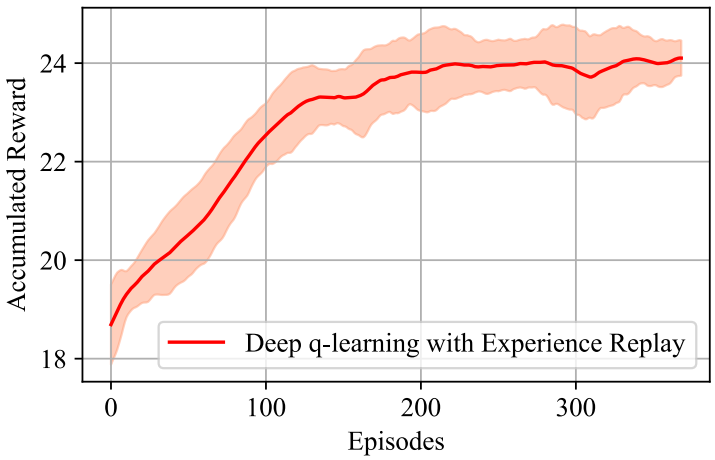

Figure 6.11: Accumulated reward vs. episodes for Alg. 2. The solid line represents the average performance over ten repeated trainings. The shaded region represents half of the standard deviation from the average performance.

In this section, we demonstrate the learning performance of our Deep Q-learning algorithm, as depicted in Alg. 2. Fig. 6.11 illustrates the learning curves for Alg. 2. We conduct 10 repeated trainings under the same parameter settings. It is observed that the cumulative reward per episode progressively increases over time, albeit with some fluctuations. In the initial 50 episodes, where the exploration rate is high, the rewards garnered are modest, reflecting the agent's preliminary adaptation and exploration of the environment. As training advances, a notable increase in rewards is seen between episodes 50 and 150, denoting the agent's improved performance and strategy optimization. Beyond 200 episodes, the rewards reach and maintain a relatively high plateau, highlighting the agent's successful derivation of an effective policy through sustained training.

6.7.4 Results under real traffic scenarios

This section compares the performance of three strategies within the two real traffic scenarios. Fig. 6.12 and Fig. 6.13 plot the price signal under the two scenarios. Fig. 6.14 and Fig. 6.15 compare the efficacy of these strategies across four critical metrics: accumulated reward, total throughput, total energy, and penalties for congestion, corresponding to scenario #1 and scenario #2, respectively. In scenario #1, where the system begins with light traffic and experiences a low traffic demand, both the CART and Deep Q-learning algorithms consistently opt for the lowest charging price ($0/kWh) at each pricing interval throughout the simulation. This leads to an increase in the number of EVs entering the WCL, thereby resulting in more energy transmitted to EVs. This phenomenon aligns with the analysis in Sec. 6.7.1, indicating that a lower charging price under light traffic conditions enhances the charging efficiency while not sacrificing the traffic efficiency. The strategy of giving the base price ($1/kWh) throughout the

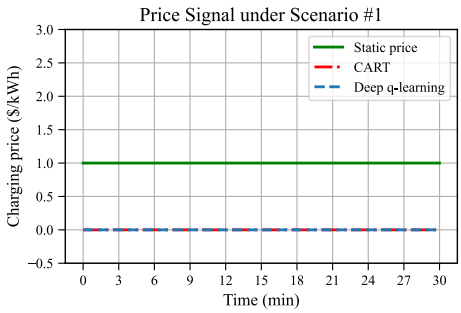

Figure 6.12: Price signal for real traffic scenario #1

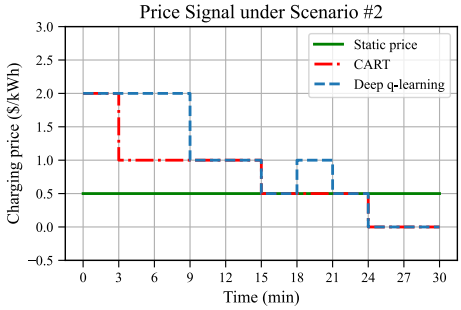

Figure 6.13: Price signal for real traffic scenario #2

simulation yields a total throughput of 1349 veh, a total energy of 17.6 kWh, and a penalty of 0.036. By contrast, the CART and Deep Q-learning algorithms yield almost the same total throughput, over 5 times energy (94.4 kWh), but a bit higher penalty for traffic congestion (0.064, though, still a low level). Consequently, the accumulated reward yielded by the dynamic pricing strategy is 6.7% higher than the static pricing strategy.

In scenario #2, the system starts under heavy traffic conditions with sustained high demand throughout the simulation. As illustrated in Fig. 6.15, the pricing trends demonstrated by the CART and Deep Q-learning algorithms start at a high price ($2/kWh) and progressively decrease, culminating in the minimum price ($0/kWh). The Deep Q-learning algorithm shows performance improvements in the final reward of 12.1% over CART and 28.3% over the static pricing strategy. The reasons are as follows. As the initial congestion on the WCL is greater than that on the GPL, both algorithms to implement a high price ($2/kWh) at the beginning. This

effectively leads more EVs to the GPL, alleviating congestion on the WCL. Subsequently, as congestion eases, the focus shifts towards maximizing energy transmission, leading to lower prices. In the final stages (24 to 30 minutes), the system reverts to light traffic conditions, similar to scenario #1, where a lower price is advantageous for maximizing energy delivery without compromising traffic efficiency. However, the pricing strategies of CART and Deep Q-learning differ significantly. CART is not capable of capturing the system dynamics or utilizing the future traffic demand information but only selects optimal prices for the current interval. Although the traffic demand remains high throughout the simulation, CART still adopts a more aggressive pricing approach at the early stages to maximize the immediate rewards. In contrast, the Deep Q-learning algorithm adopts a more nuanced strategy, maintaining a lower price of \$1/kWh between 3 and 9 minutes, which, although temporarily reduces energy growth, minimizes congestion penalties and enhances throughput. Consequently, from 9 to 15 minutes, the energy growth under both strategies aligns, yet the congestion penalty remains significantly lower under the Deep Q-learning approach. Thus, CART's strategy is myopic, whereas Deep Q-learning's farsighted approach better captures the complexities of the environment and effectively leverages future system inputs, highlighting its superior capability in managing complex dynamic traffic scenarios.

In summary, under light traffic scenarios, the dynamic pricing strategy tends to offer the lowest possible prices. It greatly enhances charging efficiency with little sacrifice of traffic efficiency. Since the traffic dynamics under light traffic are simple, CART and deep Q-learning exhibit similar performance. Under heavy traffic, however, the deep Q-learning algorithm outperforms CART due to its ability to capture the complex system dynamics of the ABM and to leverage future traffic demand information. Under both light and heavy traffic scenarios, the two dynamic pricing strategies,

which adjust charging prices according to the system state, perform better than the static pricing strategy.

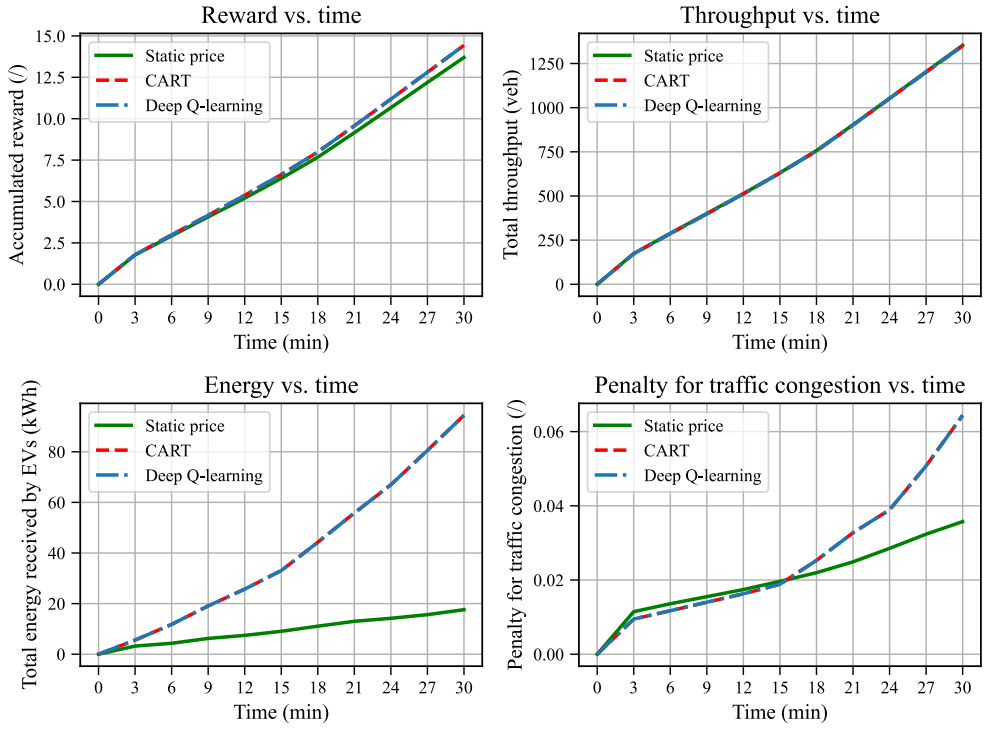

Figure 6.14: Results for real traffic scenario #1

6.8 Conclusions and Future Work

This study addresses a dynamic pricing problem within a double-lane system composed of a GPL and a WCL. EVs entering the system select lanes based on their attributes such as SOC, charging price, and travel time. It is evident that charging prices significantly influence EVs' lane choice. To this end, we developed a lane-choice model for EVs employing a Logit model, grounded in statistical data analysis. Then the problem lies in how to dynamically adjust charging prices based on the system state, thereby enhancing both traffic and charging efficiencies. We implemented an ABM using the *NetLogo* traffic simulator to establish our traffic simulation framework. To derive optimal dynamic pricing strategies, we employed both a

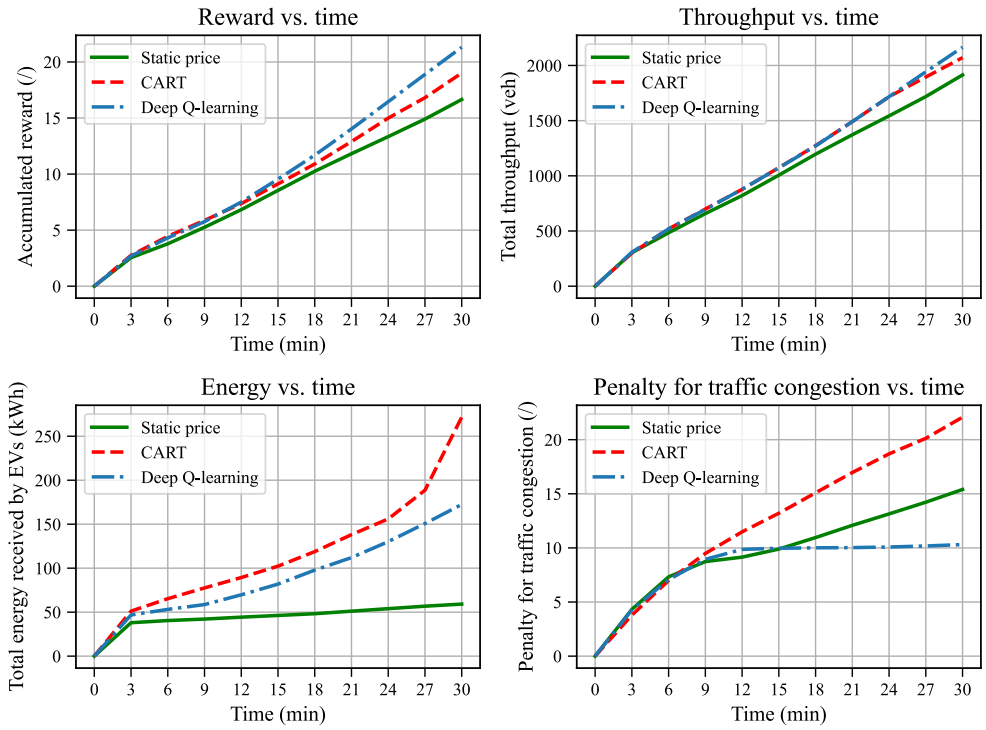

Figure 6.15: Results for real traffic scenario #2

simple decision tree (CART) algorithm and a Deep Q-learning algorithm.

A series of numerical experiments are conducted to validate the effectiveness of our model. Firstly, the one-step performance of our traffic simulation model was tested across twelve sample scenarios, confirming its validity. Subsequently, we evaluate the performance of the CART and Deep Q-learning algorithms under two real traffic scenarios. Comparisons are also made against a static pricing strategy. The simulation results reveal that both dynamic pricing strategies (CART and Deep Q-learning) outperform the static pricing strategy in effectiveness. Notably, the Deep Q-learning algorithm demonstrates superior capability in optimizing dynamic pricing strategies by leveraging system dynamics more effectively and future traffic demand information.

In conclusion, this study not only corroborates the efficacy of dynamic pricing in managing the double-lane system but also highlights the supe-

rior performance of Deep Q-learning algorithms in capturing and utilizing complex dynamic interactions within traffic systems. Future research will focus on refining these algorithms and exploring their applicability to more complex and varied traffic scenarios. In addition, there is scope to enhance the predictive accuracy of traffic demand forecasts, which is crucial for the further optimization of dynamic pricing strategies.

Chapter 7

Conclusions and future works

This thesis explores real-time management issues of traffic flows in the traffic systems with WCLs. Through three comprehensive studies, we have developed and evaluated several models and algorithms that optimize the operational efficiency of these systems.

The first two studies focused on real-time traffic control strategies, namely ramp metering and variable speed limits, using the CTM integrated with a hybrid MPC approach. We test the performance of the two control strategies under different priorities of traffic and charging efficiencies and revealed the inherent conflicts between these two objectives. We also propose a novel algorithm, *LKNMS*, to accelerate the hybrid MPC problem. The third study introduced a dynamic pricing approach within a dual-lane system (consisting of one GPL and one WCL). The system is modeled using an ABM approach. We employ a deep q-learning method to adaptively manage lane-choice behaviors and maximize overall system efficiency (a trade-off of traffic and charging efficiencies). This innovative approach proved superior to traditional static pricing strategies and highlighted the benefits of machine learning techniques in complex traffic management scenarios. The three studies provide models and algorithms tailored to the

real-time traffic management issues on WCLs, and provide some insights for policymakers and traffic departments. Besides, it is important to note that, the models and algorithms need to be established tailored to the specific scenarios.

Managerial insights are drawn from the three studies. On a fully covered WCL, the SOC of EVs is influenced by the spatial and temporal distribution of traffic flow speeds. Ramp metering control can affect the SOC by regulating on-ramp flows, though its effect is constrained by uncontrolled traffic demand. In contrast, VSL control directly impacts traffic speed profiles, making it more effective for optimizing CE. However, VSL control requires more advanced traffic technologies and complex models.

Simulation results indicate an inherent conflict between TE and CE, regardless of the control strategy, suggesting that WCLs are better suited to multi-lane systems for simultaneously optimizing both. In such systems, deploying WCLs on one lane with dynamic pricing is a viable strategy to enhance CE without sacrificing TE. However, the heterogeneity of EVs poses challenges at the model level, implying that homogenization of EV characteristics would simplify management from an operational perspective.

The limitations of this study can be categorized into three areas: Context, Modeling, and Algorithm. Each study was conducted within a specific context that may not readily generalize across different traffic systems or geographic locations. The modeling approaches, particularly the use of ABM in the third study, although powerful, require extensive computation and detailed data that may not always be available. The algorithms, especially those involving advanced machine learning, demand substantial computational resources and expertise in tuning and implementation.

Looking ahead, the future of real-time traffic management in WCL contexts appears promising but will require a more interdisciplinary approach to fully realize its potential. It is crucial to integrate knowledge from Electrical Engineering, Vehicle Engineering, Traffic Engineering, Communication Engineering, and additionally, Battery Science, which focuses on the electrochemical properties and performance characteristics of electric vehicle batteries, including charge-discharge curves that are vital for optimizing charging strategies in real-time scenarios.

Real-time management of WCLs is fundamentally an interdisciplinary problem that challenges the conventional boundaries of engineering disciplines. Although integrating these diverse fields is challenging, it is essential for addressing the more complex, real-world problems that arise as WCL technology moves towards broader deployment. Future research should continue to build on the foundations laid by this thesis, exploring new models and algorithms that can effectively integrate insights from these varied disciplines to enhance the design and operation of next-generation smart traffic systems.

Bibliography

Abdalrahman, A. and Zhuang, W. (2020). Dynamic pricing for differentiated pev charging services using deep reinforcement learning. *IEEE Transactions on Intelligent Transportation Systems*, 23(2):1415–1427.

Adriano, S., Chiara, F., Fabrizio, Z., Fabio, O., et al. (2014). Experimental analysis of the auxiliaries consumption in the energy balance of a pre-series plug-in hybrid-electric vehicle. *Energy Procedia*, 45:779–788.

Agarap, A. F. (2018). Deep learning using rectified linear units (relu). *arXiv preprint arXiv:1803.08375*.

Ahmad, A., Alam, M., and Chabaan, R. (2017). A comprehensive review of wireless charging technologies for electric vehicles. *IEEE Transactions on Transportation Electrification*, 4(1):38–63.

Alessio, A. and Bemporad, A. (2009). A survey on explicit model predictive control. In *Nonlinear Model Predictive Control*, pages 345–360. Springer, Berlin, Heidelberg.

Alwesabi, Y., Liu, Z., Kwon, S., and Wang, Y. (2021). A novel integration of scheduling and dynamic wireless charging planning models of battery electric buses. *Energy*, 230.

Alwesabi, Y., Wang, Y., Avalos, R., and Liu, Z. (2020). Electric bus scheduling under single depot dynamic wireless charging infrastructure planning. *Energy*, 213.

Amjad, M., Farooq-i Azam, M., Ni, Q., Dong, M., and Ansari, E. A. (2022). Wireless charging systems for electric vehicles. *Renewable and Sustainable Energy Reviews*, 167:112730.

Axehill, D., Besselmann, T., Raimondo, D. M., and Morari, M. (2014). A parametric branch and bound approach to suboptimal explicit hybrid mpc. *Automatica*, 50(1):240–246.

Bellemans, T., De Schutter, B., and De Moor, B. (2006). Model predictive control for ramp metering of motorway traffic: A case study. *Control Engineering Practice*, 14(7):757–767.

Bemporad, A. and Morari, M. (1999). Control of systems integrating logic, dynamics, and constraints. *Automatica*, 35(3):407–427.

Bemporad, A., Morari, M., Dua, V., and Pistikopoulos, E. N. (2002). The explicit linear quadratic regulator for constrained systems. *Automatica*, 38(1):3–20.

Bi, K., Chen, Y., Zhao, S., Ben-Arieh, D., and Wu, C.-H. J. (2019a). Modeling learning and forgetting processes with the corresponding impacts on human behaviors in infectious disease epidemics. *Computers & Industrial Engineering*, 129:563–577.

Bi, Z., Kan, T., Mi, C., Zhang, Y., Zhao, Z., and Keoleian, G. (2016). A review of wireless power transfer for electric vehicles: prospects to enhance sustainable mobility. *Applied Energy*, 179:413–425.

Bi, Z., Song, L., De Kleine, R., Mi, C., and Keoleian, G. (2015). Plug-in vs. wireless charging: Life cycle energy and greenhouse gas emissions for an electric bus system. *Applied Energy*, 146:11–19.

Bi, Z., Song, L., De Kleine, R., Mi, C., and Keoleian, G. (2019b). Life cycle assessment and tempo-spatial optimization of deploying dynamic

wireless charging technology for electric cars. *Transportation Research Part C: Emerging Technologies*, 100:53–67.

Bixby, R. E. (2002). Solving real-world linear programs: A decade and more of progress. *Operations research*, 50(1):3–15.

Bloomberg (2018). China's built a road so smart it will be able to charge your car. Accessed: January 2022.

Bolger, J., Kirsten, F., and Ng, L. (1978). Inductive power coupling for an electric highway system. In *28th IEEE Vehicular Technology Conference*, volume 28, pages 137–144. IEEE.

Borrelli, F., Bemporad, A., Fodor, M., and Hrovat, D. (2006). An mpc/hybrid system approach to traction control. *IEEE Transactions on Control Systems Technology*, 14(3):541–552.

Borrelli, F., Bemporad, A., and Morari, M. (2017). *Predictive control for linear and hybrid systems*. Cambridge University Press.

Breiman, L., Friedman, J. H., Olshen, R. A., and Stone, C. J. (1984). Classification and regression trees. wadsworth & brooks. *Cole Statistics/Probability Series*.

Camacho, E. F. and Bordons, C. (2004). *Model Predictive Control*. Springer Science & Business Media.

Canudas-de Wit, C. and Ferrara, A. (2018). A variable-length cell transmission model for road traffic systems. *Transp. Res. C, Emerg. Technol.*, 97:428–455.

Castro, P. M. (2015). Tightening piecewise mccormick relaxations for bilinear problems. *Computers & Chemical Engineering*, 72:300–311.

Celikoglu, H. B. (2014). Dynamic classification of traffic flow patterns simulated by a switching multimode discrete cell transmission model.

IEEE Transactions on Intelligent Transportation Systems, 15(6):2539–2550.

Celikoglu, H. B. and Silgu, M. A. (2016). Extension of traffic flow pattern dynamic classification by a macroscopic model using multivariate clustering. *Transportation Science*, 50(3):966–981.

Chen, F., Taylor, N., and Kringos, N. (2015a). Electrification of roads: opportunities and challenges. *Applied Energy*, 150:109–119.

Chen, F., Taylor, N., and Kringos, N. (2015b). Electrification of roads: Opportunities and challenges. *Applied Energy*, 150:109–119.

Chen, R., Zhang, T., and Levin, M. W. (2020). Effects of variable speed limit on energy consumption with autonomous vehicles on urban roads using modified cell-transmission model. *Journal of Transportation Engineering, Part A: Systems*, 146(7):04020049.

Chen, Z., He, F., and Yin, Y. (2016). Optimal deployment of charging lanes for electric vehicles in transportation networks. *Transportation Research Part B: Methodological*, 91:344–365.

Chen, Z., Liu, W., and Yin, Y. (2017). Deployment of stationary and dynamic charging infrastructure for electric vehicles along traffic corridors. *Transportation Research Part C: Emerging Technologies*, 77:185–206.

Chopra, S. and Bauer, P. (2011a). Driving range extension of ev with on-road contactless power transfer—a case study. *IEEE Transactions on Industrial Electronics*, 60(1):329–338.

Chopra, S. and Bauer, P. (2011b). Driving range extension of ev with on-road contactless power transfer—a case study. *IEEE transactions on industrial electronics*, 60(1):329–338.

Cirimele, V., Diana, M., Freschi, F., and Mitolo, M. (2018). Inductive power transfer for automotive applications: State-of-the-art and future trends. *IEEE Transactions on Industrial Applications*, 54(5):4069–4079.

Corte, M. V. and Montiel, L. V. (2021). Novel matrix hit and run for sampling polytopes and its gpu implementation. *arXiv preprint arXiv:2104.07097*.

Csikós, A. and Kulcsár, B. (2017). Variable speed limit design based on mode dependent cell transmission model. *Transp. Res. C, Emerg. Technol.*, 85:429–450.

Cui, L., Wang, Q., Qu, H., Wang, M., Wu, Y., and Ge, L. (2023). Dynamic pricing for fast charging stations with deep reinforcement learning. *Applied Energy*, 346:121334.

Da, K. (2014). A method for stochastic optimization. *arXiv preprint arXiv:1412.6980*.

Daganzo, C. F. (1995). The cell transmission model, part ii: network traffic. *Transp. Res. B, Methodol*, 29(2):79–93.

De Cauwer, C., Verbeke, W., Coosemans, T., Faid, S., and Van Mierlo, J. (2017). A data-driven method for energy consumption prediction and energy-efficient routing of electric vehicles in real-world conditions. *Energies*, 10(5):608.

Deflorio, F. and Castello, L. (2017). Dynamic charging-while-driving systems for freight delivery services with electric vehicles: Traffic and energy modelling. *Transp. Res. C, Emerg. Technol.*, 81:342–362.

Deflorio, F., Guglielmi, P., Pinna, I., Castello, L., and Marfull, S. (2015a). Modeling and analysis of wireless "charge while driving" operations for fully electric vehicles. *Transp. Res. Procedia*, 5:161–174.

Deflorio, F., Pinna, I., Castello, L., and Cantello, V. (2016a). Dynamic charging systems for electric vehicles: simulation for the daily energy estimation on motorways. *IET Intelligent Transport Systems*, 10(4):258–269.

Deflorio, F., Pinna, I., Castello, L., and Cantello, V. (2016b). Dynamic charging systems for electric vehicles: simulation for the daily energy estimation on motorways. *IET Intell. Transp. Syst.*, 10(4):258–269.

Deflorio, F. P., Castello, L., Pinna, I., and Guglielmi, P. (2015b). "charge while driving" for electric vehicles: road traffic modeling and energy assessment. *Journal of Modern Power Systems and Clean Energy*, 3(2):277–288.

Di Cairano, S., Park, H., and Kolmanovsky, I. (2012). Model predictive control approach for guidance of spacecraft rendezvous and proximity maneuvering. *International Journal of Robust and Nonlinear Control*, 22(12):1398–1427.

Doan, V., Fujimoto, H., Koseki, T., Yasuda, T., Kishi, H., and Fujita, T. (2017). Allocation of wireless power transfer system from viewpoint of optimal control problem for autonomous driving electric vehicles. *IEEE Transactions on Intelligent Transportation Systems*, 19(10):3255–3270.

Duarte, G., Silva, A., and Baptista, P. (2021). Assessment of wireless charging impacts based on real-world driving patterns: case study in lisbon, portugal. *Sustainable Cities and Society*, 71.

Esfahani, H. N., Liu, Z., and Song, Z. (2022). Optimal pricing for bidirectional wireless charging lanes in coupled transportation and power networks. *Transportation Research Part C: Emerging Technologies*, 135:103419.

Falcone, P., Borrelli, F., Asgari, J., Tseng, H. E., and Hrovat, D. (2007). Predictive active steering control for autonomous vehicle systems. *IEEE Transactions on Control Systems Technology*, 15(3):566–580.

Fernández, E., Leitner, M., Ljubić, I., and Ruthmair, M. (2022). Arc routing with electric vehicles: dynamic charging and speed-dependent energy consumption. *Transportation Science*.

Fletcher, N. (2023). Michigan to test roads with underground coils for ev charging.

Fontana, M. (2013). *Optimal routes for electric vehicles facing uncertainty, congestion, and energy constraints*. Phd thesis, Massachusetts Institute of Technology.

Foote, A. and Onar, O. (2017). A review of high-power wireless power transfer. In *2017 IEEE Transportation Electrification Conference and Expo (ITEC)*, pages 234–240. IEEE.

Frejo, J. R. D., Núñez, A., De Schutter, B., and Camacho, E. F. (2014). Hybrid model predictive control for freeway traffic using discrete speed limit signals. *Transportation Research Part C: Emerging Technologies*, 46:309–325.

Fuller, M. (2016). Wireless charging in california: Range, recharge, and vehicle electrification. *Transportation Research Part C: Emerging Technologies*, 67:343–356.

Galvin, R. (2017). Energy consumption effects of speed and acceleration in electric vehicles: laboratory case studies and implications for drivers and policymakers. *Transportation Research Part D: Transport and Environment*, 53:234–248.

García-Vázquez, C., Llorens-Iborra, F., Fernández-Ramírez, L., Sánchez-Sainz, H., and Jurado, F. (2017). Comparative study of dynamic

wireless charging of electric vehicles in motorway, highway and urban stretches. *Energy*, 137:42–57.

Ge, Y. and MacKenzie, D. (2022). Charging behavior modeling of battery electric vehicle drivers on long-distance trips. *Transportation Research Part D: Transport and Environment*, 113:103490.

Gilbert, N. (2019). *Agent-based models*. Sage Publications.

Gomes, G. and Horowitz, R. (2006). Optimal freeway ramp metering using the asymmetric cell transmission model. *Transp. Res. C, Emerg. Technol.*, 14(4):244–262.

Gomory, R. E. (1960). Solving linear programming problems in integers. *Combinatorial analysis*, 10(211-215):25.

Gomory, R. E. (1963). An algorithm for integer solutions to linear programs. *Recent advances in mathematical programming*, 64(260-302):14.

Gurobi Optimization, LLC (2024). *Gurobi Optimizer Reference Manual*. Accessed on 15 May 2024.

Ha, D. and Schmidhuber, J. (2018). Recurrent world models facilitate policy evolution. *Advances in neural information processing systems*, 31.

Hadiuzzaman, M. and Qiu, T. Z. (2013). Cell transmission model based variable speed limit control for freeways. *Canadian Journal of Civil Eng.*, 40(1):46–56.

Hajiahmadi, M., van de Weg, G. S., Tampère, C. M., Corthout, R., Hegyi, A., De Schutter, B., and Hellendoorn, H. (2015). Integrated predictive control of freeway networks using the extended link transmission model. *IEEE Transactions on Intelligent Transportation Systems*, 17(1):65–78.

Han, Y., Hegyi, A., Yuan, Y., and Hoogendoorn, S. (2017a). Validation of an extended discrete first-order model with variable speed limits. *Transportation research part C: emerging technologies*, 83:1–17.

Han, Y., Hegyi, A., Yuan, Y., Hoogendoorn, S., Papageorgiou, M., and Roncoli, C. (2017b). Resolving freeway jam waves by discrete first-order model-based predictive control of variable speed limits. *Transportation Research Part C: Emerging Technologies*, 77:405–420.

Hans, M. N. and Gupta, M. S. (2020). Trends in electric vehicle (ev) charging and key technology developments. Manuscript.

He, F., Yin, Y., and Zhou, J. (2013). Integrated pricing of roads and electricity enabled by wireless power transfer. *Transportation Research Part C: Emerging Technologies*, 34:1–15.

He, J., Huang, H.-J., Yang, H., and Tang, T.-Q. (2017). An electric vehicle driving behavior model in the traffic system with a wireless charging lane. *Physica A: Statistical Mechanics and its Applications*, 481:119–126.

He, J., Yang, H., Huang, H., and Tang, T. (2018). Impacts of wireless charging lanes on travel time and energy consumption in a two-lane road system. *Physica A: Statistical Mechanics and its Applications*, 500:1–10.

He, J., Yang, H., Tang, T.-Q., and Huang, H.-J. (2020). Optimal deployment of wireless charging lanes considering their adverse effect on road capacity. *Transportation Research Part C: Emerging Technologies*, 111:171–184.

He, M., Wang, S., and Zhuge, C. (2023). A data-driven large-scale micro-simulation approach to deploying and operating wireless charging

lanes. *Transportation Research Part D: Transport and Environment*, 121:103835.

Hegyi, A., De Schutter, B., and Hellendoorn, H. (2005). Model predictive control for optimal coordination of ramp metering and variable speed limits. *Transp. Res. C, Emerg. Technol.*, 13(3):185–209.

Hoogendoorn, S. P. and Bovy, P. H. (2001). State-of-the-art of vehicular traffic flow modelling. *Proc. of the Inst. of Mech. Eng., Part I: Journal of Syst. and Control Engineering*, 215(4):283–303.

Hu, L., Dong, J., and Lin, Z. (2019). Modeling charging behavior of battery electric vehicle drivers: A cumulative prospect theory based approach. *Transportation Research Part C: Emerging Technologies*, 102:474–489.

Hulagu, S. and Celikoglu, H. B. (2021). Electric vehicle location routing problem with vehicle motion dynamics-based energy consumption and recovery. *IEEE Transactions on Intelligent Transportation Systems*, 23(8):10275–10286.

Hussain, R., Son, J., Kim, D., Nogueira, M., Oh, H., Tokuta, A., and Seo, J. (2017). Pbf: a new privacy-aware billing framework for online electric vehicles with bidirectional auditability. *Wireless Communications and Mobile Computing*, 2017:1–17.

Hwang, I., Jang, Y., Ko, Y., and Lee, M. (2017). System optimization for dynamic wireless charging electric vehicles operating in a multiple-route environment. *IEEE Transactions on Intelligent Transportation Systems*, 19(6):1709–1726.

IEA (2021). Global electric car sales set for further strong growth after 40 Accessed November 2021.

Jang, Y. J. (2018). Survey of the operation and system study on wireless charging electric vehicle systems. *Transportation Research Part C: Emerging Technologies*, 95:844–866.

Jang, Y. J., Jeong, S., and Lee, M. (2015). System optimization of the on-line electric vehicle operating in a closed environment. *Computer & Industrial Engineering*, 80:222–235.

Jang, Y. J., Suh, E., and Kim, J. (2016a). Initial energy logistics cost analysis for stationary, quasi-dynamic, and dynamic wireless charging public transportation systems. *Energies*, 9(7):483.

Jang, Y. J., Suh, E., and Kim, J. (2016b). System architecture and mathematical models of electric transit bus system utilizing wireless power transfer technology. *IEEE Systems Journal*, 10(2):495–506.

Jansuwan, S., Liu, Z., Song, Z., and Chen, A. (2021). An evaluation framework of automated electric transportation system. *Transportation Research Part E: Logistics and Transportation Review*, 148.

Jaxa-Rozen, M. and Kwakkel, J. H. (2018). Pynetlogo: Linking netlogo with python. *Journal of Artificial Societies and Social Simulation*, 21(2).

Jeong, S., Jang, Y., and Kum, D. (2015). Economic analysis of the dynamic charging electric vehicle. *IEEE Transactions on Power Electronics*, 30(11):6368–6377.

Kim, J., Kim, J., Kong, S., Kim, H., Suh, I., Suh, N., Cho, D., Kim, J., and Ahn, S. (2013a). Coil design and shielding methods for a magnetic resonant wireless power transfer system. *Proceedings of the IEEE*, 101(6):1332–1342.

Kim, J., Kim, J., Kong, S., Kim, H., Suh, I.-S., Suh, N. P., Cho, D.-H., Kim, J., and Ahn, S. (2013b). Coil design and shielding methods for a

magnetic resonant wireless power transfer system. *Proc. of the IEEE*, 101(6):1332–1342.

Ko, Y., Jang, Y., and Lee, M. (2015). The optimal economic design of the wireless powered intelligent transportation system using genetic algorithm considering nonlinear cost function. *Computer & Industrial Engineering*, 89:67–79.

Koehler, S., Mehr, N., Horowitz, R., and Borrelli, F. (2016). Stable hybrid model predictive control for ramp metering. In *2016 IEEE 19th International Conference on Intelligent Transportation Systems (ITSC)*, pages 1083–1088. IEEE.

Kong, N. J., Li, C., Council, G., and Johnson, A. M. (2023). Hybrid ilqr model predictive control for contact implicit stabilization on legged robots. *IEEE Transactions on Robotics*.

Kponyo, J., Nwizege, K., Opare, K., Ahmed, A., Hamdoun, H., Akazua, L., Alshehri, S., and Frank, H. (2016). A distributed intelligent traffic system using ant colony optimization: a netlogo modeling approach. In *2016 International Conference on Systems Informatics, Modelling and Simulation (SIMS)*, pages 11–17. IEEE.

Land, A. H. and Doig, A. G. (2010). *An automatic method for solving discrete programming problems*. Springer.

Lee, J. H. and Cooley, B. (1997). Recent advances in model predictive control and other related areas. *IFAC Proceedings Volumes*, 30(18):347–358.

Lee, M. and Jang, Y. (2017). Charging infrastructure allocation for wireless charging transportation system. In *International Conference on Management Science and Engineering Management*, pages 1630–1644. Springer, Cham.

Lenstra, J. K. and Rinnooy Kan, A. (1978). Complexity of scheduling under precedence constraints. *Operations Research*, 26(1):22–35.

Lewis, M. (2023). Sweden is building the world's first permanent electric road that charges moving evs.

Li, C., Dong, X., Cipcigan, L. M., Haddad, M. A., Sun, M., Liang, J., and Ming, W. (2022). Economic viability of dynamic wireless charging technology for private evs. *IEEE Transactions on Transportation Electrification*, 9(1):1845–1856.

Li, M., Wu, X., Zhang, Z., Yu, G., Wang, Y., and Ma, W. (2019). A wireless charging facilities deployment problem considering optimal traffic delay and energy consumption on signalized arterial. *IEEE Transactions on Intelligent Transportation Systems*, 20(12):4427–4438.

Li, Z., Liu, P., Xu, C., Duan, H., and Wang, W. (2017). Reinforcement learning-based variable speed limit control strategy to reduce traffic congestion at freeway recurrent bottlenecks. *IEEE transactions on intelligent transportation systems*, 18(11):3204–3217.

Lighthill, M. J. and Whitham, G. B. (1955). On kinematic waves ii. a theory of traffic flow on long crowded roads. *Proceedings of the royal society of london. series a. mathematical and physical sciences*, 229(1178):317–345.

Lillicrap, T. P., Hunt, J. J., Pritzel, A., Heess, N., Erez, T., Tassa, Y., Silver, D., and Wierstra, D. (2015). Continuous control with deep reinforcement learning. *arXiv preprint arXiv:1509.02971*.

Lin, D.-Y. and Kuo, J.-K. (2021). The vehicle deployment and relocation problem for electric vehicle sharing systems considering demand and parking space stochasticity. *Transportation Research Part E: Logistics and Transportation Review*, 156.

Liu, F., Tan, Z., Chan, H. K., and Zheng, L. (2024). Ramp metering control on wireless charging lanes considering optimal traffic and charging efficiencies. *IEEE Transactions on Intelligent Transportation Systems*.

Liu, H., Zou, Y., Chen, Y., and Long, J. (2021). Optimal locations and electricity prices for dynamic wireless charging links of electric vehicles for sustainable transportation. *Transportation Research Part E: Logistics and Transportation Review*, 152.

Liu, Z. and Song, Z. (2017). Robust planning of dynamic wireless charging infrastructure for battery electric buses. *Transportation Research Part C: Emerging Technologies*, 83:77–103.

Liu, Z. and Song, Z. (2018). Dynamic charging infrastructure deployment for plug-in hybrid electric trucks. *Transportation Research Part C: Emerging Technologies*, 95:748–772.

Löfberg, J. (2004). Yalmip : A toolbox for modeling and optimization in matlab. In *In Proceedings of the CACSD Conference*, Taipei, Taiwan.

Lou, Y., Yin, Y., and Laval, J. A. (2011). Optimal dynamic pricing strategies for high-occupancy/toll lanes. *Transportation Research Part C: Emerging Technologies*, 19(1):64–74.

Lytinen, S. L. and Railsback, S. F. (2012). The evolution of agent-based simulation platforms: a review of netlogo 5.0 and relogo. In *Proceedings of the fourth international symposium on agent-based modeling and simulation*.

Machura, P. and Li, Q. (2019). A critical review on wireless charging for electric vehicles. *Renewable and Sustainable Energy Reviews*, 104:209–234.

Maggi, L., Sacone, S., and Siri, S. (2015). Freeway traffic control considering capacity drop phenomena: comparison of different mpc schemes. In

2015 IEEE 18th International Conference on Intelligent Transportation Systems, pages 457–462. IEEE.

Manshadi, S., Khodayar, M., Abdelghany, K., and Üster, H. (2018). Wireless charging of electric vehicles in electricity and transportation networks. *IEEE Transactions on Smart Grid*, 9(5):4503–4512.

Mao, P., Ji, X., Qu, X., Li, L., and Ran, B. (2022). A variable speed limit control based on variable cell transmission model in the connecting traffic environment. *IEEE Transactions on Intelligent Transportation Systems*, 23(10):17632–17643.

Marcucci, T. and Tedrake, R. (2020). Warm start of mixed-integer programs for model predictive control of hybrid systems. *IEEE Transactions on Automatic Control*, 66(6):2433–2448.

Masti, D., Pippia, T., Bemporad, A., and De Schutter, B. (2020). Learning approximate semi-explicit hybrid mpc with an application to microgrids. *IFAC-PapersOnLine*, 53(2):5207–5212.

Mayne, D. Q., Rawlings, J. B., Rao, C. V., and Scokaert, P. O. M. (2000). Constrained model predictive control: Stability and optimality. *Automatica*, 36(6):789–814.

McCormick, G. P. (1976). Computability of global solutions to factorable nonconvex programs: Part i—convex underestimating problems. *Mathematical programming*, 10(1):147–175.

McFadden, D. (1972). Conditional logit analysis of qualitative choice behavior.

McKerracher, C. (2023). Electric car sales look poised for slower growth this year.

Miller, J., Jones, P., Li, J., and Onar, O. (2015). Ornl experience and challenges facing dynamic wireless power charging of ev's. *IEEE Circuits and Systems Magazine*, 15(2):40–53.

Mitrovic, N., Dakic, I., and Stevanovic, A. (2019). Combined alternate-direction lane assignment and reservation-based intersection control. *IEEE Transactions on Intelligent Transportation Systems*, 21(4):1779–1789.

Mnih, V., Kavukcuoglu, K., Silver, D., Graves, A., Antonoglou, I., Wierstra, D., and Riedmiller, M. (2013). Playing atari with deep reinforcement learning. *arXiv preprint arXiv:1312.5602*.

Mnih, V., Kavukcuoglu, K., Silver, D., Rusu, A. A., Veness, J., Bellemare, M. G., Graves, A., Riedmiller, M., Fidjeland, A. K., Ostrovski, G., et al. (2015). Human-level control through deep reinforcement learning. *nature*, 518(7540):529–533.

Mohamed, A. A., Meintz, A., and Zhu, L. (2019). System design and optimization of in-route wireless charging infrastructure for shared automated electric vehicles. *IEEE Access*, 7:79968–79979.

Mostafizi, A., Koll, C., and Wang, H. (2021). A decentralized and coordinated routing algorithm for connected and autonomous vehicles. *IEEE Transactions on Intelligent Transportation Systems*, 23(8):11505–11517.

Mouhrim, N., Alaoui, A., and Boukachour, J. (2016). Optimal allocation of wireless power transfer system for electric vehicles in a multipath environment. In *2016 3rd International Conference on Logistics Operations Management (GOL)*, pages 1–7. IEEE.

Mubarak, M., Üster, H., Abdelghany, K., and Khodayar, M. (2021). Strategic network design and analysis for in-motion wireless charging of elec-

tric vehicles. *Transportation Research Part E: Logistics and Transportation Review*, 145.

Müller, E. R., Carlson, R. C., Kraus, W., and Papageorgiou, M. (2015). Microsimulation analysis of practical aspects of traffic control with variable speed limits. *IEEE Transactions on Intelligent Transportation Systems*, 16(1):512–523.

Muralidharan, A. and Horowitz, R. (2015). Computationally efficient model predictive control of freeway networks. *Transportation Research Part C: Emerging Technologies*, 58:532–553.

Nasr Esfahani, H., Liu, Z., and Song, Z. (2022). Optimal pricing for bidirectional wireless charging lanes in coupled transportation and power networks. *Transportation Research Part C*, 135.

Ngo, H., Kumar, A., and Mishra, S. (2020). Optimal positioning of dynamic wireless charging infrastructure in a road network for battery electric vehicles. *Transportation Research Part D: Transport and Environment*, 85.

Nguyen, J., Powers, S. T., Urquhart, N., Farrenkopf, T., and Guckert, M. (2021). An overview of agent-based traffic simulators. *Transportation research interdisciplinary perspectives*, 12:100486.

Nie, Y. and Ghamami, M. (2013). A corridor-centric approach to planning electric vehicle charging infrastructure. *Transportation Research Part B: Methodological*, 57:172–190.

Osband, I., Blundell, C., Pritzel, A., and Van Roy, B. (2016). Deep exploration via bootstrapped dqn. *Advances in neural information processing systems*, 29.

Ou, C., Liang, H., and Zhuang, W. (2015). Investigating wireless charging and mobility of electric vehicles on electricity market. *IEEE Transactions on Industrial Electronics*, 62(5):3123–3133.

Panchal, C., Stegen, S., and Lu, J. (2018). Review of static and dynamic wireless electric vehicle charging system. *Engineering Science and Technology, an International Journal*, 21(5):922–937.

Pandey, V., Wang, E., and Boyles, S. D. (2020). Deep reinforcement learning algorithm for dynamic pricing of express lanes with multiple access locations. *Transportation Research Part C: Emerging Technologies*, 119:102715.

Pelletier, S., Jabali, O., and Laporte, G. (2016). Goods distribution with electric vehicles: review and research perspectives. *Transportation Science*, 50(1):3–22.

Qin, S. J. and Badgwell, T. A. (2003). A survey of industrial model predictive control technology. *Control Engineering Practice*, 11(7):733–764.

Qiu, J. and Du, L. (2023). Cooperative trajectory control for synchronizing the movement of two connected and autonomous vehicles separated in a mixed traffic flow. *Transportation research part B: methodological*, 174:102769.

Quinlan, J. R. (1986). Induction of decision trees. *Machine learning*, 1:81–106.

Quinlan, J. R. (2014). *C4. 5: programs for machine learning*. Elsevier.

Railsback, S. F. and Grimm, V. (2019). *Agent-based and individual-based modeling: a practical introduction*. Princeton university press.

Rawlings, J. B., Mayne, D. Q., Diehl, M., et al. (2017). *Model predictive*

control: theory, computation, and design, volume 2. Nob Hill Publishing Madison, WI.

Riemann, R., Wang, D., and Busch, F. (2015). Optimal location of wireless charging facilities for electric vehicles: flow-capturing location model with stochastic user equilibrium. *Transportation Research Part C: Emerging Technologies*, 58:1–12.

Ross, B., Pilz, L., Cabrera, B., Brachten, F., Neubaum, G., and Stieglitz, S. (2019). Are social bots a real threat? an agent-based model of the spiral of silence to analyse the impact of manipulative actors in social networks. *European Journal of Information Systems*, 28(4):394–412.

Rummery, G. A. and Niranjan, M. (1994). *On-line Q-learning using connectionist systems*, volume 37. University of Cambridge, Department of Engineering Cambridge, UK.

Saharan, S., Bawa, S., and Kumar, N. (2020). Dynamic pricing techniques for intelligent transportation system in smart cities: A systematic review. *Computer Communications*, 150:603–625.

Schmitt, M., Ramesh, C., and Lygeros, J. (2017). Sufficient optimality conditions for distributed, non-predictive ramp metering in the monotonic cell transmission model. *Transportation Research Part B: Methodological*, 105:401–422.

Schwerdfeger, S., Bock, S., Boysen, N., and Briskorn, D. (2022). Optimizing the electrification of roads with charge-while-drive technology. *European Journal of Operational Research*, 299(3):1111–1127.

Shi, Y., Wang, Z., LaClair, T. J., Wang, C., Shao, Y., and Yuan, J. (2023). A novel deep reinforcement learning approach to traffic signal control with connected vehicles. *Applied Sciences*, 13(4):2750.

Shladover, S. (2007). Path at 20—history and major milestones. *IEEE Transactions on Intelligent Transportation Systems*, 8(4):584–592.

Silgu, M. A., Erdağı, İ. G., Göksu, G., and Celikoglu, H. B. (2021a). Combined control of freeway traffic involving cooperative adaptive cruise controlled and human driven vehicles using feedback control through sumo. *IEEE Transactions on Intelligent Transportation Systems*, 23(8):11011–11025.

Silgu, M. A., Erdağı, İ. G., Göksu, G., and Çelikoğlu, H. B. (2021b). H∞ state feedback controller for ode model of traffic flow. *IFAC-PapersOnLine*, 54(2):19–24.

Silver, D., Huang, A., Maddison, C. J., Guez, A., Sifre, L., Van Den Driessche, G., Schrittwieser, J., Antonoglou, I., Panneershelvam, V., Lanctot, M., et al. (2016). Mastering the game of go with deep neural networks and tree search. *nature*, 529(7587):484–489.

Sklar, E. (2007). Netlogo, a multi-agent simulation environment. *Artificial life*, 13(3):303–311.

Smith, R. L. (1996). The hit-and-run sampler: a globally reaching markov chain sampler for generating arbitrary multivariate distributions. In *Proceedings of the 28th conference on Winter simulation*, pages 260–264.

Srivastava, A. (2016). *Modified cell transmission model for bounded acceleration*. University of California, Irvine.

Srivastava, A. and Geroliminis, N. (2013). Empirical observations of capacity drop in freeway merges with ramp control and integration in a first-order model. *Transp. Res. C, Emerg. Technol.*, 30:161–177.

Suh, N. and Cho, D. (2017). Making the move: from internal combustion engines to wireless electric vehicles. In *The On-Line Electric Vehicle*, pages 3–15. Springer, Cham.

Sutton, R. S. and Barto, A. G. (2018). *Reinforcement learning: An introduction*. MIT press.

Sutton, R. S., McAllester, D., Singh, S., and Mansour, Y. (1999). Policy gradient methods for reinforcement learning with function approximation. *Advances in neural information processing systems*, 12.

Tan, Z. and Gao, H. O. (2018). Hybrid model predictive control based dynamic pricing of managed lanes with multiple accesses. *Transportation Research Part B: Methodological*, 112:113–131.

Tan, Z., Liu, F., Chan, H. K., and Gao, H. O. (2022). Transportation systems management considering dynamic wireless charging electric vehicles: review and prospects. *Transportation Research Part E: Logistics and Transportation Review*, 163:102761.

Tavakoli, R. and Pantic, Z. (2017). Analysis, design, and demonstration of a 25-kw dynamic wireless charging system for roadway electric vehicles. *IEEE Journal of Emerging and Selected Topics in Power Electronics*, 6(3):1378–1393.

Thai, J. and Bayen, A. M. (2014). State estimation for polyhedral hybrid systems and applications to the godunov scheme for highway traffic estimation. *IEEE Transactions on Automatic Control*, 60(2):311–326.

Train, K. E. (2009). *Discrete choice methods with simulation*. Cambridge university press.

Triastanto, A. N. D. and Utama, N. P. (2019). Model study of traffic congestion impacted by incidents. In *2019 International Conference of Ad-*

vanced Informatics: Concepts, Theory and Applications (ICAICTA), pages 1–6. IEEE.

Trung, N. K. and Diep, N. T. (2021). A maximum transfer efficiency tracking method for dynamic wireless charging systems of electric vehicles. *Journal of Electrical and Computer Engineering*, 2021:1–10.

U.S. Department of Energy (2024). Efficient driving to conserve fuel. Accessed: 2024-05-15.

Wang, C., Xu, Y., Zhang, J., and Ran, B. (2022a). Integrated traffic control for freeway recurrent bottleneck based on deep reinforcement learning. *IEEE Transactions on Intelligent Transportation Systems*, 23(9):15522–15535.

Wang, L., Yang, M., Li, Y., and Hou, Y. (2022b). A model of lane-changing intention induced by deceleration frequency in an automatic driving environment. *Physica A: Statistical Mechanics and its Applications*, 604:127905.

Wang, T., Yang, B., Chen, C., and Guan, X. (2019). Wireless charging lane deployment in urban areas considering traffic light and regional energy supply-demand balance. In *2019 IEEE 89th Vehicular Technology Conference (VTC2019-Spring)*, pages 1–5. IEEE.

Wang, T., Yang, B., Chen, C., and Guan, X. (2020). Double-layer game based wireless charging scheduling for electric vehicles. In *2020 IEEE 91st Vehicular Technology Conference (VTC2020-Spring)*, pages 1–5. IEEE.

Wang, X., Jiang, J., Zhou, Y., and Wang, X. (2023). Integrated infrastructure planning of charging and electricity generation. *Transportation Research Part D: Transport and Environment*, 122:103807.

Wei, S., Uthaichana, K., Žefran, M., and DeCarlo, R. (2013). Hybrid model predictive control for the stabilization of wheeled mobile robots subject to wheel slippage. *IEEE transactions on control systems technology*, 21(6):2181–2193.

Wen, Y., MacKenzie, D., and Keith, D. R. (2016). Modeling the charging choices of battery electric vehicle drivers by using stated preference data. *Transportation Research Record*, 2572(1):47–55.

Wilensky, U. (1999). Netlogo. Center for Connected Learning and Computer-Based Modeling, Northwestern University, Evanston, IL.

Wilensky, U. and Payette, N. (1998). Netlogo traffic 2 lanes model. http://ccl.northwestern.edu/netlogo/models/Traffic2Lanes. Center for Connected Learning and Computer-Based Modeling, Northwestern University, Evanston, IL.

Williams, R. J. (1992). Simple statistical gradient-following algorithms for connectionist reinforcement learning. *Machine learning*, 8:229–256.

Wu, H. (2021). A survey of battery swapping stations for electric vehicles: operation modes and decision scenarios. *IEEE Transactions on Intelligent Transportation Systems*.

Wu, X., Freese, D., Cabrera, A., and Kitch, W. (2015). Electric vehicles' energy consumption measurement and estimation. *Transportation Research Part D: Transport and Environment*, 34:52–67.

Yuan, T., Alasiri, F., and Ioannou, P. A. (2022). Selection of the speed command distance for improved performance of a rule-based vsl and lane change control. *IEEE Transactions on Intelligent Transportation Systems*, 23(10):19348–19357.

Zhang, H., Du, L., and Shen, J. (2022). Hybrid mpc system for platoon based cooperative lane change control using machine learning aided

distributed optimization. *Transportation Research Part B: Methodological*, 159:104–142.

Zhang, J., Song, C., Mo, Z., and Cao, S. (2023). A transfer learning-based approach to estimating missing pairs of on/off ramp flows. *IEEE Transactions on Intelligent Transportation Systems*.

Zhang, J., Wang, Z., Liu, P., and Zhang, Z. (2020). Energy consumption analysis and prediction of electric vehicles based on real-world driving data. *Applied Energy*, 275:115408.

Zhang, Y. and Ioannou, P. A. (2017). Coordinated variable speed limit, ramp metering and lane change control of highway traffic. *IFAC-PapersOnLine*, 50(1):5307–5312.

Zhou, S., Qiu, Y., Zou, F., He, D., Yu, P., Du, J., Luo, X., Wang, C., Wu, Z., and Gu, W. (2019). Dynamic ev charging pricing methodology for facilitating renewable energy with consideration of highway traffic flow. *IEEE Access*, 8:13161–13178.

Zhu, F. and Ukkusuri, S. V. (2014). Accounting for dynamic speed limit control in a stochastic traffic environment: A reinforcement learning approach. *Transportation research part C: emerging technologies*, 41:30–47.

Zhu, J., Hu, L., Chen, Z., Xie, H., et al. (2022). A queuing model for mixed traffic flows on highways considering fluctuations in traffic demand. *Journal of Advanced Transportation*, 2022.

Zhu, J.-J. and Martius, G. (2020). Fast non-parametric learning to accelerate mixed-integer programming for hybrid model predictive control. *IFAC-PapersOnLine*, 53(2):5239–5245.